

Breaking Barriers and Making Waves: Targeted Delivery of Gene Vector Nanoparticles to the Brain with Focused Ultrasound

A Dissertation

Presented to

the faculty of the School of Engineering and Applied Science

University of Virginia

in partial fulfillment
of the requirements for the degree

Doctor of Philosophy

by

Brian Patrick Mead

December 2017

APPROVAL SHEET

This Dissertation
is submitted in partial fulfillment of the requirements
for the degree of
Doctor of Philosophy

Author Signature: 

This Dissertation has been read and approved by the examining committee:

Advisor: Richard J. Price, Ph.D.

Committee Member: Brent French, Ph.D.

Committee Member: Jonathan Kipnis, Ph.D.

Committee Member: Alexander Klibanov, Ph.D.

Committee Member: G. Wilson Miller, Ph.D.

Committee Member: Benjamin Purow, M.D.

Accepted for the School of Engineering and Applied Science:



Craig H. Benson, School of Engineering and Applied Science

December 2017

*Breaking Barriers and Making Waves:
Targeted Delivery of Gene Vector Nanoparticles to the Brain
with Focused Ultrasound*

A Dissertation

presented to the faculty of the School of Engineering and Applied Science
in partial fulfillment of the requirements for the degree of

Doctor of Philosophy

Brian P. Mead
December 2017

Dissertation Advisor

Richard J. Price, Ph.D.

Department of Biomedical Engineering
University of Virginia

Table of Contents

Acknowledgements	ix
Chapter 1: Preface	1
1.1 Abstract.....	1
1.2 Preview of this Dissertation.....	3
Chapter 2: Drug and Gene Delivery Across the Blood-Brain Barrier with Focused Ultrasound	4
2.1 Abstract.....	5
2.2 Introduction.....	6
2.2.1 The Blood-Brain Barrier.....	6
2.2.2 Conventional Approaches for Bypassing the Blood-Brain Barrier.....	7
2.2.3 Opening the Blood-Brain Barrier with Focused Ultrasound.....	8
2.2.4 Safety and Monitoring of Blood-Brain Barrier Disruption.....	11
2.3 Drug Delivery	13
2.3.1 Unencapsulated Drugs.....	13
2.3.2 Liposomes.....	18
2.3.3 Drug Loaded Microbubbles.....	19
2.4 Gene Delivery.....	20
2.4.1 Naked Plasmid Delivery.....	21
2.4.2 Adeno-Associated Virus.....	22
2.5 Polymer-Based Delivery Systems.....	23
2.6 Therapeutic Bioeffects of Focused Ultrasound.....	25
2.6.1 Modulation of Immune Cell Activation with Focused Ultrasound.....	25
2.6.2 Changes in ECM permeability with Focused Ultrasound.....	26
2.7 Conclusions and Future Perspectives.....	28
2.8 Acknowledgements.....	29

2.9 Figures.....	30
Figure 2.1 Blood-Brain Barrier Biology.....	30
Figure 2.2 Transcranial FUS with microbubbles is the only modality capable of achieving non-invasive, safe, repeated and targeted BBB disruption, leading to improved drug or gene delivery to the brain.....	31
Figure 2.3 Mechanism of focused ultrasound mediated blood-brain barrier disruption...32	
Figure 2.4 Transcranial FUS leads to temporary and localized BBBD with no long term damage.....	33
Figure 2.5 FUS mediated delivery of anti-AB antibody reduces plaque load in the TgCRND8 mouse model of Alzheimer’s disease.....	34
Figure 2.6 Three weekly FUS BBBD treatments (weeks 1-3) mediated delivery of liposomal doxorubicin and prolonged survival in a rat glioma model.....	35
Figure 2.7 FUS mediated delivery of scAAV9 leads to a dose-dependent transgene expression in mouse brain.....	36
Figure 2.8 FUS delivers large 60-nm brain-penetrating nanoparticles across the BBB...37	
2.10. Tables.....	38
Table 2.1 Key references demonstrating drug or gene delivery with focused ultrasound.....	38

Chapter 3: Targeted Gene Transfer to the Brain via the Delivery of Brain-Penetrating DNA Nanoparticles with Focused Ultrasound.....40

3.1 Abstract.....	41
3.2 Introduction.....	42
3.3 Results and Discussion.....	45
3.4 Materials and Methods.....	50
3.4.1 Animals.....	50
3.4.2 DNA-BPN Fabrication and Characterization.....	50
3.4.3 FUS-Mediated DNA-BPN Delivery.....	51
3.4.4 Microbubble Preparation.....	51
3.4.5 In Vivo Bioluminescence Imaging.....	52

3.4.6 Ex Vivo Bioluminescence Imaging.....	52
3.4.7 Whole Brain Epifluorescence Imaging.....	52
3.4.8 Histological Processing.....	53
3.4.9 Histology.....	53
3.4.10 Immunofluorescence.....	53
3.5 Funding Sources.....	55
3.6 Figures.....	56
Figure 3.1 DNA-BPN stability in pooled human plasma.....	56
Figure 3.2 FUS-mediated delivery of pBAL DNA-BPN across the BBB leads to robust and localized transgene expression in the rat brain.....	57
Figure 3.3 FUS mediated delivery of pBACH DNA-BPN into rat brain leads to efficient and localized transfection.....	58
Figure 3.4 DNA-BPN delivered across the BBB with FUS transfect both astrocytes and neurons.....	59
Figure 3.5 Examination of brain tissues for toxicity and gliosis at 1 week after DNA-BPN delivery with FUS.....	60
3.7 Tables.....	61
Table 3.1 Physicochemical Properties of DNA-BPN.....	61
Chapter 4: Novel Focused Ultrasound Gene Therapy Approach Non-Invasively Restores Dopaminergic Neuron Function in a Rat Parkinson’s Disease Model.....	62
4.1 Abstract.....	63
4.2 Introduction.....	64
4.3 Results.....	67
4.3.1 Characterization of GDNF-BPN.....	67
4.3.2 MR Imaging Assessment of Blood-Brain Barrier Opening.....	67
4.3.3 Localized Delivery of GDNF-BPN with FUS Elicits Robust GDNF Protein Expression in the Striatum.....	68

4.3.4 Dopamine Levels are Elevated in 6-OHDA Lesioned Rats that Subsequently Received FUS-Targeted GDNF-BPN Delivery.....	69
4.3.5 Dopaminergic Neuron Density is Restored in 6-OHDA Lesioned Rats that Subsequently Received FUS-Targeted GDNF-BPN Delivery.....	69
4.3.6 Locomotor Function is Markedly Improved in 6-OHDA Lesioned Rats that Subsequently Received FUS-Targeted GDNF-BPN Delivery.....	70
4.3.7 Safety Analysis.....	70
4.4 Discussion.....	71
4.4.1 Gene Delivery to the CNS with FUS.....	71
4.4.2 Comparison to Previous Preclinical Studies with GDNF.....	72
4.4.3 Relevance to Clinical Trials.....	74
4.5 Materials and Methods.....	76
4.5.1 Animals.....	76
4.5.2 6-OHDA Lesions.....	76
4.5.3 Plasmid Design.....	76
4.5.4 DNA-BPN Fabrication and Characterization.....	77
4.5.5 Microbubble Fabrication and Characterization.....	77
4.5.6 FUS-Mediated DNA-BPN Delivery.....	78
4.5.7 Behavioral Testing.....	79
4.5.8 Histological Processing.....	80
4.5.9 Immunohistochemistry.....	80
4.5.10 Quantitative Morphology.....	81
4.5.11 Sample Preparation for Biochemical Analysis.....	81
4.5.12 Measurement of Striatal Catecholamines.....	82
4.5.13 GDNF Protein Levels Measured by ELISA.....	82
4.5.14 Statistical Analysis.....	82
4.5.15 Data Availability.....	83

4.6 Acknowledgements.....	83
4.7 Author Contributions.....	83
4.8 Figures.....	85
Figure 4.1 MR imaging for guidance, confirmation, and safety evaluation of FUS treatments.....	85
Figure 4.2 FUS-mediated delivery of GDNF-BPN to the striatum of PD rats leads to a significant increase in GDNF protein levels in the striatum.....	86
Figure 4.3 FUS-mediated delivery of GDNF-BPN improves dopamine levels in the ipsilateral hemisphere.....	87
Figure 4.4 Delivery of GDNF-BPN to the striatum with FUS increases dopaminergic neuron density in the striatum and SNpc.....	88
Figure 4.5 Delivery of GDNF-BPN with FUS restores locomotor function in PD rats.....	89
4.9 Supplemental Figures.....	90
Figure 4.S1 GDNF-BPN are colloiddally stable when incubated in water or artificial cerebrospinal fluid (aCSF).....	90
Figure 4.S2 FUS-mediated delivery of GDNF-BPN to the striatum of PD rats does not change GDNF protein levels in the SNpc or other major organs.....	91
Figure 4.S3 FUS-mediated delivery of GDNF-BPN to the striatum of PD rats does not lead to systemic or local toxicity.....	92
Figure 4.S4 Time schedule of study.....	93
4.9 Supplemental Tables.....	94
Table 4.S1 Dopamine metabolites in the Ipsilateral Striatum.....	94
Chapter 5: Mechanisms and Applications of Augmented Nanoparticle Dispersion and Non-Viral Transfection via Brain Tissue Pre-Treatment with Pulsed Focused Ultrasound.....	95
5.1 Abstract.....	96
5.2 Introduction.....	97
5.3 Results.....	100
5.3.1 Characterization of Gene Vector BPN.....	100
5.3.2 Pre-Exposure of Rodent Brain to Pulsed FUS Prior to Convection Enhanced	

Delivery of ZsGreen-BPN, both with and without MBs, improves volume of transfection.....	100
5.3.3 Pulsed FUS enhances transfection volume by activating TrpA1 channels, but not TrpV1 channels.....	101
5.3.4 Pulsed FUS enhances transfection volume after CED administration of ZsGreen-BPN into the U87 model of human GBM.....	102
5.3.5 Application of Pulsed FUS to Brain Tissue Before Trans-BBB Delivery of Luc-BPN Markedly Enhanced Transfection.....	102
5.3.6 Passive Cavitation Detection Reveals No Change in Cavitation Detected During BBB Opening.....	103
5.3.7 Histology.....	103
5.4 Discussion.....	104
5.4.1 Rationale for Testing Pulsed FUS as a Means for Enhancing Transfection in the CNS.....	104
5.4.2 Improving Transfection Volume in the CNS by Combining Ultrasound and Direct Injection.....	105
5.4.3 Increased Volume of Transfection After FUS Pre-Treatment is Attenuated in TrpA1 Knockout Mice.....	107
5.4.4 FUS Pre-Treatment as a Strategy to Enhance Glioma Transfection.....	108
5.4.5 Pre-Treatment of CNS Tissue with FUS to Enhance Delivery of Systemically Administered Agents with FUS and MBs.....	109
5.5 Materials and Methods.....	111
5.5.1 Animals.....	111
5.5.2 Plasmid Design.....	111
5.5.3 DNA-BPN Fabrication and Characterization.....	111
5.5.4 Microbubble Fabrication and Characterization.....	112
5.5.5 FUS Pre-Exposure and Convection Enhanced Delivery.....	112
5.5.6 Histological Processing and Imaging After Convection Enhanced Delivery....	113
5.5.7 U87mg-mCherry Tumor Inoculation.....	114
5.5.8 MRI-guided FUS Delivery of Luc-BPN.....	115

5.5.9 Passive Cavitation Detection.....	116
5.5.10 <i>In Vivo</i> Bioluminescence Imaging.....	117
5.5.11 <i>Ex Vivo</i> Bioluminescence Imaging.....	117
5.5.12 Histological Processing for Safety Analysis.....	117
5.5.13 Immunolabeling and Histology for Safety Analysis.....	118
5.5.14 Statistical Analysis.....	118
5.5.15 Data Availability.....	118
5.6 Acknowledgements.....	119
5.7 Figures.....	120
Figure 5.1 Pre-treatment of rat brain with FUS with or without MBs increases volume of distribution after CED administration of ZsGreen-BPN.....	120
Figure 5.2 Enhancement of ZsGreen-BPN volume of distribution with FUS is attenuated in TrpA1 ^{-/-} mice, but not in TrpV1 ^{-/-} mice.....	121
Figure 5.3 Pre-Treatment of an intracranial mCherry-expressing U87 human glioma tumor in a mouse increases volume of distribution after CED administration of ZsGreen-BPN.....	122
Figure 5.4. Pre-Exposure of rat brain to 4 MPa or 2 MPa FUS (2.25% duty cycle, 10 mins) without MBs increases bioluminescence after delivery of Luc-BPN with FUS compared to non-pre-treated controls.....	123
Figure 5.5 Pre-treatment with 4 MPa or 2 MPa FUS does not alter SCD or ICD during BBB-opening.....	124
Figure 5.6 Pre-treatment with FUS at either 4 MPa or 2 MPa does not lead to signs of damage.....	125
5.8 Tables.....	126
Table 5.1 Physiochemical Properties of BPN.....	126
Chapter 6: Direction of Future Research Projects.....	127
6.1 Focused Ultrasound as a Strategy for Treating Brain Disease.....	128
6.2 Integrating Alternative Nanoparticle Formulations into Focused Ultrasound Treatment Paradigms.....	128

6.3 Development of GDNF-BPN delivery with FUS as a Clinical Treatment Strategy for Parkinson's Disease.....	129
6.4 Secondary Mechanisms of Focused Ultrasound to Enhance Nanoparticle-based treatment strategies.....	131
6.5 Promise for Therapeutic Genome and Transcriptome Engineering strategies with Focused Ultrasound.....	133
6.6 Pre-treatment with Focused Ultrasound as a Strategy to Enhance Immune Infiltration and Activation.....	133
6.7 Summary.....	134
References.....	135

Acknowledgements

Throughout my work toward this dissertation, I have been supported by an inestimable amount of support. I am deeply indebted to my advisor, Dr. Richard Price, who drove me to take ownership of my work and encouraged me to pursue lofty goals that have led to the conclusions of this dissertation. Through all the surprising results and troubleshooting, I have learned a great deal and will be forever grateful.

The work in this dissertation could not have been accomplished without an exceptional network of lab-mates, class-mates and friends. In particular, thank you to the lab-mates with whom I have spent the most time, Ji Song, Colleen Curley and Kelsie Timbie, who, in addition to showing me the ropes, helped maintain a dynamic and scientifically stimulating lab environment by introducing different and enlightening perspectives to challenges. Each of you have made unique and lasting impacts on me. I am also grateful to the hard-working and dedicated undergrads who put their faith in me during their time at UVa. Thank you to in particular to David Hodges, Lena Badr and Grace Wusk, whose hard work inspired me to become a better teacher.

Thank you to the many collaborators I have been able to work with. To Panos Mastorakos, Namho Kim, Jung Soo Suk and Justin Hanes and the rest of the Hanes Lab at John's Hopkins University, I am grateful for your incalculable support and challenging questions. To Wilson Miller, thank you for being one of my closest mentors and for teaching me to always see the humor in every situation.

To the members of my dissertation committee, including Drs. Brent French, Alexander Klibanov, Jonathan Kipnis, Wilson Miller and Benjamin Purow: thank you for your guidance. Each of you has helped push me out of my comfort zone and helped me focus on the broader goals in both my career and the science.

Finally, I am profoundly grateful to my family. Thank you in particular to my parents, Diane and Alan, for giving me love and continued support throughout my time here at UVa.

It was not until recently that I fully realized the extent to which their support helped me keep my spirits up and focused on the most important things. Thank you also to my brothers, David and Paul, for your encouragement

Chapter 1: Preface

1.1 Abstract

Gene therapy in the central nervous system (CNS) has the potential to slow or reverse pathology in numerous neurological diseases including Parkinson's disease, Alzheimer's disease, and brain tumors. However, while clinical gene therapy trials have been largely unsuccessful, outcomes may be improved by a) enhancing delivery efficiency and transfection volume, b) improving reproducibility of treatments and c) treating patients at earlier or prodromal stages prior to onset of irreversible pathology. While currently the gold standard for treatments in the CNS, direct administration strategies are invasive and may yield poor gene vector distribution. Less invasive strategies capable of targeted and homogenous delivery in the CNS are required.

In this dissertation, we demonstrate a novel strategy for delivery of gene vector nanoparticles into the brain capable of circumventing two major barriers to drug delivery in the brain; namely, the blood-brain barrier (BBB) and the nanoporous extracellular matrix (ECM). Focused ultrasound (FUS), when used in conjunction with ultrasound contrast agent microbubbles (MBs) is capable of non-invasive and spatially localized disruption of the BBB, capable of delivering agents as large as 100 nm in diameter into the CNS. We use this strategy in combination with non-viral gene vector nanoparticles which are coated in exceptionally dense coats of polyethylene glycol in a "brain-penetrating" nanoparticle (BPN) formulation, capable of rapidly diffusing through brain tissue. With this novel strategy, we are able to achieve robust reporter gene expression in the brain of healthy rats that lasted at least 28-days and was localized to the site targeted with FUS. Importantly, we demonstrate transfection of both neurons and astrocytes without signs of toxicity or astrocyte activation.

Next, we sought to apply our strategy to a rat model of Parkinson's disease (PD). PD is a common and idiopathic neurodegenerative disorder commonly characterized by degeneration of

dopamine-generating neurons in the substantia nigra and their axonal projections into the striatum. We packaged a gene for the glial cell line-derived neurotrophic factor (GDNF), a neurotrophic factor shown by other groups to be therapeutic in this model, into a BPN and delivered it to the striatum of a PD rat model. With just a single treatment, we were able to achieve therapeutically relevant levels of GDNF protein content in the FUS-targeted striatum, restore dopamine levels, and dopaminergic neuron density and eliminate behavioral indicators of Parkinsonism.

Finally, we explored strategies to enhance BPN dispersion and uptake in the CNS. By using a unique approach in which pulsed FUS was used to pre-treat the target tissue, we found significant enhancement in BPN dispersion through healthy rat and mouse brain as well as in the U87 model of human glioblastoma multiforme after infusion into the brain parenchyma with convection enhanced delivery. Next, by applying this pre-treatment regimen prior to opening of the BBB with FUS and MBs, we demonstrate up to 5-fold enhancement of delivery of BPN compared animals whose BBB was opened with FUS and MBs but did not receive pre-treatment FUS.

Overall, these studies demonstrate the ability of FUS to target the delivery of gene vectors across the BBB and elicit robust and homogenous transgene expression that is localized to the FUS-targeted site. Importantly, the non-invasive nature allows treatment of neurological disorders earlier time points than current invasive direct administration strategies. These results will be important in the development and, ultimately, translation of FUS-based strategies for gene delivery and gene therapy in the CNS.

1.2 Preview of this dissertation

In chapter 2, this dissertation will introduce broad topics related to FUS and its ability to delivery drugs and genes across the blood-brain barrier. This chapter will also include discussion of outstanding questions in the larger field. Chapter 3-5 will report our studies involving the development of FUS and non-viral gene vector nanoparticles as a novel strategy for delivery of gene vectors to the brain, our application of this strategy to treat a rat model of Parkinson's disease and, finally, a novel strategy to enhance delivery across the blood-brain barrier with FUS. Chapter 6 will provide a discussion of the future directions of the work discussed in this dissertation.

**Chapter 2: Drug and Gene Delivery Across the Blood-Brain Barrier with Focused
Ultrasound**

Kelsie F. Timbie*, Brian P. Mead*, Richard J. Price. *Journal of Controlled Release* 219: 61-75, 2015

*Authors contributed equally to this work.

2.1 Abstract

The blood-brain barrier (BBB) remains one of the most significant limitations to treatments of central nervous system (CNS) disorders including brain tumors, neurodegenerative diseases and psychiatric disorders. It is now well-established that focused ultrasound (FUS) in conjunction with contrast agent microbubbles may be used to non-invasively and temporarily disrupt the BBB, allowing localized delivery of systemically administered therapeutic agents as large as 100 nm in size to the CNS. Importantly, recent technological advances now permit FUS application through the intact human skull, obviating the need for invasive and risky surgical procedures. When used in combination with magnetic resonance imaging, FUS may be applied precisely to pre-selected CNS targets. Indeed, FUS devices capable of sub-millimeter precision are currently in several clinical trials. FUS mediated BBB disruption has the potential to fundamentally change how CNS diseases are treated, unlocking potential for combinatorial treatments with nanotechnology, markedly increasing the efficacy of existing therapeutics that otherwise do not cross the BBB effectively, and permitting safe repeated treatments. This article comprehensively reviews recent studies on the targeted delivery of therapeutics into the CNS with FUS and offers perspectives on the future of this technology.

Keywords: Focused ultrasound, blood-brain barrier, CNS drug delivery, nanoparticles

Abbreviations: AAV, adeno-associated virus; BBB, blood-brain barrier; BBBD, blood-brain barrier disruption; BCNU, bis-chloroethylnitrosourea, or carmustine; BNCT, boron neutron capture therapy; BPN, brain-penetrating nanoparticle; CNS, central nervous system; DOX, doxorubicin; FUS, focused ultrasound; GBM, glioblastoma multiforme; GDNF, glial-cell derived neurotrophic factor; MB, microbubble; MR, magnetic resonance; NTN, neurturin; NP, nanoparticle; PCD, passive cavitation detection; PEG, polyethylene glycol; SPIO, superparamagnetic iron oxide; SWI, susceptibility weighted imaging; TMZ, temozolomide

2.2. Introduction

Many diseases of the central nervous system (CNS) present tremendous challenges for clinicians. Both primary and metastatic brain tumors carry dismal survival rates (11, 12), and the increasing age of the population in the developed world has created a dramatic increase (13) in the number of people living with age-related neurodegenerative diseases like dementia, Alzheimer's and Parkinson's. Additionally, nearly 20% of the adult population (14) experiences the debilitating effects of a mental illness like obsessive-compulsive disorder or clinical depression each year, generating over \$44 billion in lost productivity in the US alone (15). The commonality in this wide range of CNS disorders is the inherent difficulty of treatment. The blood-brain barrier (BBB) provides excellent protection for the body's most privileged organ, preventing the vast majority of molecules in circulation from entering brain tissue. However, because of this, the BBB also presents a significant challenge for CNS treatments, as systemic therapies are rarely capable of crossing the BBB. Recently, the ability of focused ultrasound (FUS) in conjunction with microbubbles (MBs) to facilitate the noninvasive, localized, and reversible opening of the BBB has led to the emergence of this technology as a viable new option for delivering therapeutics to the CNS. Here, we review recent studies on FUS-mediated delivery of drugs and genes into the CNS. For convenience, we have included a table of key references (Table 1).

2.2.1 The Blood-Brain Barrier

The BBB provides a formidable obstacle for drug delivery in the brain (Figure 1). Through a unique combination of transmembrane proteins and tightly regulated channels not seen elsewhere in the body, the BBB prevents nearly 100% of large molecule (>500 Da) drugs including recombinant proteins and antibodies and 98% of small molecule drugs from passing into the brain (5). Lipid soluble small molecule drugs may cross the BBB if they are capable of

diffusing through the endothelial cell membrane itself (5), but few drugs fall into this category. The BBB's remarkable exclusionary capability is attributed to tight junctions that join the endothelial cells lining the vasculature throughout the brain (16). Tight junctions are comprised of several proteins, including various claudins, occludins, junctional adhesion molecules, and cadherins, which function to prevent molecules from passively diffusing between cells and out of the vasculature (16). Rather, small molecules must pass through the endothelial cells themselves, either through diffusion (for lipid soluble molecules) or active transport (most nutrients and other substances necessary for normal brain function) (16). Furthermore, if a certain molecule does manage to pass through the endothelial cell layer, the basement membrane provides an additional barrier to diffusion. Simply stated, nature's best defense against infection significantly hinders our ability to treat diseases of the CNS by preventing drug delivery to the brain.

2.2.2 Conventional Approaches for Bypassing the Blood-Brain Barrier

Given the central role of the BBB in limiting drug and gene delivery to the CNS, numerous methods have been developed to bypass this barrier. For example, specific viruses or nanoparticles (NPs) with BBB-targeting ligands can cross the BBB after systemic administration(17). However, in order to achieve effective concentrations in the brain, they must be administered in doses which are associated with adverse effects in peripheral organs(18). For this reason, the majority of preclinical and clinical studies have used direct intracranial administration as a strategy to locally increase therapeutic concentration without off-target effects. Specific brain regions can be accessed with needles or catheters and more recent strategies have utilized fluid convection to enhance distribution of therapeutics in the brain(19). By maintaining bulk flow with hydrostatic pressure differentials, convection enhanced delivery has demonstrated marked improvement over conventional direct intracranial injection

methodologies(20, 21). Unfortunately, despite promising results for direct injection in several preclinical and clinical trials(22–26), these strategies are risky and surgical complications have hindered widespread adoption. Furthermore, macromolecular agents require long dissemination times and typically cannot spread beyond a few millimeters(20). Indeed, the invasive nature of strategies like intracranial injections is not compatible with drugs that need to be dosed repeatedly.

In order to reduce risks associated with direct injection, less-invasive strategies to enhance therapeutic delivery across the BBB have been developed. These include intranasal administration and chemical disruption of the BBB by intra-arterial infusion of the osmotic agent mannitol(27) or vasodilators(28–30). Intranasal administration permits transport to the brain through perineural or perivascular channels(31). While intranasal drug delivery is non-invasive and obviates peripheral side effects associated with intravenous administration, it is limited by poor absorption across the nasal epithelium, inconsistent delivery efficiency and poor localization(31, 32). Similarly, mannitol infusions lead to global BBB disruption, causing non-specific uptake and potentiating adverse off-target effects. Infusion of mannitol into the carotid artery leads to an osmotic-driven movement of fluid out of endothelial cells(33), shrinking them and leading to fenestration of cerebral vessels. While disruption of the BBB with mannitol is reasonably safe, therapeutic delivery is inconsistent with up to 10-fold variations in drug concentrations(34).

2.2.3 Opening the Blood-Brain Barrier with Focused Ultrasound

FUS has the advantage of being the only modality capable of achieving non-invasive, safe, repeated, and targeted BBB disruption to enhance drug or gene delivery to the CNS. With the advent of MR-compatible transducers with sub-millimeter precision, it is now possible to apply image-guided transcranial FUS to the human brain (35–38) in an extremely localized manner,

greatly reducing the risk of off-target effects. FUS treatments can be performed on awake patients, eliminating the need for general anesthetic and permitting real-time patient feedback. Importantly, MR and integrated passive cavitation detection (PCD) facilitate real-time intraoperative treatment monitoring, while post-treatment MR imaging allows confirmation of treatment success(39–42) and safety(43, 44). The development of transcranial FUS has been a long process. Groundbreaking research by the Fry brothers performed over 50 years ago demonstrated that ultrasound could produce bioeffects in the human brain(45). However, it wasn't until recent technological advances were made in both ultrasound and MRI that the field experienced a surge in interest. In the past ten years, there has been an increase in the number of papers investigating the potential applications of ultrasound in the brain.

Ultrasound is, at its most basic, a pressure wave. As the wave passes through the tissue, the tissue experiences alternating periods of high pressure (compression) and low pressure (rarefaction). Ultrasound can be applied in a continuous fashion, common in treatments that require heat deposition, or in a pulsed manner, which is utilized for BBBD. Focusing the ultrasound beam (i.e. FUS) provides high spatial accuracy (less than 1 mm resolution in some cases) and localizes bioeffects. However, reflection and diffraction of the ultrasound wave at material interfaces (i.e. skull-tissue interface) can distort the focus and decrease the energy delivered at the target. While the favorable skull geometry of rats or mice allows the use of single-element transducers in pre-clinical trials (Figure 2), the far more complex topography of the human skull requires the use of a multi-element array with phase-correction software to re-focus the ultrasound beam as it passes through the skull. There are many combinations of FUS parameters (frequency, pressure, pulsing protocol) suitable for BBBD, but lower frequencies (≤ 1.0 MHz) experience less attenuation and distortion by the skull.

Transcranial FUS is typically applied in conjunction with intravenously administered MBs to effect blood-brain barrier disruption (BBBD). MBs are small (1-10 μm) lipid or protein shelled

bubbles filled with an inert gas, most commonly a perfluorocarbon and are FDA-approved as a contrast agent during ultrasound imaging. Importantly, circulating MBs reduce the acoustic energy required to open the BBB by two orders of magnitude and confine mechanical effects to the vasculature(46). This permits the use of low pressure FUS and virtually eliminates any concerns about skull heating during treatment. Extended off-time (low duty cycle) between FUS pulses allows MB reperfusion and thermal dissipation at the focus. At the lower ultrasonic pressures used for BBBD, MBs oscillate stably in the FUS field, expanding during rarefaction and contracting during compression, producing mechanical shear forces(47) and microstreaming(48) effects which act on the vessel wall. This behavior domain, called stable oscillation, is preferred for BBBD as its effects are more predictable. In contrast, at higher acoustic pressures, MBs experience unstable oscillations and eventually collapse inward, producing elevated local temperatures and high-pressure jet streams in a process termed inertial cavitation. While FUS-MB induced BBBD occurs in both regimes, inertial cavitation is more violent and is generally avoided for applications in healthy brain tissue. However, it may find use in diseased tissue, or for the delivery of very large (~100 nm) therapeutics, when the potential benefits outweigh the risks.

A collection of *in vitro* and *ex vivo* work(49–51) has demonstrated that the mechanical forces exerted by stably oscillating MBs cause vessel distension and invagination, as well as changes in the endothelial cells' cytoskeletons and cell-cell interactions (Figure 3). Together, these effects produce BBBD via three mechanisms: disruption of tight junctions, induction of transcytosis and sonoporation of the vascular endothelium. Work using transmission electron microscopy imaging(52) has demonstrated both a reduction and altered distribution of claudins 1 and 5, occludin, and ZO-1 after FUS exposure. Most notably, tight junction proteins were no longer clustered along the edges of endothelial cells, suggesting that they were no longer contributing to tight junction complexes. Furthermore, penetration of horse radish peroxidase

between endothelial cells was evident, demonstrating that tight junctions were no longer sealing paracellular pathways from the vasculature to the brain parenchyma. In addition to this paracellular pathway, horseradish peroxidase was also taken up by the vascular endothelial cells after sonication. Later work (53–55) demonstrated increased expression of caveolin-1 in the vascular endothelium after sonication, identifying caveolae as the most likely transcytotic pathway. A unique approach using two-photon microscopy provided further support for both paracellular and transcellular pathways. Here, it was noted that dextrans crossed the BBB after FUS via either a fast or slow mechanism (i.e. less/greater than 10 min) and postulated that the fast and slow pathways were most likely paracellular (tight junction disruption) and transcellular (increased transcytosis and sonoporation), respectively (56). Interestingly, 70kDa dextrans appeared to have a higher pressure threshold for BBB crossing than smaller 10kDa dextrans, in agreement with other studies indicating that the extent of BBBD (particularly the size of junctional clefts) is related to pressure (57). Furthermore, smaller vessels (i.e. less than ~25-30 μm) were significantly more likely to be disrupted by FUS (58) than larger vessels, and fast leakage (56) (i.e. paracellular) was the dominant mode of transport in these vessels. This difference is attributed to the interactions between MBs and the vessel wall – in smaller vessels, oscillating MBs are more likely to come in close contact with the vessel wall, generating larger circumferential stresses than in larger vessels. Going forward, achieving a better understanding of the dynamics of these transport pathways will be critical for enabling more predictable BBBD, especially with the increased use of larger therapeutics.

2.2.4 Safety and Monitoring of Blood-Brain Barrier Disruption

While it is well known that driving MBs into inertial cavitation with high acoustic pressures can lead to irreversible capillary damage and the leakage of blood across the BBB (59), thresholds have been established wherein BBBD can be achieved without toxicity or damage.

BBBD is transient and, depending on acoustic pressure(60), barrier function is typically restored within 4-6 hours after treatment (Figure 4A,B) (52, 61, 62). Importantly, no motor or acuity deficits were found after repeated BBBD procedures with FUS at numerous targets in monkeys(63, 64). Interestingly, some of these monkeys had T2* hypointensities in post-FUS MR imaging, indicating minor red blood cell accumulation; however, these minor capillary leakages did not lead to any changes in visual acuity or motor skills. Furthermore, it is important to emphasize that, even in the rare occurrence of erythrocyte extravasation at the lower pressures used in these studies, no apoptotic bodies were found and cognitive function of the animals was not impaired(63). These findings are in agreement with other studies suggesting that minor capillary damage and red blood cell extravasation is not expected to lead to long term effects(41, 65). Indeed, it is possible that such damage would be acceptable in treatment of debilitating or life-threatening neurological diseases. It is important to further emphasize that FUS-related safety issues would be minor compared to those of other treatment strategies like intracranial injection, which can lead to extensive damage along the needle tract, or even non-invasive treatments like gamma knife radiosurgery(66, 67).

While FUS-mediated BBBD has been shown to be safe in numerous animal models, intraoperative monitoring with passive cavitation detection or MR imaging further reduces chances of aberrant FUS treatments. Passive cavitation detection (PCD) allows real-time assessment of MB cavitation(68). While stable cavitation is most likely responsible for reversible BBBD(59, 69), inertial cavitation has been linked with tissue damage(70). Importantly, acquired PCD intensity is well correlated with BBBD(59, 69). PCD non-invasively detects the acoustic signatures resulting from MB oscillations, and can distinguish between stable oscillations and MB collapse.(71). Stably oscillating MBs emit harmonic, subharmonic or ultraharmonic frequency acoustic emissions, whereas collapsing MBs emit broadband acoustic signals(72, 73). PCD has been used to ensure safe FUS settings in several large animal BBBD models(63,

74) and systems are currently in development that will allow fully automatic feedback to control FUS sonications(75). Once the FUS treatment is complete, MR imaging sequences including T2* and susceptibility weighted imaging (SWI) are sensitive tools that can be used to detect blood products present in tissue(43, 61, 76) and have been shown to be sensitive to measure even minor capillary damage(63).

2.3. Drug Delivery

FUS-mediated BBBD permits the delivery of a wide range of therapeutics, and improves the efficacy and safety profile of the few drugs which can cross the BBB by reducing the required systemic dose. FUS has demonstrated remarkable ability to deliver a wide range of payloads, including small molecule drugs[79,85], ~150 kDa antibodies(79), recombinant proteins(80) and even ~100 nm liposomal drug vehicles(81, 82). As FUS technology has improved over the last decade, work has progressed from the delivery of free small molecule drugs [79,85] such as temozolomide to larger plaque-binding antibodies (79) and ~100 nm liposomal drug vehicles (81, 82). In addition, functionalized MBs (83), targeting moieties(84) and two-step processes like boron neutron capture therapy (85) have also been investigated in conjunction with FUS to further enhance delivery efficiency into the CNS. Here, we review work demonstrating the delivery of systemically administered small molecule-, recombinant protein- and antibody-based therapeutics in the brain using FUS-mediated BBBD.

2.3.1 Unencapsulated Drug

Temozolomide (TMZ), a small molecule drug, is currently part of the recommended approach to the clinical treatment of glioblastoma multiforme (GBM), and many clinical trials continue to test various TMZ dosing regimens as well as drug combinations (86–89). Although TMZ has produced moderate improvements in patient survival, GBM is notorious for tumor recurrence

after surgical resection because infiltrating tumor cells, which are protected from systemic drug delivery by the BBB, inevitably remain after surgery. Thus, it has been hypothesized that the delivery of TMZ via FUS-mediated BBBD may improve patient outcomes by providing drug delivery to these “protected” infiltrating cells (77, 90). In support of this hypothesis, in a rat model of GBM, BBBD in combination with orally administered medium dose TMZ significantly increased survival ($IST_{\text{median}}=15\%$ compared to controls) and controlled tumor growth as well as high dose TMZ alone (90). A study using the U87 glioma model in mice further demonstrated that FUS treatment improves tumor growth control and survival over TMZ alone across a range of TMZ doses ($IST_{\text{median}}=111\%$ compared to control for highest dose TMZ + FUS), although the benefit is most pronounced for low dose regimens (77). This effect appeared to be due to an increase in TMZ concentration and retention time (2.7- and 1.5-fold, respectively) in sonicated tissue (77). These studies demonstrate that BBBD with FUS can enhance the efficacy of even “gold standard” drugs in GBM.

While able to cross the BBB, carmustine (bis-chloroethylnitrosourea, BCNU) is another small molecule chemotherapeutic drug whose effectiveness could be enhanced by improved local delivery, as it is highly toxic and degrades within 15 minutes. BCNU-loaded polifeprosan 20 Gliadel wafers were one of the first uses of biodegradable polymers for drug delivery in humans (91–94), representing a unique solution to the problems posed by BCNU. Disappointingly, Gliadel produced only mild improvements in patient survival (2.3 months compared to placebo), and is now only recommended for patients with fully resectable tumors(94). Given these limitations, FUS-mediated delivery has been hypothesized to provide similar benefits. To this end, intravenous BCNU has been administered in conjunction with FUS-mediated BBBD, which doubled BCNU deposition in a C6 glioma model. It was shown that this combined treatment provides better tumor growth control and improved animal survival ($IST_{\text{median}}=86\%$ compared to control) (95). This study also indicates that it may be possible to decrease the intravenous dose

administered while maintaining therapeutically relevant drug concentrations in the brain, thus reducing systemic toxicity effects without the need for surgery. Ultimately, it is evident that BBBD with FUS can improve outcomes, even when used in conjunction with drugs that are able to cross the BBB, by increasing local drug concentrations and decreasing systemic toxicity.

PEGylated liposomal doxorubicin formulations are able to extravasate and collect in tumors, and they have been used in the treatment of glioma with some success, increasing progression free survival to 12 months in 15% of patients (96–98). The liposomal formulation is necessary since free doxorubicin (DOX) exhibits systemic toxicity and is unable to cross the BBB (96). However, liposomal DOX is also able to extravasate and collect in other tissues, notably the skin, producing tissue damage and discomfort (98). FUS-mediated BBBD may facilitate the use of free DOX, generating high intratumor drug concentrations while preventing systemic toxicities associated with the liposomal formulation. While FUS was capable of delivering up to 17-fold increases in DOX concentration in healthy brain tissue, in the GL261 mouse model of GBM, treatment with FUS and free DOX increased DOX concentrations in the tumors by only 4-fold compared to contralateral controls, although this increase was significant. Animals treated with FUS + free DOX had improved survival times ($IST_{\text{median}} = 68\%$) as well, and did not show effects of systemic drug toxicities (99). While this work indicates that FUS can improve the delivery of free drug across the blood-tumor barrier, it is also apparent that FUS parameters may need to be optimized for tumor biology rather than healthy brain tissue.

Boron neutron capture therapy (BNCT) offers the ability to eradicate tumor cells without damaging healthy tissue, a characteristic which is particularly appealing for brain applications. It relies on the accumulation of a stable boron isotope in the tumor tissue, followed by irradiation with low-energy neutrons. The accumulated boron absorbs the neutrons and releases high energy particles, destroying the tumor cells (100). BNCT has achieved some success in head-and-neck cancers (101), as well as GBM (102, 103), but it is believed that FUS-mediated BBBD

may improve BNCT efficacy by increasing the concentration of boron in the tumor tissue. Several rodent studies (85, 104, 105) have demonstrated that FUS significantly increases the concentration of BPA-f, a boron containing drug, in tumor tissue, as well as homogenizing distribution (85). Nonetheless, it remains to be seen whether this increase correlates to an improvement in treatment efficacy.

Therapeutic antibodies, while currently showing promise in the treatment of numerous cancers, are too large to cross the BBB. Therefore, antibodies which have shown success against various cancers are not beneficial for patients with brain metastases (106), and antibodies designed to treat neurodegenerative diseases require a delivery system (107). Early work indicated that FUS-mediated BBBD could be used to deliver endogenous IgG antibodies (108) as well as functionally intact D(4) receptor targeting antibody(109), opening the door for therapeutic applications. An exciting recent study in the TgCRND8 model of Alzheimer's disease showed that FUS-mediated BBBD increased glial cell activation and the delivery of endogenous IgG and IgM antibodies, which led to a reduction in plaque load (110). Further work in this model demonstrated the delivery of anti-A β across the BBB (Figure 5A), which then bound to the plaques (Figure 5B) and caused a significant 23% decrease in plaque surface area (Figure 5C). Plaque number and size were both decreased in the anti-A β + FUS group (79). An earlier study in the APP^{swe}/PSEN1^{dE9} Alzheimer's model indicated that FUS-mediated BBBD produces a 3-fold increase in plaque-bound anti-A β compared to non-sonicated tissue (111). These studies suggest the potential use of FUS-mediated antibody delivery for the treatment of neurodegenerative disorders. Indeed, compared to other transcranial delivery methods, FUS is particularly suited for the long term repeated treatments necessitated by the nature of these disorders due to its noninvasive application and highly localized effects.

Trastuzumab (Herceptin), a monoclonal antibody which binds to the Her2 receptor, has shown promise in the treatment of breast cancer (106), which frequently metastasizes to the

brain. In healthy animals, FUS-mediated BBBD significantly increased the delivery of trastuzumab in sonicated tissue with no apparent toxicity (112). In a rat model of breast cancer brain metastasis, animals receiving FUS + trastuzumab had significantly smaller tumors (4 of 10 tumors resolved completely) with an IST_{median} of 32% compared to untreated controls.

Commonly, patients with brain metastases are omitted from clinical trials, as many therapeutics which work well against the primary tumor do not cross the BBB and have no efficacy against brain metastases. FUS-mediated delivery across the BBB can significantly improve drug delivery and efficacy in the brain, and may permit a wider range of treatment options for patients with brain metastases.

Neurotrophic factor administration has been shown to ameliorate a variety of CNS disorders, including schizophrenia (113), depression (114), autism (115), and Parkinson's (116). However, like most large molecules, neurotrophic factors do not cross the BBB. BDNF, which shows promise as a neuroprotective agent (116), maintains its bioactivity after FUS-mediated delivery across the BBB and generates significant downstream signaling activity(117). Neurturin (NTN), another factor that has been identified as a potential therapy for neurodegenerative diseases (116), has also been delivered successfully (117) . FUS-mediated delivery increased NTN bioavailability by 25-fold compared to direct injection, and activation of signaling downstream of NTN indicated retention of function (80). Nonetheless, despite the success with BDNF and NTN, glial cell-line derived neurotrophic factor (GDNF) continues to pose problems for FUS-based delivery. One study (118) demonstrated a significant increase in the delivery of GDNF in FUS-treated regions; however, another was unable to detect GDNF delivery across the BBB due to rapid breakdown in the bloodstream (117).

Immunotherapy is especially intriguing for brain tumor applications, because toxicities associated with traditional drugs pose significant problems for healthy brain tissue(119, 120). However, the presence of the BBB confounds most traditional immunotherapeutic approaches.

FUS-mediated delivery of immunostimulatory interleukin-12 (IL-12) significantly increased IL-12 deposition in intracranial C6 gliomas, improved tumor growth control and increased survival ($IST_{\text{median}}=43\%$) (121). This effect was attributed to a significant improvement in the cytotoxic T-lymphocyte/regulatory T-cell ratio in the FUS + IL-12 group, presumably due to a combination of increased IL-12 concentration and vascular permeability, which permitted enhanced cytotoxic T-lymphocyte infiltration (121). With the success of recent immunotherapy trials, we speculate that FUS-mediated immunotherapy delivery may permit the inclusion of patients with brain metastases who would normally be denied treatment and ultimately represent a turning point in how brain metastases are treated.

2.3.2 Liposomes

Liposomal drug formulations are popular due to their versatility and biocompatibility (122). Their structure, comprised of an aqueous core and a lipid shell, permits the loading of both hydrophilic and hydrophobic drugs (123), and the formulation of the lipid shell can be easily modulated for PEGylation (124), thermosensitivity, and/or targeting (125). Furthermore, both the size and composition of the liposome can be altered to control circulation time and degradation rate (126). Liposomes are particularly beneficial for packaging highly toxic drugs, since encapsulated drugs are not bioavailable. Conversely, their larger size makes them more difficult to deliver and FUS may trigger release of the drug payload. The liposomal formulation of doxorubicin, a potent anthracycline, was one of the first drug delivery systems used in combination with FUS (81, 82, 84, 127–129). Treat et al demonstrated that a single treatment combining FUS and liposomal DOX delayed tumor growth and improved survival time ($IST_{\text{median}}=24\%$ compared to 16% for liposomal DOX alone) in a rat gliosarcoma model. Later work by the same group showed that 3 weekly FUS + liposomal DOX treatments drastically improved survival (Figure 6B) compared to the liposomal DOX-only group ($IST_{\text{median}}=100\%$ and

16%, respectively), with complete tumor resolution (Figure 6A) in several animals in the FUS + liposomal DOX group (82). Nonetheless, several animals did suffer from side effects, including skin toxicity, neural loss and intratumoral hemorrhage (82). To verify that the combination of FUS and liposomal DOX was not causing additional toxicity, a safety study in healthy animals was conducted that demonstrated only minor damage at the focus in animals that received both liposomal DOX and FUS, believed to be due to high local concentrations of DOX deposited by aggressive FUS settings. Of note, the authors also demonstrated that administering liposomal DOX after treatment caused a 32% decrease in DOX delivery across the BBB, a finding we have substantiated with 60 nm polymeric NPs (unpublished studies). A study with animals bearing bilateral 9L gliosarcomas indicated that even late stage tumors benefit from FUS-mediated delivery, with treated tumors showing a two-fold increase in DOX concentration compared to unsonicated controls (81). FUS treatment also significantly increased the delivery of tumor targeted liposomal DOX formulations in an intracranial mouse xenograft model (84, 128), while decreasing some elements of DOX-related toxicity (128), presumably due to lower levels of drug in circulation post sonication. While it is still unclear whether intact liposomes cross the BBB, it is clear that the combination of liposomal encapsulation and FUS-mediated delivery provide excellent therapeutic results, increasing drug concentrations at the target while minimizing systemic toxicities.

2.3.3 Drug Loaded Microbubbles

Microbubbles can also be functionalized for use as drug delivery vehicles. Although drug loading is limited to the lipid or protein shell, the relatively large surface area ($\sim 50 \mu\text{m}^2$) permits conjugation for both targeting and therapeutics (130). Because of its hydrophobicity, BCNU has been incorporated into the shell of lipid MBs with some success (83, 131–133). Encapsulation of BCNU within the MB's lipid shell permitted simultaneous BBB opening and local drug delivery

similar to that seen with unencapsulated drug, with the added benefit of increased tissue retention time at the target(133). Treatment with BCNU-MBs and FUS showed excellent tumor control 30 days post inoculation and median survival time was increased by 12% compared to controls in a C6 glioma model (133). The addition of VEGF-R2 to the BCNU-MBs provided antiangiogenic targeting capabilities and further improvements in tumor control and animal survival (83). The same group also developed DOX-loaded MBs conjugated with superparamagnetic iron oxide (SPIO) NPs(134), which showed a two-fold increase in DOX deposition within a rat glioma compared to a non-sonicated control. FUS treatment followed by magnetic targeting also deposited SPIO NPs released from the MBs within the tumor tissue, permitting MR-based treatment monitoring. While drug-loaded MBs offer the benefit of highly localized delivery, they may also require higher pressure to release the drug and are limited to the circulation time of the MB itself.

2.4 Gene Delivery

Gene therapy in the CNS is emerging as an attractive strategy for the treatment of neurological diseases like Parkinson's disease(2, 135–137), Alzheimer's disease(138, 139), lysosomal storage diseases(140, 141) and brain tumors (142). Indeed, despite the ability of traditional small molecule drug regimens to treat early symptoms of diseases like Parkinson's disease, continued disease progression ultimately leads to recurrence(143). Furthermore, the BBB requires these drugs to be administered at high systemic doses to reach effective concentrations in the brain, ultimately causing adverse peripheral side effects (18). Alternatively, gene therapy offers the ability to treat the underlying causes of the disease and ultimately slow progression or even reverse disease pathology. Moreover, continuous transgene expression leads to long term efficacy, reducing required treatments and overall patient costs when

compared to drugs or liposomes, which need to be dosed periodically. While numerous gene therapy trials for neurological disease have yielded early positive results, limited vector distribution(20) and the risk of infection(144) after intracranial injection have slowed widespread adoption. Toward this end, it has been postulated that outcomes could be improved by enhancing therapeutic distribution within the target structures(145). High capillary density in the brain allows multiple points of entry into the CNS after FUS application, potentiating improved distribution compared to intracranial injection. Therefore, delivery of therapeutic genes into the CNS with FUS may prove to be a powerful new method for treating neurological diseases.

Despite a high number of publications demonstrating the ability FUS to deliver gene bearing liposomes(146, 147), non-viral polyplexes(148–150), viruses(151–153) and free or MB bound plasmid DNA(154) to the periphery, there are very few studies that have shown the delivery of systemically administered gene-bearing agents to the CNS with FUS. Indeed, the first successful studies showing delivery of reporter gene-bearing agents across the BBB with FUS were completed as recently as 2012(155–157). In these studies, it was shown that FUS could deliver either naked plasmid or adeno-associated virus (AAV) across the BBB to mediate transgene expression in the brain. Recently, however, excitement for this application has led to a flurry of new studies, which will be reviewed here.

2.4.1 Naked Plasmid Delivery

Anionic plasmid DNA can be electrostatically bound to cationic MBs to create MB-DNA carriers. As a result, DNA will be immediately exposed to the vasculature being disrupted by FUS-activated MBs, potentiating DNA extravasation and trans-BBB delivery. Several studies have shown that linking the plasmid DNA to the MB will enhance the transfection compared to free circulating plasmid delivered with FUS(130, 158–160). Interestingly, MRIGFUS exposure to MB-DNA carriers bearing a gene for eGFP led to a significant enhancement of transgene

expression in neurons in a young mouse model(156). Using a similar system, it was shown a MB-DNA carrier bearing a gene for BDNF led to a ~20-fold increase in BDNF protein content(157). Unfortunately, very high doses of plasmid DNA were required due to susceptibility to degradation from nucleases in the blood and the cell, which reduce the efficiency of this vector system.

2.4.2 Adeno-Associated Virus

Adeno-associated virus (AAV) with its small ~20 nm size, transduction efficiency, and limited immunogenicity is a well-suited vector for delivery applications across the BBB. Indeed, some AAV vectors like the self-complementary AAV9 (scAAV9) vector are able to cross the BBB and mediate global transgene expression in the brain after intravenous injection. However, very high doses of scAAV9 are required with up to 1×10^{11} vg/g found to only transduce 19% of motor neurons in adult mice(161). In contrast, FUS-mediated BBBD can yield transduction efficiencies of 80% in the brain (155) and 87% in the spinal cord (Figure 7) (162) at doses as low as 2.5×10^9 or 2×10^9 vg/g, respectively. This marks a robust enhancement of transgene expression in the CNS after intravenous administration of scAAV9. In each case, transgene expression was localized to the anatomical location targeted with FUS. In addition to scAAV9, other studies have shown the delivery of AAV1(163, 164) or AAV2(165) across the BBB with FUS. Importantly, these studies showed that transgene expression can be limited to neurons through the use of the synapsin-1 promoter(163). Moreover, it was found that a transgene under the CMV promoter and packaged into the AAV2 capsid led to predominantly astrocytic expression after delivery with FUS(165), in contrast to intracranial injection of the same vector which led to mostly neuronal expression(166, 167). To this end, it has been suggested that FUS could alter cellular receptor concentrations including heparan sulfate proteoglycans. This receptor, in

addition to being the cellular receptor for AAV2(168) is also known to have roles in the CNS injury response(169).

Despite its efficiency, AAV has shown significant limitations when considered in the context of CNS gene delivery applications. Concerns about safety, limited packaging capacity, difficulties in scale-up and high production costs limit its scope as a long-term solution to CNS gene delivery. Furthermore, repeated administration of AAV leads to production of neutralizing antibody immune responses that may ultimately reduce the efficiency of the vector(170, 171). Finally, scAAV vectors and AAV vectors have packaging capacities of just 2.4 kb or 4.8 kb (172), respectively, which hampers the versatility of this vector.

2.5. Polymer-Based Delivery Systems

Polymer based NP delivery systems offer several advantages over non-encapsulated drugs or viral delivery systems. These include tailorability, ease of manufacture, improved drug-release profiles and protection from degradation or clearance(173, 174). Combined, these properties can reduce drug doses and drug-associated toxicity while improving therapeutic efficacy (175–180). Polymer NPs can be loaded with a variety of payloads including soluble or non-soluble drugs(160, 177, 181, 182), imaging or theranostic agents(183–185), or nucleic acids(148, 174, 186, 187).

It is well known that enhancing therapeutic distribution in the brain parenchyma will improve efficacy(145). Indeed, while the limitations imposed by the BBB are widely known, the brain parenchyma itself presents a further barrier to delivery in the brain. The brain tissue barrier consists of a dense nanoporous mesh of electrostatically charged macromolecules including chondroitin sulfate proteoglycans, hyaluronan and tenascins (188, 189). These charged molecules form a microstructure that hampers diffusion of macromolecules and vectors including NPs (8, 190) and viruses (21) via steric or adhesive interactions. In addition, tumors

like GBM contain dense and heterogeneous networks of collagen(191) and high interstitial pressures(192) that further limit macromolecule diffusion(193–196). As a result, until recently, it was thought that the upper size limit to diffusion in healthy brain was as small as 64 nm (197). However, it has been shown that an extremely dense (> 9 PEG/100 nm²) coat of the bioinert and neutrally charged polymer polyethylene glycol (PEG) shields NP surface charge and reduces ECM interactions in brain tissue, permitting the diffusion of particles up to 114 nm in size (6, 8, 198) and improving circulation time(199), which leads to enhanced accumulation in tumors through the enhanced permeability and retention effect(200, 201). Dense PEG coats have demonstrated remarkable improvements in diffusivity and efficacy with multiple types of polymer(6, 148, 174, 186). For example, highly-PEGylated “brain-penetrating” NPs (BPNs) continue to diffuse up to 24 hours after delivery, leading to a more homogeneous distribution within the parenchyma (Figure 8A-E) (198) In contrast, all sizes of un-PEGylated controls were rapidly immobilized within the ECM (Figure 8F,G). Unsurprisingly, drug-loaded BPNs are more effective than their un-PEGylated counterparts in limiting tumor growth after intracranial administration. Additionally, BPNs are also an effective vehicle for gene delivery in the brain, and have demonstrated remarkable efficiency after intracranial administration(186). Gene bearing BPN are an easily adaptable and versatile option for applications in the brain, devoid of the limitations of viral vectors. FUS is capable of delivering 60 nm BPNs across the BBB (Figure 8A-E) (6). These BPN represent an important advance in polymeric delivery systems, as evading the BBB is only the first major obstacle to drug and gene delivery in the brain – a point eloquently demonstrated by the lack of success with the Gliadel wafers. Therapeutics must be delivered well beyond the vasculature, and particles that are able to diffuse within the brain parenchyma greatly increase treatment volume and efficacy.

Polymer-based NP delivery systems are well suited for brain therapies after FUS mediated BBBD. Ideal drug delivery systems for applications in the CNS would include (i) ability to

homogeneously distribute within the target volume, (ii) sustained drug release and (iii) long circulation times by avoiding rapid clearance. In combination with FUS as a non-invasive strategy to bypass the BBB, polymeric brain-penetrating NPs have potential to overcome many of the hurdles associated with drug and gene delivery in the brain.

2.6. Therapeutic Bioeffects of Focused Ultrasound

This chapter is focused on the delivery of drugs and genes across the BBB with FUS; however, it is also important to note that recent advances in our understanding of biological responses to FUS have potentiated novel approaches to treatments of brain disease. FUS is now being explored both pre-clinically and clinically for its potential to treat brain diseases, even the absence of additional therapeutic agents. Recent advances in this field has led to considerable excitement and a flurry of new studies which will be reviewed here.

2.6.1 Modulation of Immune Cell Activation with Focused Ultrasound

Focused ultrasound-mediated modulation of the brain immune environment may potentiate novel treatment strategies for brain diseases including brain cancers and neurodegenerative diseases without need for pharmacological agents(202, 203). For example, BBBD with FUS alone in a mouse model of Alzheimer's disease led to a significant reduction of plaque burden four days after a single treatment(110). The authors showed that plaque reduction was linked to significant enhancement of endogenous antibodies bound to the A β plaque as well as to activation of microglia and astrocytes in the FUS-treated region. Further studies, using FUS to deliver an antibodies against amyloid- β (79) or have also been shown to reduce plaque burden. Additionally, five successive treatments with FUS and MBs were shown to lead to further plaque clearance and improved subject performance on several memory tasks(204) and, in combination with anti-tau antibodies(205) was able to elicit even more robust effects.

FUS and MBs have also been used to enhance the body's anti-tumor immune response with great success (202, 206). Earlier in this chapter we reviewed a variety of papers that used FUS and MBs to delivery antibodies across the blood-tumor barrier in order to enhance immune activation in a tumor. However, FUS with or without MBs has been shown to enhance activation and/or trafficking of immune cells into tumors and is being explored as an adjuvant strategy to enhance immunomodulatory anti-cancer drugs. These studies have been extensively reviewed elsewhere(202) and are outside the scope of this dissertation.

Finally, in addition to alterations in immune function and cell behavior within the brain, FUS-mediated BBBD has been shown to enhance neurogenesis(207), which is attributed to the demonstrated upregulation of BDNF(208) and Akt (209) after FUS. This observation has led to suggestions that FUS could be used as a non-invasive alternative to deep brain stimulation for treatment of depression(210). Importantly, low intensity FUS has also shown ability to transiently stimulate neurons in both animals(208, 211–214) and humans(215, 216), and has the ability to elicit acute sensory responses in the fingers and hands(216), potentially allowing non-invasive brain mapping. Ultimately, we believe that FUS will permit several therapeutic options in the CNS, beyond those dependent upon drug and/or gene delivery across the BBB.

2.6.2 Changes in ECM structure with Focused Ultrasound

Recent studies have demonstrated the ability of FUS to enhance delivery and/or transport of therapeutic agents even after they cross into the brain parenchyma. Ultrasound treatments are now being explored preclinically to enhance dispersion of therapeutic agents when applied during direct injection of small molecule tracers(217, 218) or liposomes(219) into rodent or non-human primate brain. ARF driving infusate...

In addition to using FUS simultaneously during infusion, additional data argues that FUS exposure prior to administration of agents into the brain can lead to significant

enhancement in transfection volume. One such study used FUS and MBs (1.5 MHz, 0.72 MPa, 5% duty cycle, 2.5×10^6 MB/g), with a regime similar to that used for BBB opening, prior to direct infusion of AAV2 vectors and found approximately 3-fold enhancement of transduction volume(220). Importantly, MBs do not appear necessary to this treatment and ultrasound exposure (~ 0.36 MPa, 10% duty cycle) of *ex vivo* brain slices (i.e. without MBs) revealed increases in perivascular and extracellular spaces of the brain(221). Interestingly, another recent study used acoustic radiation force imaging to show that pulsed FUS exposure reduced tissue elasticity and interstitial fluid pressures and increased penetration of fluorescent tracer nanoparticles(223) with FUS PNP of 8.95 MPa and a duty cycle of 5%. While this study did not assess thermal changes, temperature rise with similar FUS intensities was shown in a previous study to be $<5^\circ\text{C}$ (328). Nonetheless, It has been postulated that the increase in fluid conductivity of the tumor after FUS pre-treatment results in more rapid fluid flow away from the high pressure tumor core to the relatively lower pressure tumor periphery(329). High interstitial fluid pressures remain a major barrier to uptake of intravascularly circulating therapeutic agents into tumors(330), which is typically dependent on differences in capillary hydrostatic pressure and tumor interstitial fluid pressure. While the mechanisms of increased tissue permeability after FUS pre-treatment has been hypothesized to be primarily non-thermal(221), additional investigation is required to better understand cellular and tissue-level responses to FUS.

2.7. Conclusions and Future Perspectives

FUS is currently the only modality which allows repeated, non-invasive, and temporary BBBD to deliver drugs or genes to the CNS(39). Numerous studies have demonstrated the ability of FUS to deliver a wide range of payloads across the BBB including imaging agents, small molecule drugs, ~150 kDa antibodies, recombinant proteins, ~20 nm viruses, ~60 nm NPs, 100 nm liposomes and even 10 μ m stem cells. As a result, FUS has opened doors to novel treatments for CNS disorders like neurodegenerative disease, GBM, and psychiatric disorders. Particularly, despite its advantages and immense potential, nanotechnology has largely been excluded from applications in the brain owing to difficulties in delivery, which can be overcome with FUS. While the BBB has long been considered the greatest bottleneck in the development of treatments for CNS disease, FUS may fundamentally revolutionize how such diseases are approached.

2.8. Acknowledgements

The authors of this work have been supported by NIH R01 CA164789 and the NHLBI-sponsored Basic Cardiovascular Research Training Grant (5 T32 HL007284).

2.9 Chapter 2 Figures:

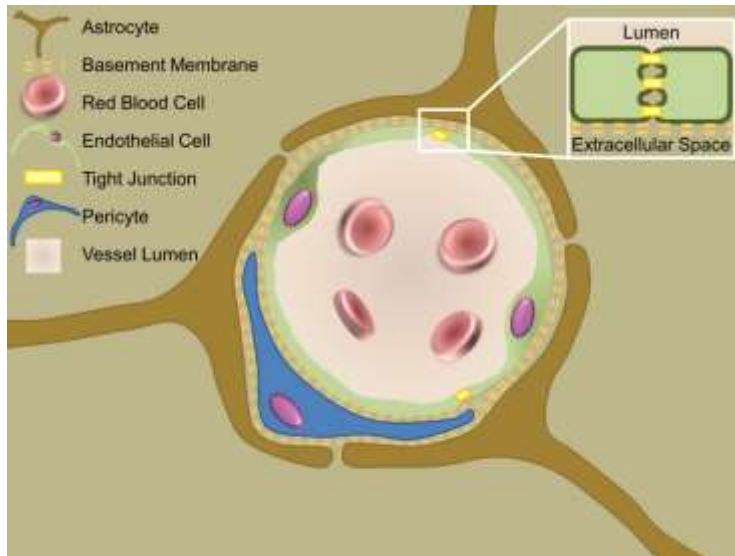


Figure 2.1. Blood-Brain Barrier Biology. The blood-brain barrier presents a major obstacle to therapeutic delivery in the central nervous system. It is comprised of unusually abundant and structurally unique tight junctions between the vascular endothelial cells and a thick basement membrane. Regulation via astrocytes and pericytes maintain this barrier, preventing the passage of the vast majority of therapeutics.

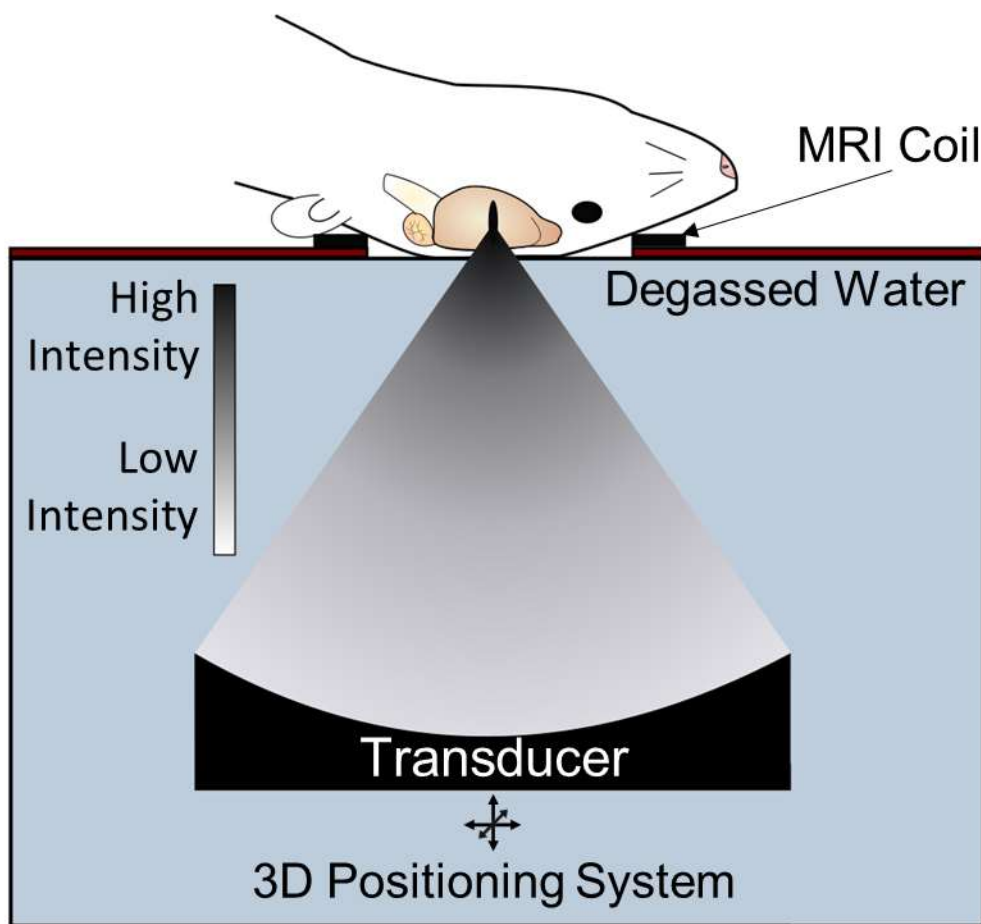


Figure 2.2. Transcranial FUS with microbubbles is the only modality capable of achieving non-invasive, safe, repeated and targeted BBB disruption, leading to improved drug or gene delivery to the brain. Pre-clinical FUS studies in animals including mice and rats permit use of a single-element FUS transducer, due to favorable skull geometry. FUS can be guided with MR imaging and is capable of sub-millimeter resolution allowing precise targeting of structures in the CNS with minimal off-target effects.

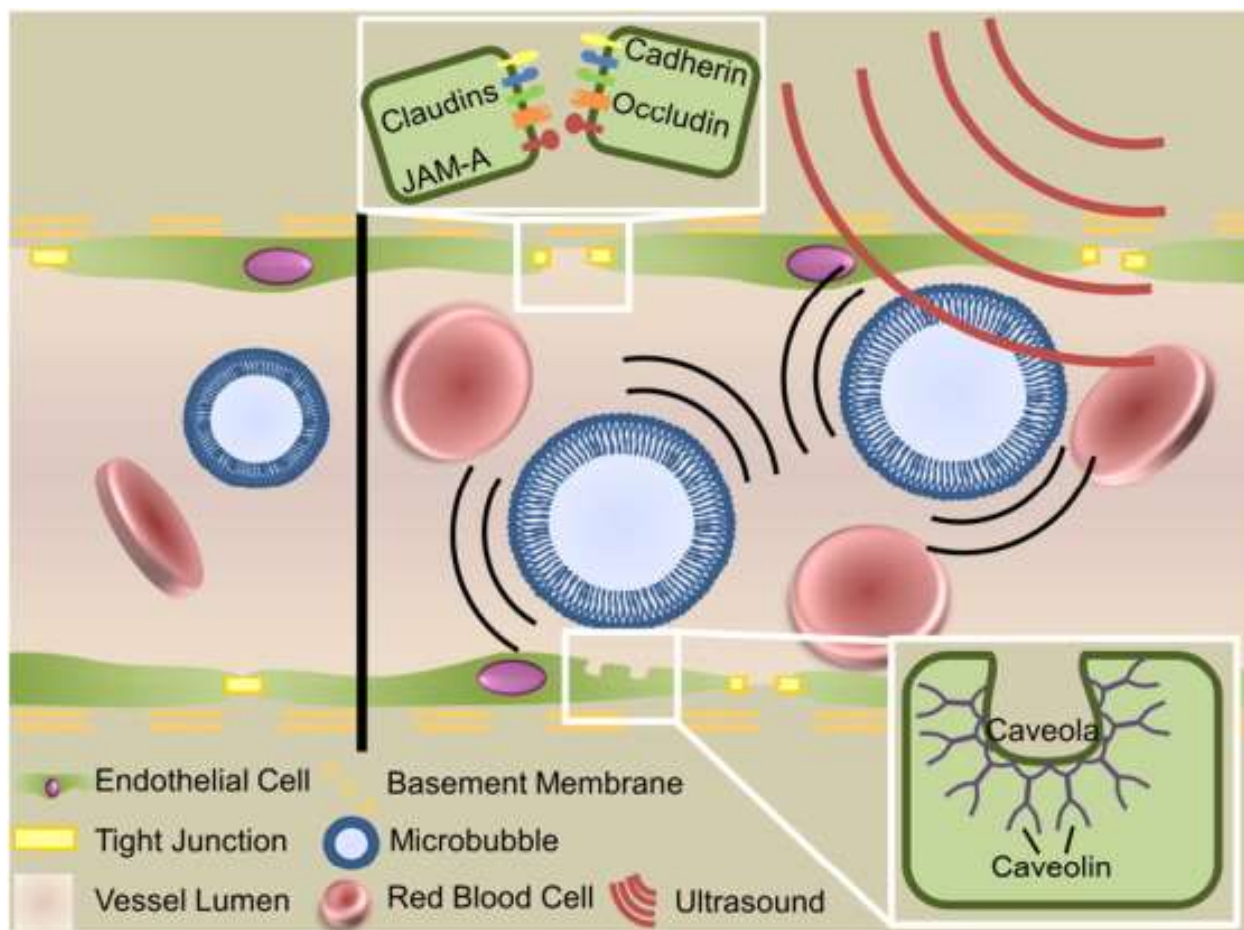


Figure 2.3. Mechanism of focused ultrasound mediated blood-brain barrier disruption. Circulating microbubbles oscillate in the ultrasonic field, producing forces that act on the vessel wall to generate three bioeffects that permit transport across the blood-brain barrier: disruption of tight junctions, sonoporation of the vascular endothelial cells and upregulation of transcytosis.

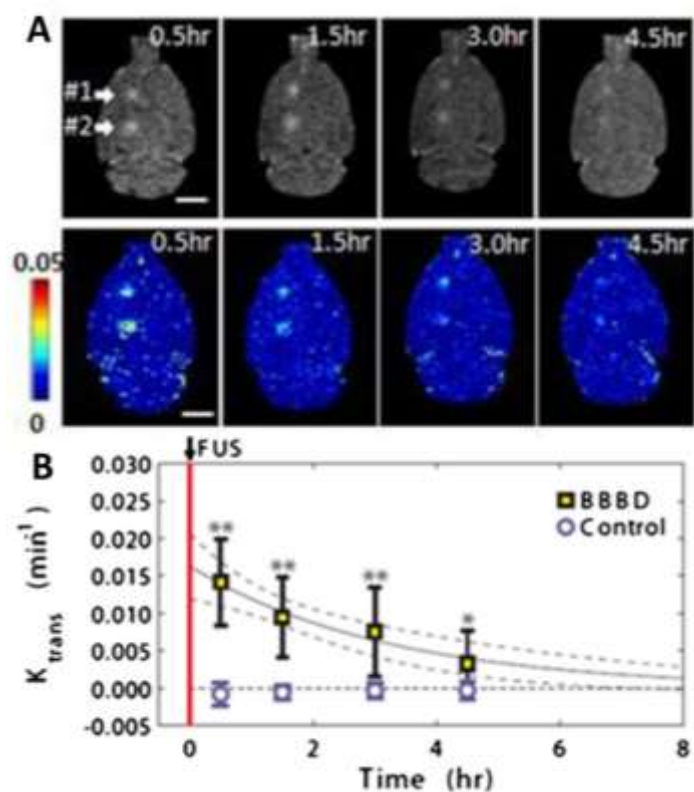


Figure 2.4. Transcranial FUS leads to temporary and localized BBBD with no long term damage. A. Representative transverse contrast enhanced T1 MRI (top) and permeability maps (bottom) obtained at four time points after FUS-mediated BBBD. Arrows indicate the two FUS-treated regions. K_{trans} values indicated by the color bar. B. Mean K_{trans} values over time in FUS treated regions. Control indicates contralateral hemisphere at same anatomical location. Reprinted from *Journal of Controlled Release*, 162, J. Park, Y. Zhang, N. Vykhodtseva, F. a Jolesz, N.J. McDannold, The kinetics of blood brain barrier permeability and targeted doxorubicin delivery into brain induced by focused ultrasound, 134-42, (2012) with permission from Elsevier.

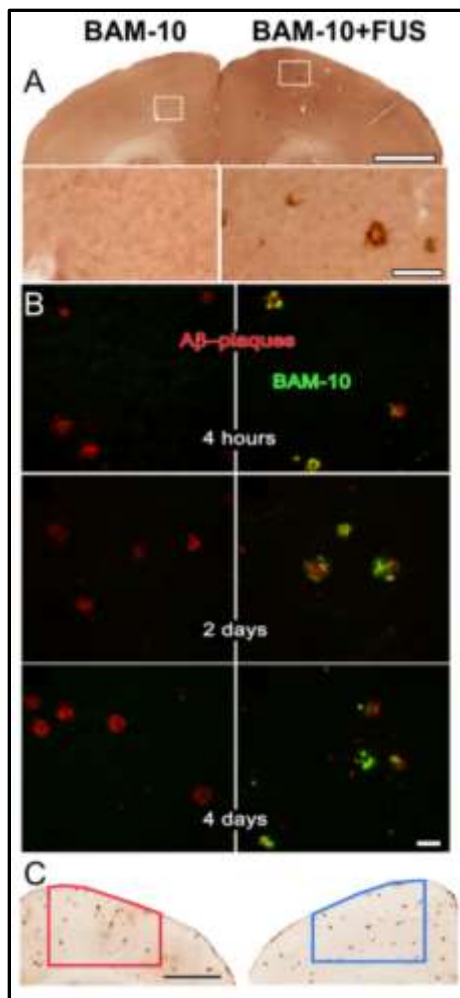


Figure 2.5. FUS mediated delivery of anti-AB antibody reduces plaque load in the TgCRND8 mouse model of Alzheimer's disease. A) Treatment with FUS increases delivery of anti-AB antibody BAM-10 in the targeted region (right) compared to the non-sonicated control (left). White boxes indicate area selected for inset. Scale bar 1mm, inset 100 μ m. B) BAM-10 delivered with FUS (right column) colocalizes with plaque within 4 hrs post-delivery and remains up to 4 days. Unsonicated control regions (left column) show no BAM-10 delivery. Scale bars 50 μ m. C) FUS-MB enhanced delivery of BAM-10 reduces plaque load 4 days post treatment. Scale bar 1mm. Reprinted from PLoS One, 5(5), Jordão JF, Ayala-Grosso CA, Markham K, Huang Y, Chopra R, McLaurin J, Hynynen K, Aubert I, Antibodies targeted to the brain with image-guided focused ultrasound reduces amyloid-beta plaque load in the TgCRND8 mouse model of Alzheimer's disease, e10549, (2010) with permission.

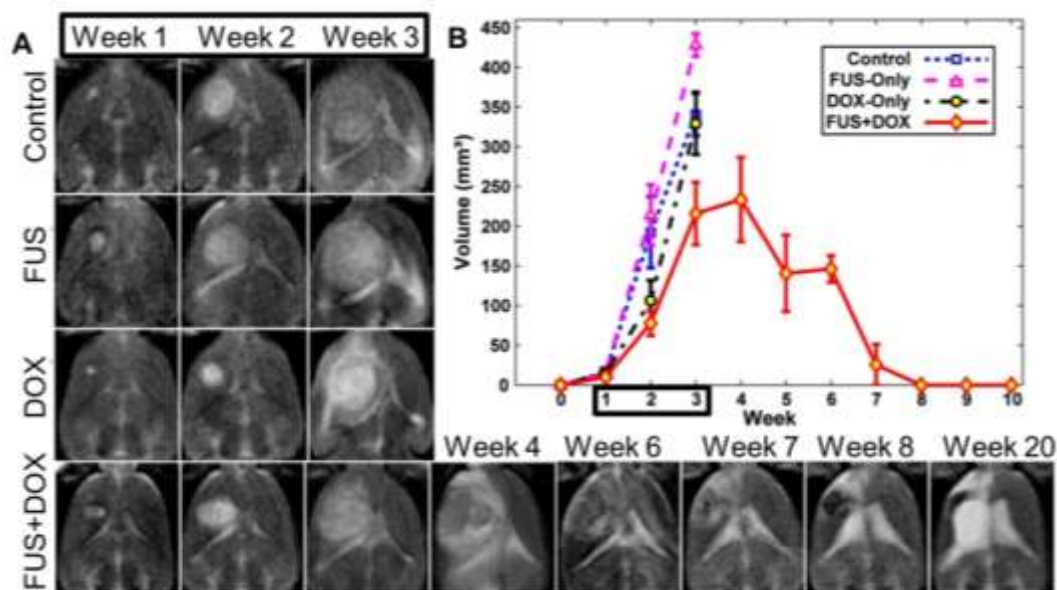


Figure 2.6. Three weekly FUS BBBB treatments (weeks 1-3) mediated delivery of liposomal doxorubicin and prolonged survival in a rat glioma model. A) T2 weighted images of control, FUS-only and DOX-only groups showing rapid tumor growth during weeks 1-3. T2 weighted images of a long-term survivor in the FUS+DOX group shows rapid tumor growth in weeks 1-4 followed by tumor resolution. Hyperintensity at week 20 is due to an enlarged ventricle. Black box indicates treatment period. B) Tumor growth as measured by MRI for each experimental group. Note that no control animals survived past week 3. Black box indicates treatment period. Reprinted from J Control Release, 169, Aryal M, Vykhodtseva N, Zhang YZ, Park J, McDannold N. Multiple treatments with liposomal doxorubicin and ultrasound-induced disruption of blood-tumor and blood-brain barriers improve outcomes in a rat glioma model, 103-11, (2015) with permission from Elsevier.

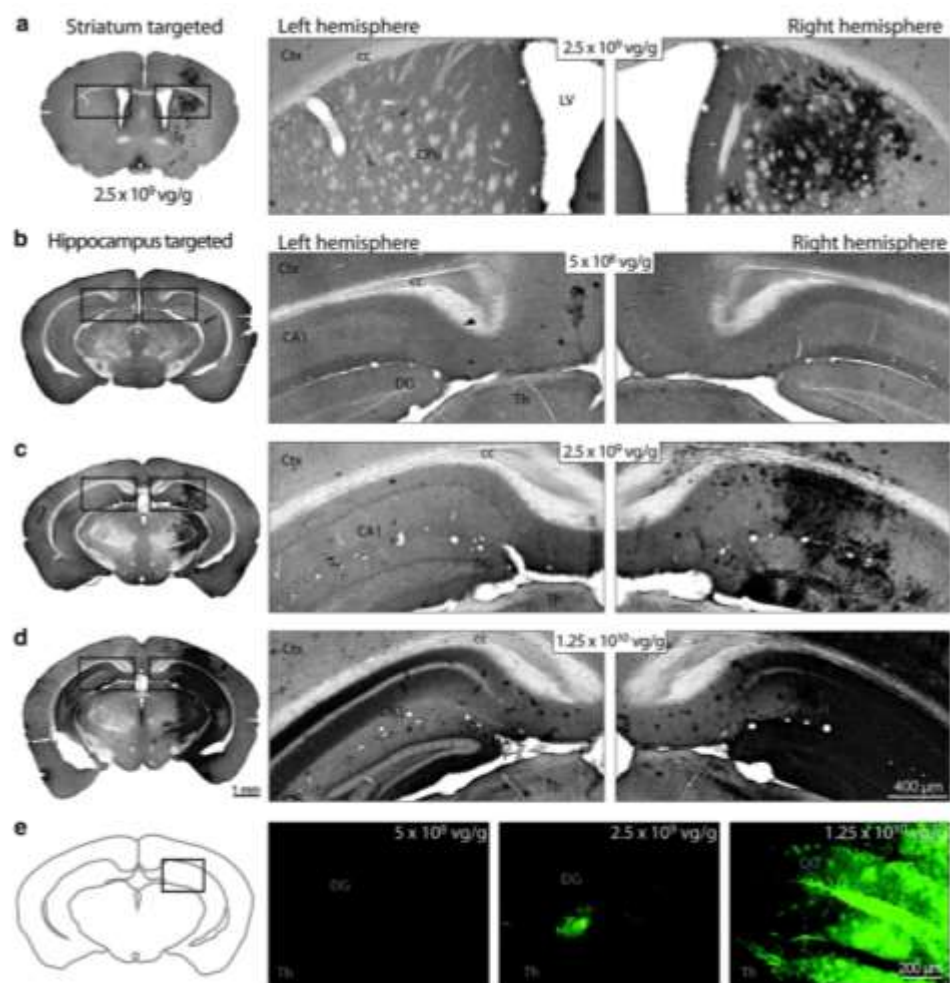


Figure 2.7. FUS mediated delivery of scAAV9 leads to a dose-dependent transgene expression in mouse brain. Mice were treated with MRI guided FUS in the right striatum (a) or hippocampus (b-e) immediately prior to intravenous injection of scAAV9 bearing a gene for GFP under the ubiquitously active chicken β -actin promoter at doses of 5×10^8 (a,c,e left), 2.5×10^9 (b,e middle) or 1.25×10^{10} (d,e right) vg/g . Twelve days after treatment, GFP expression was assessed in coronal brain sections with immunohistochemistry (a-d) or fluorescence microscopy (e). GFP expression was higher on the FUS-treated region (a,c,d,e, right) than the corresponding anatomical location on the contralateral hemisphere (a,c,d,e, left) at the two higher doses, but not the lowest dose. The publisher for this copyrighted material is Mary Ann Liebert, Inc. publishers.

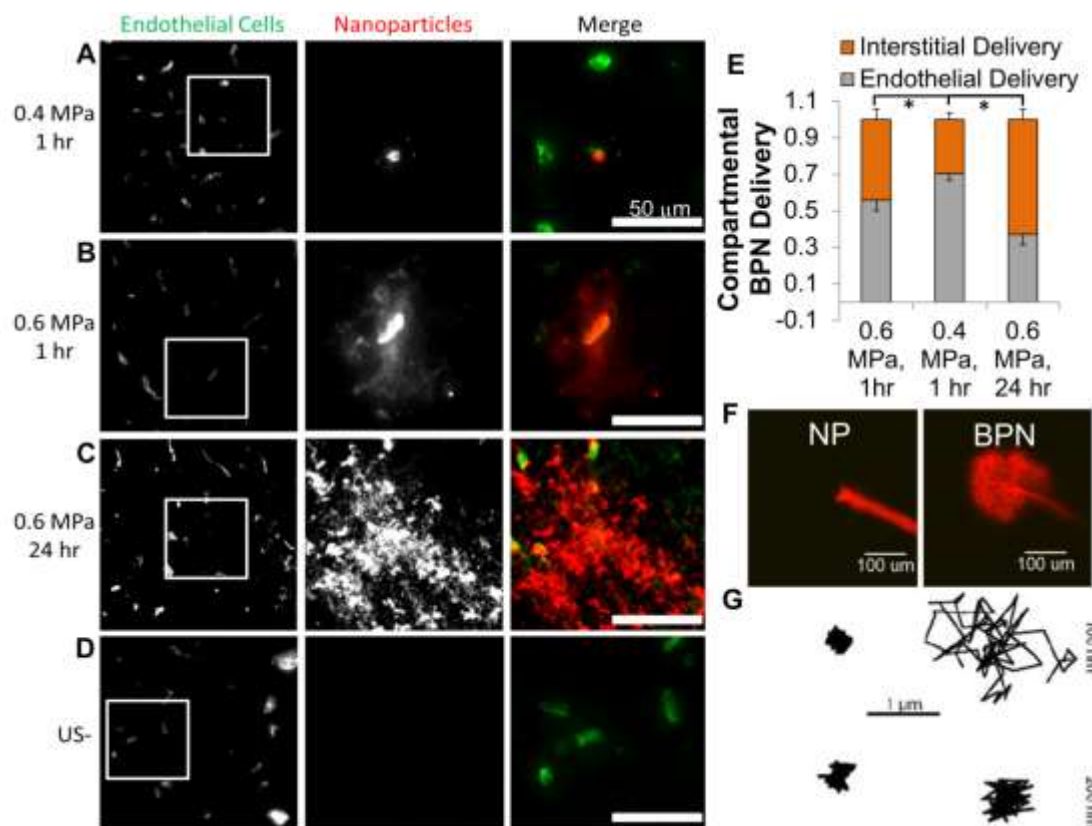


Figure 2.8. FUS delivers large 60-nm brain-penetrating nanoparticles across the BBB. At one hour post sonication, low pressure sonication primarily delivers nanoparticles to the endothelium (A) while higher pressure delivers particles to the interstitium (B). After 24 hours, brain-penetrating particles have diffused away from the vessel, significantly increasing nanoparticle coverage in the interstitial space compared to both low and high pressure 1 hr timepoints (C, G). Control regions show no nanoparticle delivery (D). 60 nm brain-penetrating nanoparticles (BPN) diffuse in *ex vivo* brain tissue after injection, while uncoated particles (NP) are immobilized (E). 100 nm BPNs also exhibit diffusive behavior in brain tissue, as demonstrated by traces taken by particle tracking software, while 200 nm BPNs and both 100 and 200 nm uncoated NPs are immobilized (F). * indicates $p < 0.05$. A,B,D,G,E reprinted from J Control Release, 189, Nance E, Timbie K, Miller GW, Song J, Louttit C, Klivanov AL, Shih TY, Swaminathan G, Tamargo RJ, Woodworth GF, Hanes J, Price RJ, Non-invasive delivery of stealth, brain-penetrating nanoparticles across the blood-brain barrier using MRI-guided focused, 123-32, (2014) with permission from Elsevier. F reprinted from ACS Nano, 8(10), Nance E, Zhang C, Shih TY, Xu Q, Schuster BS, Hanes J, Brain-penetrating nanoparticles improve paclitaxel efficacy in malignant glioma following local administration, 10655-64, (2013) with permission from AAAS.

2.10 Chapter 2 Tables

Table 1. Key references demonstrating drug or gene delivery with focused ultrasound.					
Disease Application	Author, Year	Animal Model	Substance Delivered	Vehicle	Ref.
Generalized	Kinoshita 2006	Swiss-Webster mice	Dopamine D4 receptor-targeting antibody	Unencapsulated	(109)
Generalized	Burgess 2012	Wistar Rats	siRNA oligonucleotide	Unencapsulated	(223)
Generalized	Huang 2012	Kunming Mice	BDNF-eGFP Plasmid	Cationic MBs	(157)
Generalized	Huang 2012	Kunming Mice	CMV-EGFP Plasmid	Cationic MBs	(156)
Generalized	Thevenot 2012	C56BL/6 Mice	CB-GFP Gene	scAAV9	(155)
Generalized	Alonso 2013	Wistar Rats	CMV-nlsLacZ Gene	AAV2/1	(164)
Generalized	Hsu 2013	Mice	CMV-GFP Gene	AAV2	(165)
Generalized	Nance 2014	Sprague-Dawley Rats	Polystyrene Tracer	PEGylated NPs	(224)
Generalized	Wang 2014	Mice	Synapsin-eGFP Gene	AAV1 and AAV2	(163)
Generalized	Weber-Adrian 2015	Wistar Rats	CB-GFP Gene	scAAV9	(162)
Alzheimer's	Raymond 2008	APPswe:PSEN1 dE9 and PDAPP Mice	Anti-A β antibody	Unencapsulated	(111)
Alzheimer's	Jordão 2010	TgCRND8 Mice	Anti-A β antibody	Unencapsulated	(79)
Alzheimer's	Jordão 2013	TgCRND8 Mice	Endogenous IgG	Unencapsulated	(110)
Alzheimer's	Leinenga 2015	APP23 Mice	NA	Unencapsulated	(225)
Brain Metastasis	Kinoshita 2006	Swiss-Webster Mice	Herceptin	Unencapsulated	(112)
GBM	Ting 2012	C6 glioma in Sprague-Dawley Rats	BCNU	MBs	(133)
GBM	Treat 2012	9L gliosarcoma in Sprague-Dawley Rats	Doxorubicin	PEGylated liposomes	(127)
GBM	Yang 2012	GBM8401 in NOD- <i>scid</i> Mice	Doxorubicin	PEGylated liposomes, AP-1 targeted, ¹¹¹ In-labeled	(128)

GBM	Yang 2012	GBM8401 in NOD- <i>scid</i> Mice	Doxorubicin	PEGylated liposomes, AP-1 targeted	(84)
GBM	Alkins 2013	9L glioma in Fischer 344 Rats	BPA-f	Unencapsulated	(85)
GBM	Aryal 2013	9L gliosarcoma in Sprague-Dawley Rats	Doxorubicin	PEGylated liposomes	(82)
GBM	Fan 2013	C6 glioma in Sprague-Dawley Rats	Doxorubicin	SPIO-conjugated MBs	(134)
GBM	Fan 2013	C6 glioma in Sprague-Dawley Rats	BCNU	VEGF-targeted MBs	(83)
GBM	Kovacs 2014	GL261 or SMA-560 glioma in Mice	Doxorubicin	Unencapsulated	(99)
GBM	Yang 2014	F98 glioma in Fischer 344 Rats	BPA-f	Unencapsulated	(105)
GBM	Aryal 2015	9L gliosarcoma in Sprague-Dawley Rats	Doxorubicin	PEGylated liposomes	(81)
GBM	Aryal 2015	9L gliosarcoma in Sprague-Dawley Rats	Doxorubicin	PEGylated liposomes	(129)
GBM	Chen 2015	C6 glioma in Sprague-Dawley Rats	IL-12	Unencapsulated	(121)

Chapter 3: Targeted Gene Transfer to the Brain via the Delivery of Brain-Penetrating DNA Nanoparticles with Focused Ultrasound

Brian P. Mead, Panagiotis Mastorakos, Jung Soo Suk, Alexander L. Klibanov, Justin Hanes, Richard J. Price. *Journal of Controlled Release*, 223: 109-117, 2016

Abbreviations

FUS, Focused ultrasound; DNA-BPN, gene-bearing brain penetrating nanoparticles; NP, nanoparticle; PEG, polyethylene glycol; MB(s), microbubble(s); BBB, blood brain barrier; CNS, central nervous system; GFAP, glial cell fibrillary acidic protein; NeuN, Neuronal nuclear antigen, AAV, adeno-associated virus; MR, magnetic resonance

3.1 Abstract

Gene therapy holds promise for the treatment of many pathologies of the central nervous system (CNS), including brain tumors and neurodegenerative diseases. However, the delivery of systemically administered gene carriers to the CNS is hindered by both the blood-brain barrier (BBB) and the nanoporous and electrostatically charged brain extracellular matrix (ECM), which acts as a steric and adhesive barrier. We have previously shown that these physiological barriers may be overcome by, respectively, opening the BBB with MR image-guided focused ultrasound (FUS) and microbubbles (MBs) and using highly compact “brain penetrating” nanoparticles (BPN) coated with a dense polyethylene glycol corona that prevents adhesion to ECM components. Here, we tested whether this combined approach could be utilized to deliver systemically administered DNA-bearing BPN (DNA-BPN) across the BBB and mediate localized, robust, and sustained transgene expression in the rat brain. Systemically administered DNA-BPN delivered through the BBB with FUS led to dose-dependent transgene expression only in the FUS-treated region that was evident as early as 24 h post administration and lasted for at least 28 days. In the FUS-treated region ~42% of all cells, including neurons and astrocytes, were transfected, while less than 6% were transfected in the contralateral non-FUS treated hemisphere. Importantly, this was achieved without any sign of toxicity or astrocyte activation. We conclude that the image-guided delivery of DNA-BPN with FUS and MBs constitutes a safe and non-invasive strategy for targeted gene therapy to the brain.

KEYWORDS: Focused Ultrasound, Non-Viral Gene Delivery, CNS Diseases, Blood Brain Barrier

3.2 Introduction

Gene therapy approaches have shown promise for the treatment of Parkinson's disease,(2, 4, 24, 135–137) Alzheimer's disease,(138, 139) lysosomal storage diseases(140, 141) and brain tumors.(226) Viral gene vectors have been used in clinical trials for neurological disorders and shown to be therapeutically effective.(227) However, viral vectors, such as adenovirus, adeno-associated viruses and herpes simplex viruses have significant limitations, including safety concerns, limited packaging capacity, technical difficulties in scale up and high production costs.(228) Moreover, prior exposures and/or repeated administrations of these vectors lead to neutralizing immune responses that ultimately reduce the efficiency of transgene delivery.(170, 171) DNA-bearing nanoparticles (DNA-NP) have emerged as a versatile and easily adaptable platform for gene therapy devoid of the aforementioned limitations.

Regardless of the type of gene vectors used, the blood brain barrier (BBB) prohibits delivery of systemically administered vectors to the central nervous system (CNS), resulting in minimal transgene expression.(5) Even specific viral vectors or DNA-NP with BBB-targeting ligands achieve only minimal accumulation in the brain when administered at very high doses, which are associated with potential adverse effects in peripheral organs.(18) For this reason, the majority of preclinical and clinical studies have focused on direct intracranial administration of gene vectors. However, the invasive nature of this approach and the risks associated with surgery limit the applicability of this strategy and its potential use for repeated administrations. Various methods for circumventing the BBB, such as intra-arterial infusion of osmotic agents, have been proposed, but they are invasive and non-targeted,(229, 230) leading to transgene expression in an uncontrolled fashion.

Currently, focused ultrasound (FUS) is the only modality allowing repeated, non-invasive, and temporary BBB permeabilization, leading to localized drug and gene delivery to the brain.(6, 39) Circulating ultrasound contrast agent microbubbles (MBs), when exposed to low intensity

FUS, oscillate in volume with acoustic rarefaction and compression.(231) Ultimately, interactions between these activated MBs with the vascular wall lead to disruption of tight junctional complexes(108) and induction of active transport processes across the BBB.(232) Importantly, high capillary density in the brain permits many points of entry after FUS application, potentiating improved distribution compared to local injection. BBB opening is temporary, typically resolving within 4-6 h,(39, 233) and has shown safety in several experimental animal models, including rhesus macaques.(63) Furthermore, both preclinical and clinical studies have demonstrated the potential of FUS to deliver systemically administered payloads including imaging agents,(65, 234) ~100 nm liposomes,(78, 127) ~150 kDa antibodies,(110, 112) recombinant proteins,(118) ~20 nm viruses(155, 164) and ~10 μ m neural stem cells(235) into the brain. Toward this end, the size of BBB opening is dependent on FUS acoustic pressures(57), suggesting the FUS parameters can be tuned to accommodate delivery of therapeutics of different sizes. FUS can be aimed with guidance from magnetic resonance imaging systems, allowing for accurate targeting of predefined brain structures; devices capable of targeting ultrasound through the human skull with sub-millimeter precision are currently in clinical trials.(36, 37)

Once beyond the BBB, the brain parenchyma provides an additional barrier to the diffusion of nanoparticles (NP). This brain-tissue barrier (BTB) consists of a nanoporous microstructure of negatively charged ECM macromolecules that hampers the distribution of NP(8, 190) and viruses(21) via adhesive interactions and/or steric obstruction. It has recently been shown that sub-115 nm NP densely coated with neutrally charged and bio-inert polyethylene glycol (PEG) are able to overcome the BTB and rapidly diffuse within the brain tissue.(8) We have demonstrated that BBB opening with MR-guided FUS and MBs can facilitate the delivery of colloidally stable, densely PEGylated 60 nm fluorescent tracer brain-penetrating NP (BPN) across the BBB.(6) Once delivered across the BBB, BPN exhibited wide dispersion

into the tissue away from the vessels of entry, allowing for homogeneous distribution in the FUS-treated tissue.

In this study, we used colloiddally stable DNA-NP with a dense PEG coating (DNA-BPN) previously shown to achieve remarkable penetration through the BTB and high levels of transfection following direct intracranial administration.⁽¹⁸⁶⁾ By combining FUS-mediated BBB opening with systemically administered DNA-BPN, we formulated a non-invasive strategy to achieve safe, highly localized, robust, and sustained transgene expression in the CNS.

3.3 Results and Discussion:

We formulated highly PEGylated DNA-BPN based on a gold-standard cationic polymer, polyethylenimine (PEI), as previously described.^(148, 174, 186) This technique allowed the formulation of highly compact and colloiddally stable 56 ± 2 nm DNA-BPN with a PEG to PEI w/w ratio of 50 that is substantially higher than PEGylation ratios used traditionally^(236–238). Effective shielding of the NP positive surface charge was confirmed by the near-neutral ζ -potential ($+1.5 \pm 0.3$ mV; Table 1). We further measured the stability of DNA-BPN in pooled human plasma (PHP; Innovative Research, Novi, MI); DNA-BPN retained their colloidal stability following incubation in PHP at 37°C, as evidenced by the well-preserved hydrodynamic diameters (65 ± 7 nm), near-neutral surface charge (-1.8 ± 0.8 mV) and polydispersity index (PDI) of 0.25 (Table 1). Despite a minimal increase in size, DNA-BPN did not aggregate, retained their sub-100 nm diameter and DNA compaction over at least 30 min of incubation in PHP at 37°C, as demonstrated by the hydrodynamic diameter histograms and transmission electron micrographs (Figure 1a, b).

To measure the *in vivo* transfection efficiency of DNA-BPN, we formulated DNA-BPN with a plasmid containing a luciferase reporter gene driven by a long-acting β -actin promoter (pBAL). These DNA-BPN were intravenously co-injected at 3 different concentrations (50 μ g, 100 μ g and 200 μ g) with MBs in Sprague-Dawley rats and FUS was applied to the striatum of the left hemisphere. Gene expression was measured using an *In Vivo* Imaging System (IVIS100; Xenogen, Alameda, CA). FUS-mediated BBB permeabilization led to targeted DNA-BPN delivery to the brain and robust bioluminescence at the ultrasound focus (i.e. anatomical location where FUS was applied) (Figure 2a). Off-target (i.e. outside the ultrasound focus) bioluminescence was not observed. *Ex vivo* bioluminescent imaging was performed on freshly excised brains at day 28 after DNA-BPN administration in order to confirm that the *in vivo* transfection measurements were not due to signal from extra-axial tissues such as the skin

and/or the skull (Figure 2b). *Ex vivo* images offer higher resolution and thus confirmed luciferase transgene expression through the entire ultrasound focus without off-target transgene expression. Repeated IVIS imaging demonstrated persistent dose-dependent reporter transgene expression for at least 28 days. Of note, even the lowest DNA-BPN dose led to bioluminescence signal significantly above the background (Figure 2c, d). Importantly, gene expression was observed as early as 24 hours after FUS-mediated delivery of DNA-BPN. Compared to commonly used viral vectors, this constitutes a very short lag time.⁽²³⁹⁾ Some viral vectors (e.g. AAV2) require up to 5 weeks to achieve maximal expression,⁽²⁴⁰⁾ indicating that their expression kinetics are less favorable than that of DNA-BPN. Importantly, expression persistence represents a marked improvement over previously published results using non-viral gene vectors. For example, in a study wherein MB bound pDNA was delivered across the BBB with FUS, expression dropped to ~10% of maximum after just 14 days.⁽¹⁵⁶⁾

We next determined the transfection efficiency and neuron-astrocyte tropism following FUS-mediated delivery of DNA-BPN. We used DNA-BPN containing an mCherry plasmid driven by the β -actin promoter (pBACH). The hydrodynamic diameter (56 ± 2 nm) and ζ -potential (1.5 ± 0.3 mV) of these pBACH-carrying DNA-BPN were consistent with those of DNA-BPN complexed with pBAL. One week after FUS mediated delivery of pBACH bearing DNA-BPN, whole-brain *ex vivo* epifluorescence imaging confirmed mCherry transgene expression in the FUS-targeted region (Figure 3a). Microscopic examination of the FUS-targeted regions of nuclear counterstained (Draq5) brain cross-sections (Figure 3b) yielded visually detectable levels of mCherry expression, even at the lowest DNA-BPN dose. DNA-BPN achieved efficient transfection throughout the ultrasound focus region, in good agreement with a previous study suggesting the ability of densely PEGylated DNA-BPN to distribute homogeneously throughout brain parenchyma.⁽¹⁸⁶⁾ At the 200 μ g DNA-BPN dose, 42.3% of cells in the ultrasound focus expressed the transgene compared to only 5.8% in the non-FUS treated contralateral

hemisphere (Figure 3c). The population of cells transfected by the 200 μg dose was significantly greater than the transfection efficiency of 30.2% or 28.0% found at the 100 μg or 50 μg doses, respectively. Consistent with our results generated using pBAL, mCherry gene expression appeared to be dose dependent (Figure 3c). Furthermore, we confirmed that transgene expression is directly dependent on FUS treatment because, even at a very high DNA-BPN dose, transgene expression beyond the intact BBB of the contralateral hemisphere was minimal. The highly efficient transfection of a large cell population within the FUS focus is most likely attributed to the contribution of FUS to improving DNA-BPN penetration through the BBB,⁽¹⁴⁸⁾ as well as the widespread distribution of DNA-BPN within the brain tissue. This is in good agreement with previous findings in which ultrasound enhanced delivery and transfection efficiency in FUS-treated tissue following systemic administration of NP.^(159, 160) In fact, ultrasound mediated delivery of pBAL bearing NP, similar to the formulation used in the current study, led to strong and localized expression in hard-to-transfect skeletal muscle *in vivo*,⁽¹⁴⁸⁾ even greater than the level achieved by direct injection.

To then determine which cell types are transfected with this approach, additional cross-sections were immunolabeled for NeuN (neuronal marker), GFAP (astrocyte marker), and mCherry (Figure 4). DNA-BPN vectors entered both astrocytes and neurons in FUS-targeted tissue (Figure 4a). Out of the transfected neuron-astrocyte cell population, approximately 42% of transfected cells were neurons and the remaining 58% of transfected cells were astrocytes. Numerous studies have shown the importance of restricting transgene expression to particular cell types. To this end, cell-specific transgene expression can be achieved by the use of specific promoters. In the brain, transgene expression can be limited to astrocytes with a GFAP promoter⁽³⁾ or neurons with a synapsin⁽¹⁶³⁾ or MeCP2⁽²⁴¹⁾ promoter. Several recent studies have demonstrated the importance of astrocytes in neurodegenerative disease,^(242, 243) and

astrocyte-specific overexpression of neurotrophic factors leads to similar therapeutic efficacy as neuron-derived expression.(3)

FUS has previously demonstrated the ability to improve efficiency of several different gene vectors in the brain after systemic administration. For example, while self-complementary adeno-associated virus 9 (scAAV9) broadly transfects cells beyond the BBB even without additional targeting mechanisms, doses as high as $\sim 1 \times 10^{11}$ vg/g have been found to transduce only 19% of motor neurons in adult mice.(161) Delivery of scAAV9 into the brain(155) or spinal-cord(162) with FUS achieved almost 80% total transduction efficiency in the brain and 87% of neurons in the spinal cord at 2.5×10^9 or 2×10^9 vg/g, respectively. While scAAV9 currently yields higher transfection than DNA-BPN in the brain after delivery with FUS, scAAV9 has a packaging capacity of just 2.4 kb(172), which limits the versatility of this vector. To this end, tailorability, high packaging capacity and ease of manufacture make non-viral gene vector systems enticing, and further optimization of DNA-BPN formulation may enhance efficiency in the CNS.

Finally, we histologically examined brain tissues for signs of toxicity and/or gliosis. Hematoxylin and eosin (H&E) stained brain tissues that had been transfected via the delivery of DNA-BPN with FUS-mediated BBB opening were used to assess local toxicity (Figure 5a); comparisons were made to contralateral control hemispheres (i.e. FUS⁻, DNA-BPN⁺) and animals receiving no treatment. Importantly, no cellular damage was observed at any dose in either the FUS-treated or contralateral control hemispheres. Hemosiderin staining was found in the FUS treated region in only 2 of the n=18 brains tested. When examined as fraction of tissue area coverage, less than 0.1% of the observed H&E stained tissue area was hemosiderin positive, thereby indicating that erythrocyte leakage across the BBB after FUS treatment was an exceptionally rare occurrence. GFAP immunolabeling was used to assess potential astrocyte activation (i.e. gliosis) (Figure 5a). Comparisons of average grayscale intensity in GFAP stained

images across several depths in the brain revealed that GFAP staining intensity was unchanged when compared to both the contralateral region (i.e. FUS-, DNA-BPN+) and untreated controls (FUS-,DNA-BPN-). This indicates that no long-term astrocyte activation occurred in response to DNA-BPN delivery via FUS-mediated permeabilization of the BBB (Figure 5b). We also note that no long-term changes in animal behavior were observed following FUS-mediated delivery of DNA-BPN.

While the long term safety of BBB opening with FUS and MBs has been confirmed in animals through both tissue histology and animal behavior tests, it is also well known that driving MBs beyond a mode of stable cavitation and into an inertial cavitation mode can lead to blood pooling in tissue.(59, 244) Nonetheless, inertial cavitation is avoidable and it has been argued that minor erythrocyte extravasation would have minimal impact(41, 65) and such minor effects would be acceptable in treatments of diseases like tumors or neurodegenerative disease. With regard to PEI, its high positive charge density has raised concerns about toxicity.(238) In particular, non-PEGylated PEI NP have been shown to lead to cell death *in vitro* and *in vivo* after intracranial administration(186, 245). However, when the surface of PEI-based NP are densely coated with PEG, such as with the DNA-BPN used in the current study, toxicity is negligible.(186) Our safety results are consistent with those reported for convection enhanced delivery of PEI-based DNA-BPN, wherein no vector-induced toxicity was observed at high doses in rats.(186)

In conclusion, we provide here the first demonstration of targeted, robust, and sustained CNS transfection achieved by delivering systemically administered DNA-BPN across the BBB with FUS and MBs. This platform approach for gene delivery to the CNS has potential as a targeted and non-invasive modality for treatment of a variety of neurological diseases, including brain tumors and neurodegenerative diseases.

3.4 Materials and Methods:

3.4.1 Animals

Female Sprague-Dawley rats were purchased from Harlan and maintained on a 12/12h light/dark cycle. Rats used in the experiments weighed between 180-220 g and were given food and water *ad libitum*. All animal experiments were approved by the Animal Care and Use Committee at the University of Virginia and conformed to the National Institutes of Health regulations for the use of animals in research.

3.4.2 DNA-BPN Fabrication and Characterization

To synthesize a PEG_{5k}-PEI copolymer, methoxy-PEG-N-hydroxysuccinimide (mPEG-NHS; 5 kDa; Sigma-Aldrich, St. Louis, MO) was conjugated to 25 kDa branched PEI (Sigma-Aldrich), as previously described (PEG_{5k}-PEI)(148, 174, 186). Nuclear magnetic resonance (NMR) was used to confirm a PEG: PEI ratio of 50; a ratio previously shown to provide sufficient shielding of the DNA-NP positive surface charge(186). ¹H NMR (500 MHz, D₂O): δ 2.48 – 3.20 (br, CH₂CH₂NH), 3.62 – 3.72 (br, CH₂CH₂O). The pBAL and pBACH plasmids were produced by Copernicus Therapeutics Inc. (Cleveland, OH). DNA-NP were formulated by the drop-wise addition of 10 volumes of plasmid DNA (0.2 mg/ml) to 1 volume of polymer solution. PEI solutions were prepared at a previously optimized nitrogen to phosphate (N/P) ratio of 6 and at PEG_{5k}-PEI to PEI molar ratio of 3. Gene vectors were washed with 3 volumes of ultrapure water, and concentrated to 1 mg/ml using Amicon® Ultra Centrifugal Filters (100,000 MWCO; Millipore Corp., Billerica, MA) so as to remove free polymers. DNA concentration was determined using a NanoDrop ND-1000 spectrophotometer (NanoDrop Technologies, Wilmington, DE).

To characterize DNA-NP in water as well as PHP we used a Nanosizer ZS90 (Malvern Instruments, Southborough, MA). Hydrodynamic diameter and PDI were measured in 10 mM

NaCl at pH 7.0 by dynamic light scattering (DLS); ζ -potential was similarly measured by laser Doppler anemometry. In order to determine the DNA-NP morphology, transmission electron microscopy (TEM) was used (Hitachi H7600; Hitachi High Technologies America, Schaumburg, IL). PEI gene vector stability was assessed following incubation of DNA-NP in PHP, filtered through Amicon® Ultra Centrifugal Filters (100,000 MWCO), at 37°C. We conducted DLS before and immediately after treatment with PHP as well as at 5 min, 10 min, 20 min and 30 min of incubation. TEM was also conducted immediately after treatment with PHP and at 10 min, 20 min and 30 min of incubation.

3.4.3 FUS-Mediated DNA-BPN Delivery

Female Sprague-Dawley rats (180-220 g) were anesthetized with an intraperitoneal injection of ketamine (40 mg/kg; Fort Dodge, IA) and dexdomitor (0.2 mg/kg, Pfizer, New York, NY) in sterilized 0.9% saline. A tail vein catheter was inserted to allow intravenous injections of DNA-BPN and microbubbles. Animal heads were shaved and depilated before being secured prone in a stereotaxic frame (Stoelting, Wood Dale, IL). Rat heads were ultrasonically coupled to a FUS transducer and positioned such that the ultrasound focus was localized to the left striatum. Rats received a co-injection of DNA-BPN (50 μ g, 100 μ g or 200 μ g) and MBs (3×10^5 MBs/g body weight) followed by 0.3 ml of 2% heparinized saline to clear the catheter. Sonication began immediately after clearance of the catheter.

All sonications were performed using a 1 MHz single element FUS transducer (Olympus, Center Valley, NJ) operating at a 0.5% duty cycle for 2 min. Peak negative pressure was 0.6 MPa for all treatments. The waveform pulsing was amplified using a 55 dB RF power amplifier (ENI 3100LA; Electronic Navigation Industries, Richardson, TX).

3.4.4 Microbubble Preparation

MBs used in this study are similar to Optison (GE Healthcare, Little Chalfont, Buckinghamshire, UK). To produce MBs, a 1% solution of serum albumin in saline was sonicated (20 kHz, 30 s) with an ultrasound disintegrator (XL2020; Misonix, Farmingdale, NY) with an extended ½-inch titanium probe. The flask containing the solution had its headspace filled with octafluoropropane gas prior to sonication. MBs were sized and counted using a Coulter Counter (Multisizer 3, Beckman Coulter, Fullerton, CA).

3.4.5 *In Vivo Bioluminescence Imaging*

Animals were anesthetized and maintained on 2-2.5% isoflurane in oxygen. D-Luciferin (Gold Biotechnology, St. Louis, MO) was administered by intraperitoneal injection at 150 mg/kg. Animals were serially imaged using an IVIS100 imaging system (Xenogen, Alameda, CA, USA). Photons were collected and integrated for a period of 1 minute. Images were processed using Xenogen's Living Image software. Total flux intensities were measured from a region of interest over the FUS targeted region.

3.4.6 *Ex Vivo Bioluminescence Imaging*

Immediately following the final *in vivo* bioluminescence imaging session, rats treated with FUS and DNA-BPN bearing β -actin-luciferase plasmid rats were euthanized and decapitated. The brains were quickly dipped in 10 mg/ml D-luciferin and imaged using the IVIS100 imaging system. Photons emitted were collected over 2 min.

3.4.7 *Whole Brain Epifluorescence Imaging*

One week after delivery of pBACH-bearing DNA-BPN with FUS, rats were euthanized. Immediately following euthanasia, left and right carotid arteries were cannulated and perfused with 20 ml of 2% heparinized 0.9% saline followed by 10 ml of 4% paraformaldehyde. Brains

were immediately placed into 0.9% saline and imaged using an IVIS100 imaging system with the 605 nm excitation and 650 nm emission filters.

3.4.8 Histological Processing

Immediately following euthanasia, left and right carotid arteries were cannulated and perfused with 20 ml of 2% heparinized 0.9% saline followed by 10 ml of 4% paraformaldehyde. Brains were suffusion-fixed in 4% paraformaldehyde for 24 h at 4°C prior to desiccation in 30% sucrose for 24 h at 4°C. Desiccated brains were placed in OCT compound for 1 h prior to flash freezing and ultimate storage at -80°C. Brains were mounted with OCT and sectioned in a cryostat (Leica, Buffalo Grove, IL). Transverse 8 µm thick sections were mounted and stained.

3.4.9 Histology

Hematoxylin and Eosin (H&E) staining was performed on mounted sections according to standard protocols. Tissues were imaged on a bright field microscope (Zeiss, Jena, Germany) equipped with a color CCD Camera (Olympus, Center Valley, NJ)

3.4.10 Immunofluorescence

Mounted sections were washed 3x for 10 min in phosphate buffered saline (PBS) then incubated with blocking solution (Vector Labs, Burlingame, CA). Next, sections were incubated overnight at 4°C with mouse anti-mCherry (1:200; Abcam, Cambridge, MA). After washing 3x for 10 min in PBS, sections were incubated for 1 h at room temperature with Alexafluor-488 conjugated goat anti-mouse IgG (1:250; Invitrogen, Grand Island, NY) and Draq5 (1:1000; Thermo Scientific, Waltham, MA). After washing 3x for 10 min in PBS, slides were mounted using Prolong Gold (Invitrogen) and a coverslip. Sections were imaged on a Nikon Eclipse TE2000 confocal microscope (Nikon, Melville, NY) equipped with a 20x oil objective.

Transfection efficiency was assessed using ImageJ by manually counting Draq5+ cells and comparing this to Draq5+ mCherry+ cells. At least three representative fields of view were counted from at least three different section depths within the rat brain.

To assess cell tropism, mounted sections were washed 3x for 10 min in PBS and incubated with blocking solution (Vector Labs, Burlingame, CA). Sections were next incubated overnight with mouse anti-mCherry (1:200; Abcam). After washing 3x for 10 min in PBS, sections were incubated for 1 hr at room temp with Alexa Fluor 647 conjugated goat anti-mouse IgG (Invitrogen). After washing 3x for 10 min in PBS, sections were incubated with mouse anti-glia fibrillary acidic protein (GFAP) (1:500; Millipore Corp.) and mouse anti-neuronal nuclear antigen (NeuN) (1:500; Millipore Corp.). After washing 3x for 10 min in PBS, sections were mounted using Prolong Gold (Invitrogen). Sections were imaged on a Nikon Eclipse TE2000 confocal microscope equipped with a 20x oil objective. Cellular tropism was assessed using ImageJ by manually comparing localization of mCherry+ cells with NeuN+ cells and GFAP+ cells. At least three representative fields of view were counted from at least three different section depths within the rat brain.

3.5 Funding Sources

Supported by NIH CA164789, NIH EB016784, NIH R01 CA197111, NIH R01 EB020147, NHLBI
5 T32 HL007284 and the Focused Ultrasound Foundation.

3.6 Chapter 3 Figures

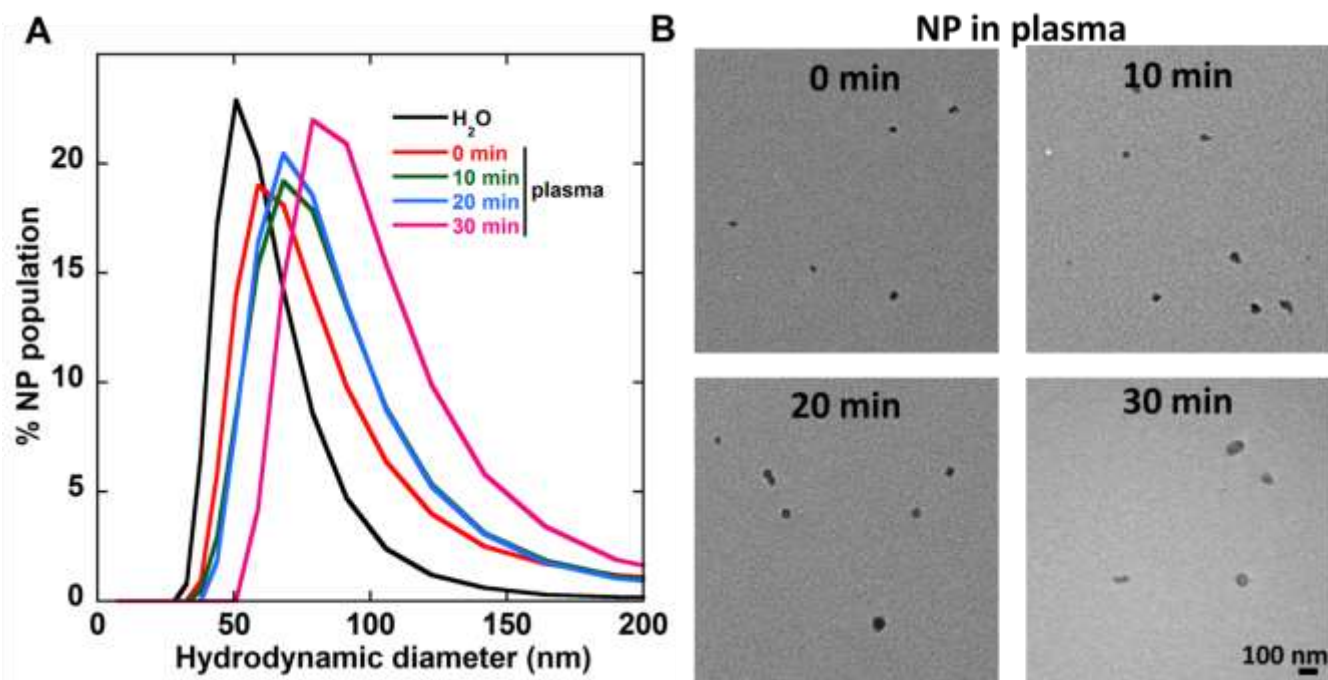


Figure 3.1. DNA-BPN stability in PHP (A) Gene vector hydrodynamic diameter (number mean) distribution following incubation in PHP at 37°C for 0, 10, 20 and 30 min. Size was measured by DLS in 10 mM NaCl at pH 7.0. (B) Transmission electron microscopy images of gene vectors following incubation in PHP at 37°C. Scale bar: 100 nm.

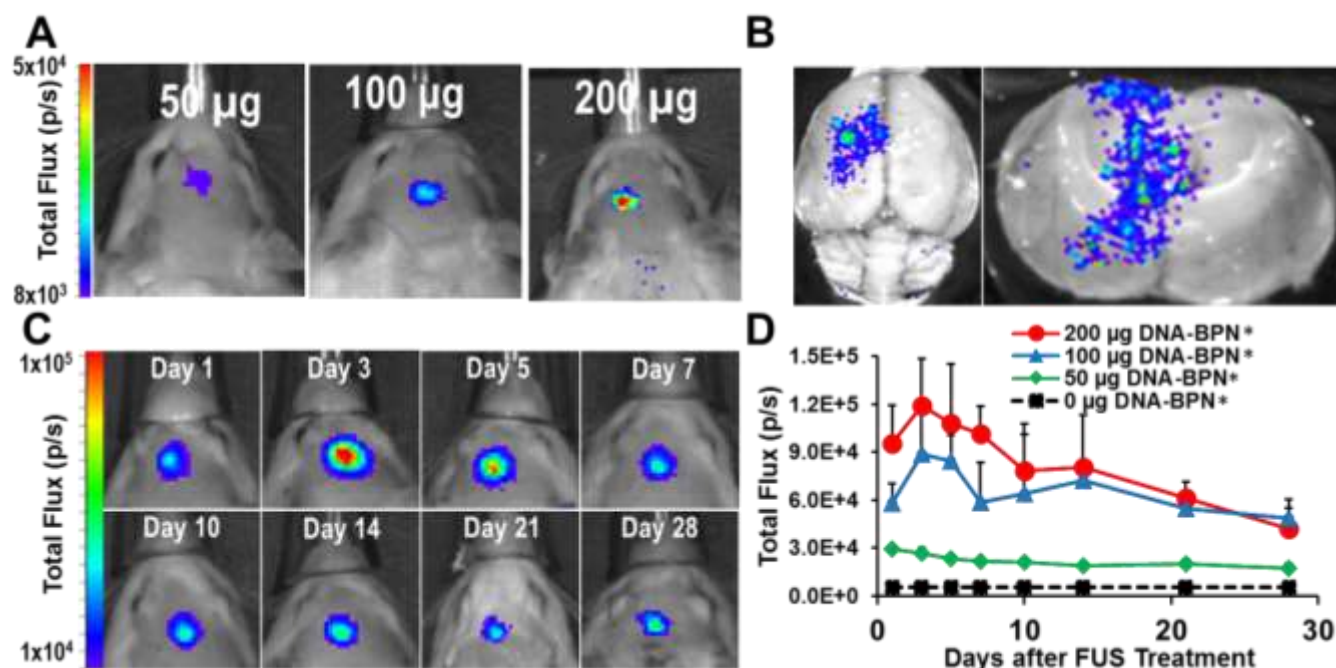


Figure 3.2. FUS-mediated delivery of pBAL DNA-BPN across the BBB leads to robust and localized transgene expression in the rat brain. (A) Representative IVIS bioluminescence scans acquired 7 days after delivery of luciferase-bearing DNA-BPN into the rat brain with FUS. Bioluminescence was dependent on the DNA-BPN dose. (B) *Ex vivo* bioluminescence IVIS scans showing transgene distribution through axial plane (left) and coronal plane (right) 28 days after FUS treatment. (C) Representative IVIS bioluminescence images in a rat given 200 µg luciferase bearing DNA-BPN over 28 days. (D) Line graph of bioluminescence total flux over the 28 day test period. *Significantly different than all other doses tested ($p < 0.05$).

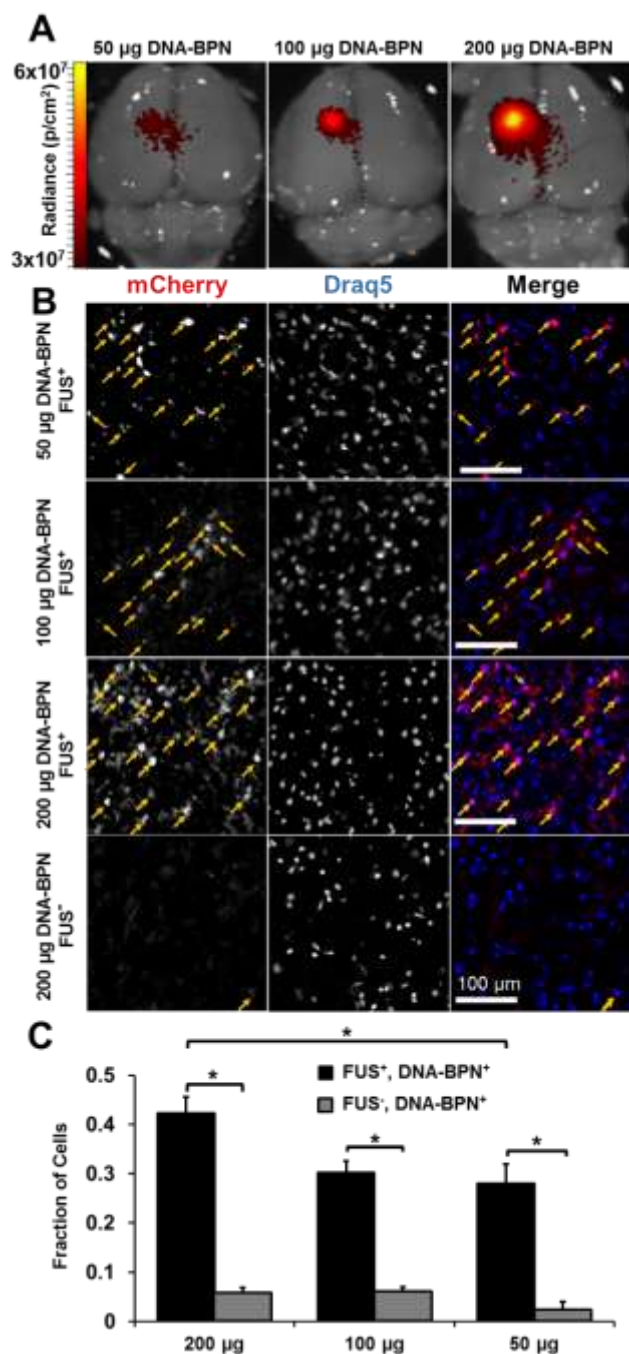


Figure 3.3. FUS mediated delivery of pBACH DNA-BPN into rat brain leads to efficient and localized transfection. (A) Representative whole brain *ex vivo* epifluorescence IVIS scans taken 7 days after delivery of DNA-BPN. (B) Confocal fluorescence images show mCherry (red, left column), Draq5 (blue, middle column) and merge (right column) images 7 days after FUS-mediated delivery of DNA-BPN. Arrows indicate co-localization of mCherry and Draq5. Scale bar = 100 μm . (C) Bar graphs showing transfection efficiency 7 days after DNA-BPN delivery with FUS compared to contralateral non-FUS treated hemisphere. *Significantly different ($p < 0.05$).

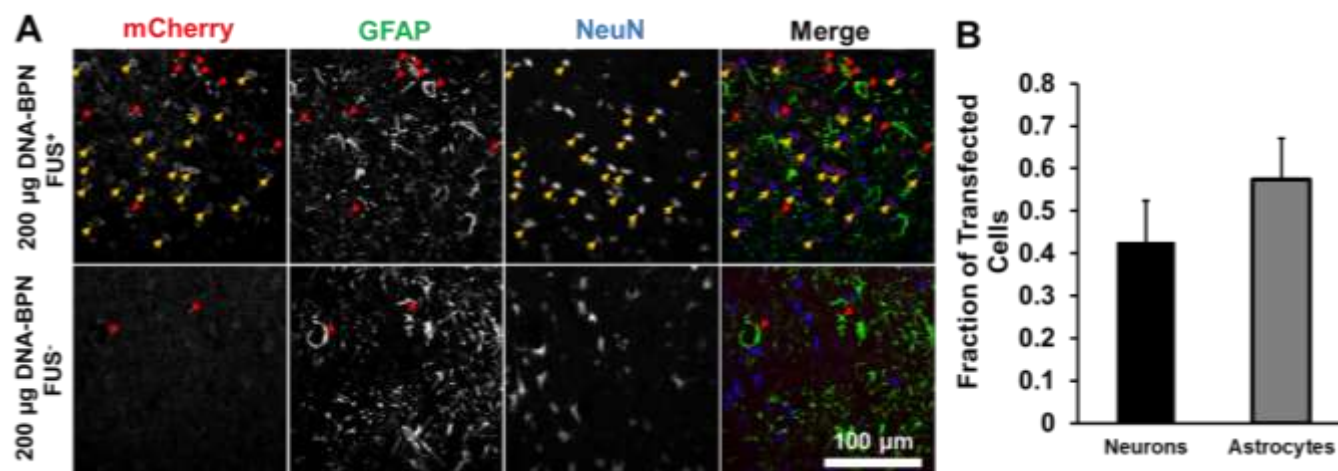


Figure 3.4. DNA-BPN delivered across the BBB with FUS transfect both astrocytes and neurons. (A) Representative confocal fluorescent images show mCherry (red, left column), GFAP (green, middle-left column), NeuN (blue, middle-right column), and merge (right column) images 7 days after delivery of pBACH DNA-BPN with FUS (top row) or without FUS (bottom row). Arrows indicate colocalization of mCherry and GFAP (red) or NeuN (yellow). Scale bar = 100 µm. (B) Bar graph showing the relative fraction of mCherry⁺ cells that colocalize with the GFAP astrocytic marker or the NeuN neuronal marker.

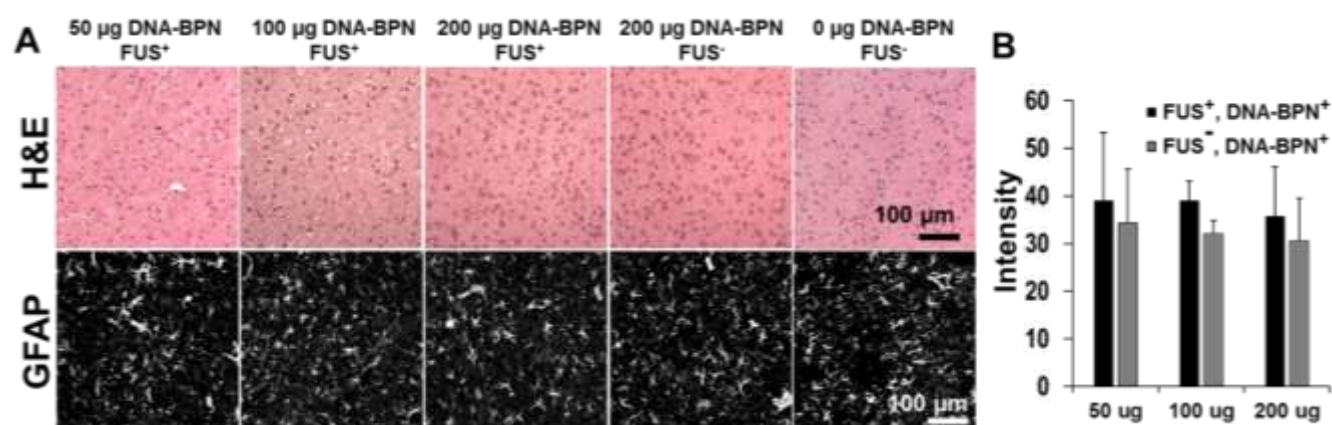


Figure 3.5. Examination of brain tissues for toxicity and gliosis at 1 week after DNA-BPN delivery with FUS. (A) Representative images from $n=6$ H&E-stained sections (top) or confocal GFAP-immunofluorescence sections 7 days after DNA-BPN delivery with FUS. No signs of toxicity were found in brains treated with FUS and DNA-BPN. Hemosiderin staining was found in 11% of $n=18$ brains tested. (B) Bar graph of GFAP grayscale intensity in the FUS⁺ and DNA-BPN treated regions as well as the contralateral FUS⁻ hemisphere. No statistical differences were found.

3.7 Chapter 3 Tables

Table 3.1. Physicochemical properties of DNA-BPN.

	Hydrodynamic Diameter \pm SEM (nm) ^a		ζ -potential \pm SEM (mV) ^b	PDI ^a
	Number mean	z-average		
DNA-BPN	56 \pm 2	106 \pm 1	1.5 \pm 0.3	0.18
DNA-BPN in plasma^c	65 \pm 7	130 \pm 2	-1.8 \pm 0.8	0.25

^a Size and PDI were measured by DLS in 10 mM NaCl at pH 7.0 and data are presented as the average of at least 3 measurements \pm standard error of the mean (SEM).

^b ζ -potential was similarly measured by laser Doppler anemometry and data are presented as the average of at least 3 measurements \pm SEM.

^c Physicochemical characteristics were measured following 5 min incubation in PHP at 37°C.

Chapter 4: Novel focused ultrasound gene therapy approach non-invasively restores dopaminergic neuron function in a rat Parkinson's disease model

Brian P. Mead, Namho Kim, G. Wilson Miller, David Hodges, Panagiotis Mastorakos, Alexander L. Klibanov, James W. Mandell, Jay Hirsh, Jung Soo Suk, Justin Hanes, Richard J. Price. *Nano Letters* 17: 3533-3542, 2017.

4.1 Abstract

Therapies capable of decelerating, or perhaps even halting, neurodegeneration in Parkinson's disease (PD) remain elusive. Clinical trials of PD gene therapy testing the delivery of neurotrophic factors, such as the glial cell-line derived neurotrophic factor (GDNF), have been largely ineffective due to poor vector distribution throughout the diseased regions in the brain. In addition, current delivery strategies involve invasive procedures that obviate the inclusion of early-stage patients who are most likely to benefit from GDNF-based gene therapy. Here, we introduce a two-pronged treatment strategy, composed of MR image-guided focused ultrasound (FUS) and brain-penetrating nanoparticles (BPN), that provides widespread but targeted GDNF transgene expression in the brain following systemic administration. MR image-guided FUS allows circulating gene vectors to partition into the brain tissue by non-invasive and transient opening of the blood-brain barrier (BBB) within the areas where FUS is applied. Once beyond the BBB, BPN provide widespread and uniform GDNF expression throughout the targeted brain tissue. After only a single treatment, our strategy led to therapeutically relevant levels of GDNF protein content in the FUS-targeted regions in the striatum of the 6-OHDA-induced rat model of PD, which lasted at least up to 10 weeks. Importantly, our strategy restored both dopamine levels and dopaminergic neuron density and reversed behavioral indicators of PD-associated motor dysfunction with no evidence of local or systemic toxicity. Our combinatorial approach overcomes limitations of current delivery strategies, thereby potentially providing a novel means to treat PD.

Keywords: Focused Ultrasound, Non-Viral Gene Delivery, Parkinson's Disease, Blood-Brain Barrier

4.2 Introduction

Parkinson's disease (PD) is a largely idiopathic neurodegenerative disorder affecting approximately 2% of the population over 65(246). It is estimated that PD costs more than 14 billion dollars each year in the US alone(247) and incidence is expected to double as early as 2040(116). One of the primary hallmarks of PD is the degeneration of dopaminergic neurons with cell bodies in the substantia nigra pars compacta (SNpc) and axon projections extending into the striatum. The resulting dopamine deficiency leads to progressive and debilitating motor control deficits including bradykinesia, rigidity, and resting tremor. While pharmacological dopamine replacement or surgical therapies like deep brain stimulation can ameliorate symptoms at early stages in PD, they are not neuroprotective and continued neuronal degeneration ultimately leads to recurrence of symptoms(248, 249). Furthermore, late stage patients often develop motor symptoms that are refractory to dopamine replacement therapies or complications stemming from long-term dopamine-replacing drug use(250). Therapies that can slow or stop the neurodegenerative process have remained elusive(251).

Gene therapy approaches aimed at slowing or reversing neurodegeneration in PD have been developed and tested in both pre-clinical and clinical settings for many years. Neurotrophic factors, like the glial cell-line derived neurotrophic factor (GDNF), are attractive candidates for gene therapy due to their ability to protect neurons from continued degeneration, induce neuronal regeneration and sprouting, and enhance dopamine generation from the remaining neuronal population(252, 253). Numerous gene therapy clinical trials for PD have been completed using genes that encode for neurotrophic factors like GDNF or its close structural and functional relative, neurturin (NTRN). While these clinical trials showed safety, therapeutic outcomes were disappointing. Going forward, it has been hypothesized that therapeutic outcomes may be improved by: a) enhancing delivery efficiency, transfection volume, and reproducibility of delivery within the target structures(254), b) treating earlier stage (or even

prodromal) patients prior to the onset of extensive irreversible neurodegeneration(255, 256), and c) further adjusting dosing parameters to ensure appropriate levels of neurotrophic factor expression throughout the target volume. While advances in direct injection strategies, including convection enhanced delivery (CED), may improve outcomes, concerns over their invasive and risky nature have obviated the inclusion of early stage PD patients in clinical trials. More effective and minimally-invasive approaches that can be used for patients regardless of their disease stages are required.

To date, clinical gene therapy studies have relied upon direct administration methods that are invasive and may yield poor transgene distribution. Systemic administration has not been considered because the BBB prevents nearly 100% of molecules larger than ~400 Da in size from entering the brain. Indeed, the BBB remains one of the most significant impediments to therapeutic delivery to the brain following systemic administration(5). To achieve efficacy, both viral vectors and nanoparticles with BBB-targeting ligands often require very high systemic doses, which can lead to peripheral adverse side effects(18). Other strategies for circumventing the BBB, such as intranasal administration or intra-arterial infusion of the osmotic agent mannitol, have been proposed and are being tested. However, they also have weaknesses that may hinder translation to the clinic, including invasiveness, inconsistency, and/or poor targeting and tissue distribution(229, 230).

MR image-guided focused ultrasound (FUS) is currently the only modality capable of non-invasively opening the BBB for spatially targeted therapeutic delivery into the brain(7). Through the activation of ultrasound contrast agent microbubbles (MBs) in stable cavitation, FUS permits the targeted delivery of nanoparticles as large as 100 nm across the BBB(6, 7). Activated MBs exert mechanical forces on the vessel wall, temporarily disrupting tight junctional complexes(108) and inducing active transport processes(232). Barrier function is typically fully restored within 4-6 hours(233, 257), and safety has been demonstrated in several large animal

models(63, 64). Advances in transducer technology now permit sub-millimeter precision, and with guidance from magnetic resonance (MR) imaging, it is possible to apply FUS across the human skull in an extremely localized manner, limiting the potential for unwanted side effects(258, 259). Furthermore, MR imaging allows semi-real time intraoperative treatment feedback and post-operative confirmation of success. Indeed, MR image-guided FUS is now FDA approved for use in humans with essential tremor(259), and clinical trials for other CNS disorders including tremor dominant PD are underway(260).

Once across the BBB, vectors must traverse a dense, nanoporous, and negatively charged extracellular matrix (ECM) that impedes the dispersion of traditional nanoparticles(8, 190) and viruses(21) through both adhesive interactions and steric obstruction. Importantly, it has recently been shown that sub-114 nm nanoparticles densely coated with hydrophilic and neutrally charged polyethylene glycol (PEG) are able to overcome this barrier and diffuse rapidly within the brain parenchyma(8, 186, 261, 262). These “brain-penetrating nanoparticles” (BPN) can be complexed into nano-sized and colloidally stable gene vectors(263, 264). We have previously demonstrated that FUS can target BPN delivery to rat brain(6), which can provide robust and long-term reporter gene expression in the FUS-targeted region when the BPN is loaded with plasmid DNA(265). In the current study, we used a BPN formulation to deliver a GDNF gene-bearing plasmid (GDNF-BPN) to the striatum of PD rats whose BBB was transiently opened in a targeted manner with MR image-guided FUS. We demonstrate a clinically-relevant strategy to restore dopaminergic neuronal function without the need for invasive surgical procedures.

4.3 Results

4.3.1 Characterization of GDNF-BPN.

The GDNF plasmid was previously engineered for long term expression in the brain(266). By using a long-lasting polyubiquitin C promoter, optimized Kozak consensus sequence to improve translation initiation, and a CpG depleted plasmid backbone to reduce DNA silencing(267), this gene cassette was found to have peak expression after approximately 7 days and lasting at least 6 months after direct injection into mouse striatum(266). We condensed GDNF plasmids or negative control reporter gene bearing plasmids (i.e. pBAL) with a blend of polyethylenimine (PEI) and PEI-PEG conjugates to yield GDNF-BPN or pBAL-BPN, respectively. We have shown that the large amount of PEG in these systems greatly reduces, if not eliminates, potential *in vivo* toxicity induced by the highly cationic nature of PEI(148, 186, 265). The GDNF-BPN and pBAL-BPN formulations both possessed very small hydrodynamic diameter (50 +/- 3 nm), near neutral surface charge (ζ -potential of 1.5 +/- 0.2 mV), and a tight size distribution (polydispersity index of 0.2); we have shown that nanoparticles that possess this combination of physicochemical properties rapidly penetrate within brain tissue(186) and provide uniform and efficient reporter gene expression in the rat striatum after delivery with FUS(265). GDNF-BPN and pBAL-BPN were colloiddally stable without any significant change in size and morphology for at least 6 hours when incubated in artificial cerebrospinal fluid (aCSF) at 37 °C (Figure S1).

4.3.2 MR Imaging Assessment of Blood-Brain Barrier Opening.

FUS treatments were guided by peri-operative MRI (Figure 1). Pre-FUS T1-weighted and T2-weighted (Figure 1A) MR images were acquired and used to plan 4 equally-spaced treatment sites within the ipsilateral (6-OHDA treated) striatum. We targeted only the striatum because previous studies suggest that this approach leads to a greater functional recovery than treatment of both the striatum and SNpc(268). FUS parameters (1.15 MHz, 0.6 MPa non-

derated peak-negative pressure), MB dose (3×10^5 MB/g), and GDNF-BPN dose ($0.5 \mu\text{g/g}$ body weight) were chosen based on previous BPN delivery and safety studies from our group (6, 265). To confirm BBB disruption after FUS-application, Gd-DPTA was injected intravenously and contrast-enhanced T1-weighted images were acquired (Figure 1C) and compared to pre-FUS T1-weighted images. Enhancement in signal intensity in the FUS-treated striatum was found in all ($n = 32$) animals treated with FUS. In addition, T2*-weighted imaging, which detects extensive red blood cell extravasation, was performed pre- and post-FUS (Figure 1 B,D). Red blood cell extravasation, which would have been indicated by hypointense regions on T2* MRI, was never detected at the FUS-treated sites ($n = 128$) in this study.

4.3.3 Localized delivery of GDNF-BPN with FUS Elicits Robust GDNF Protein Expression in the Striatum.

Two weeks after unilateral partial lesioning with 6-OHDA, GDNF-BPN were injected intravenously and delivered to the 6-OHDA lesioned striatum with MRI-guided FUS. Delivery of GDNF-BPN with FUS to the striatum led to an 11-fold increase in ipsilateral striatal GDNF protein when compared to 6-OHDA only control animals (Figure 2). GDNF protein levels remained elevated through week 12, reaching 12.3 ± 3.5 ng/mg. Application of 6-OHDA alone, in conjunction with GDNF-BPN without FUS, or in conjunction with FUS-mediated delivery of pBAL-BPN, had no significant effect on GDNF protein levels. GDNF levels were not elevated above baseline levels in the contralateral striatum or the SNpc (Figure S2A) of either hemisphere in any group, indicating that FUS application yielded target-site specific GDNF expression. Importantly, GDNF expression in animals receiving GDNF-BPN was not significantly elevated in off-target major organs (Figure S2B) when compared to 6-OHDA only animals.

4.3.4 Dopamine Levels are Elevated in 6-OHDA Lesioned Rats that Subsequently Received FUS-Targeted GDNF-BPN Delivery.

Two weeks after administration of 6-OHDA into the striatum of control animals, ipsilateral striatal dopamine (DA) levels dropped to ~10% of those measured in the contralateral striatum (Figure 3). Furthermore, DA levels remained low at weeks 6 and 12 in the 6-OHDA only control group. In agreement with the locomotor function data, animals in both the 6-OHDA + GDNF-BPN (no FUS) and 6-OHDA + FUS + pBAL-BPN control groups showed no improvement in ipsilateral DA levels compared to animals who received no treatment after 6-OHDA administration.

Importantly, 6-OHDA lesioned animals treated with GDNF-BPN and FUS exhibited 2.8-fold and 2.2-fold increases in DA levels compared to 6-OHDA only control animals at weeks 6 and 12, respectively. Ipsilateral DA levels in these treated animals were not significantly different from contralateral striatal DA levels at week 12, suggesting that the treatment regimen normalized DA levels. In addition, in the ipsilateral striatum, the DA metabolites 3,4-dihydroxyphenylacetic acid (DOPAC) and homovanillic acid (HVA) were elevated 3.8-fold and 4.3-fold, respectively, in 6-OHDA +FUS + GDNF-BPN animals at week 12 compared to 6-OHDA rats, indicative of DA turnover (Table S1).

4.3.5 Dopaminergic Neuron Density is Restored in 6-OHDA Lesioned Rats that Subsequently Received FUS-Targeted GDNF-BPN Delivery.

Both dopaminergic (TH⁺) neuron cell number in the SNpc and nigrostriatal neuronal projection density in the striatum were assessed through quantitative morphology at weeks 2, 6, and 12 after 6-OHDA administration (Figure 4). In control animals, 6-OHDA administration led to a 74% reduction in dopaminergic cell number in the SNpc and an 87% reduction in dopaminergic staining density in the striatum at two weeks. Control animals receiving 6-OHDA only, 6-OHDA + GDNF-BPN, or 6-OHDA + FUS + pBAL-BPN showed no improvement in dopaminergic

neuron number in the SNpc nor in dopaminergic staining density in the striatum. In contrast, 6-OHDA rats treated with GDNF-BPN and FUS showed, respectively, 3.2-fold and 5.0-fold increases in dopaminergic cell number in the SNpc and dopaminergic density in the striatum at week 12. Qualitatively, 6-OHDA + FUS + GDNF-BPN treatment also appeared to enhance TH+ fiber density in the substantia nigra pars reticulata (SNpr), which lies ventral to the SNpc, when compared to 6-OHDA controls.

4.3.6 Locomotor Function is Markedly Improved in 6-OHDA Lesioned Rats that Subsequently Received FUS-Targeted GDNF-BPN Delivery.

Unilateral striatal 6-OHDA lesioning without treatment led to extensive locomotor deficits, including apomorphine-induced rotational bias and forepaw use bias after two weeks (Figure 5). Control animals that received no treatment after 6-OHDA administration, intravenous GDNF-BPN only, or pBAL-BPN and FUS maintained both drug induced and voluntary locomotor bias throughout the entire 12-week course of the study, indicating extensive neurodegeneration (Figure 5). In contrast, 6-OHDA lesioned animals that received the FUS + GDNF-BPN treatment demonstrated markedly improved locomotor function. At week 2, treated animals exhibited a 54% reduction in apomorphine-induced rotational bias when compared to 6-OHDA only control animals. At week 4, forepaw use bias was restored to normal levels. In the 6-OHDA + FUS + GDNF-BPN treatment group, these improvements in locomotor function, as assessed by both tests, were fully retained through the 12 week duration of the experiment.

4.3.7 Safety Analysis

Animals in the 6-OHDA + FUS + GDNF-BPN treatment group did not show changes in weight gain compared to controls (Figure S3A). Brain tissue sections were stained with H&E and scored for signs of toxicity by a board certified neuropathologist (JWM) blinded to the

treatment conditions. No evidence of neural damage, ischemic injury, or gliosis was found beyond that caused by the 6-OHDA probe injection tract in any slide throughout the course of the 12-week study (Figure S3B).

4.4 Discussion

Clinical strategies capable of slowing or reversing neurodegeneration in Parkinson's disease remain elusive. It has been hypothesized that clinical gene therapy trials using viral vectors to deliver neurotrophic factors, including GDNF, have failed to meet primary efficacy outcomes due to both incomplete delivery to the target structures and invasive surgical strategies that obviate the inclusion of early stage PD patients(254, 255). Using a clinically relevant treatment paradigm, wherein treatment was applied when the nigrostriatal motor neuron pathway had experienced an ~80% reduction in dopaminergic neuron density, we demonstrated that the MR image-guided delivery of brain-penetrating GDNF gene nanovectors with FUS is capable of generating marked improvements in locomotor function, nigrostriatal dopaminergic neuron density, and DA levels, with some metrics showing complete restoration. Given the minimally-invasive nature of this gene delivery strategy, we postulate that it may eventually be translated to the clinic for treatment of early stage or prodromal PD patients.

4.4.1 Gene Delivery to the CNS with FUS

It is now well established that MR image-guided FUS may be used to non-invasively and temporarily open the BBB, allowing localized delivery of systemically circulating agents as large as 100 nm in size to the CNS(6, 7). We have previously demonstrated the ability of FUS to target the delivery of reporter gene-bearing BPN to the brains of healthy rats, leading to efficient, targeted, and localized transgene expression without signs of toxicity or astrocyte activation(265). Importantly, we found that ~30% of cells, including an equal ratio of neurons

and astrocytes, were transfected at a similar dose as the current study(265). We note that FUS has recently been shown to facilitate the delivery of systemically administered GDNF-loaded liposomes ~200 nm in diameter to the brain, leading to neuroprotection in a mouse model of PD(269). While a modest but significant increase in GDNF protein content was observed (< 2-fold increase over control animals), a total of 12 FUS + GDNF plasmid treatments, at doses of 1 µg/g, were required to achieve this level of GDNF expression. Moreover, transgene expression was detected in non-targeted brain and some peripheral organs, as determined by *in vivo* imaging. In contrast, our GDNF-BPN, possessing smaller diameters of ~50 nm, elicited an 11-fold increase in GDNF protein content that was achieved with a single treatment only (dose = 0.5 µg/g) and precisely localized to the FUS-treated striatum. Thus, we postulate that GDNF plasmid delivered via this unique combination of FUS-targeted BBB opening and BPN-mediated brain distribution offers a single treatment approach with improved spatial specificity, greater GDNF expression, and enhanced functional therapeutic outcomes.

FUS has also been shown, in studies by other investigators, to be capable of delivering naked plasmids(156, 157) and adeno-associated viruses (~20 nm size)(155, 163) to the CNS after systemic administration. The appeal of viral-based gene vectors is reduced by neutralizing immune responses to the virus, which are often observed following administration or prior exposure, that reduce efficiency of transgene delivery(171). Other limitations of viral vector approaches include low packaging capacity, high production costs, and/or safety risks(228). The non-viral BPN vectors used in the current study are versatile, highly tunable, and devoid of the intrinsic limitations associated with viral vectors.

4.4.2 Comparison to Previous Pre-Clinical Studies with GDNF

Our treatment strategy yielded long-term and spatially localized GDNF expression at levels that did not elicit local toxicity. GDNF protein content remained elevated (~10-fold over controls)

in the FUS + GDNF-BPN treated striatum for at least 10 weeks post-treatment, suggesting long-term GDNF expression at functional levels at least on the order seen in other gene delivery studies with the same plasmid(270). Elevated GDNF levels were not found in the ipsilateral SNpc, the contralateral striatum, or the contralateral SNpc, highlighting the ability of FUS to spatially localize the delivery of GDNF-BPN. While the mechanisms of restoration of dopaminergic cell number in the SNpc due to enhanced GDNF expression are not yet clear, it has been postulated(3) that this could be elicited by GDNF-induced signaling at axon terminals rather than retrograde GDNF transport. This is consistent with our finding that dopaminergic neurons were restored in the SNpc despite GDNF levels remaining at normal levels. There appears to be a fairly large therapeutic window for GDNF in the brain, as previous studies have shown that while small (3-4 fold) increases in GDNF protein levels in the striatum were sufficient to protect most neurons from 6-OHDA lesioning, much higher levels (~100-300-fold increases) of GDNF expression can lead to adverse side effects, including lower tissue DA and TH levels after 6-12 weeks(271, 272). However, appropriate targeting within the brain is critical, as off-target GDNF overexpression in the hypothalamus(273, 274) or infusion into the ventricles(275) can lead to weight loss. Studies using systemically administered recombinant GDNF protein have not reported adverse events associated with off-target GDNF uptake(276), which is consistent with the observation that animal weight gain was normal in our study.

Previous studies have used direct administration of viral vectors to overexpress GDNF in both toxin-based and α -synuclein-based preclinical models of PD. While studies in toxin-based models have demonstrated restoration of motor function and/or dopaminergic density after GDNF gene therapy, these studies have utilized less severe models of PD, wherein animals only exhibited ~30-50% dopaminergic neuron loss at the time of treatment(2, 3, 277). In contrast, animals in the current study were treated when ~70-80% of dopaminergic neurons had been lost, thereby replicating the level of neurodegeneration seen in early stage human PD

patients(278, 279). While the 6-OHDA model recapitulates many aspects of human PD, going forward, it may be useful to determine whether our approach is efficacious in other PD models, such as an α -synuclein overexpression model. Nonetheless, it is important to note that α -synuclein-based PD models have previously demonstrated lack of efficacy of GDNF gene therapies(280), presumably due to GDNF receptor (Ret) downregulation(281); therefore, alternative models may be more appropriate for this application.

4.4.3 Relevance to Clinical Trials

Despite the success of gene therapies for neurotrophic factors in pre-clinical animal studies (2, 3, 271, 282), clinical PD trials have generally failed to meet primary outcomes. While early gene therapy trials with AAV2-NTRN administered intracranially by convection-enhanced delivery did produce preliminary evidence for clinical improvement, results were inconsistent(22, 23). Following this clinical trial, post-mortem results demonstrated that only ~20% of the targeted putamen expressed detectable levels of NTRN (283), suggesting that increasing putaminal coverage could improve outcomes. A follow-up phase 2b trial used an ~3-fold higher dose of AAV2-NTRN and increased the CED-injected volume ~4-fold(284). Unfortunately, putaminal coverage was increased to only ~30% and these trials again failed to meet primary outcomes. Ongoing clinical trials using AAV2-GDNF (www.clinicaltrials.gov, NCT01621581) are aimed at improving volume of distribution using highly-invasive intracranial infusion.

Additional data argue for treatments at earlier stage or even prodromal PD. PD symptoms typically appear after loss of ~70-80% of dopaminergic neurons(278, 279), and degeneration is nearly complete within 10 years after diagnosis, rendering the disease irreversible(285). Consistent with this paradigm, a recent post-hoc analysis of earlier AAV2-NTRN clinical trials demonstrated that patients treated less than 5 years after PD diagnosis had a significantly (~2.5-fold) greater improvement in unified PD rating scale (UPDRS) scores when compared to

patients treated more than 10 years after diagnosis. Importantly, PD patients treated with AAV2-NTRN more than 10 years after diagnosis (constituting more than half of the treated patients) exhibited no improvement when compared to sham controls(284). The FDA has so far been unwilling to treat PD patients at earlier stages owing to the invasive nature and risks associated with intracranial injection/infusion strategies(255).

In contrast, FUS has the advantage of being a non-invasive treatment strategy that can even be performed on awake patients, obviating risks associated with surgical procedures and general anesthetics (286). Moreover, the high capillary density in the brain provides a large surface area for delivery from the systemic circulation after FUS application. Coupling of FUS with highly diffusive BPN that can access all the cells between opened capillaries allows exceptionally homogenous and efficient DNA delivery over a large volume within the FUS-targeted region. FUS mediated delivery of GDNF-BPN, therefore, represents an enticing alternative capable of overcoming many of the hurdles associated with conventional treatment strategies.

4.5 Materials and Methods

4.5.1 Animals

Female Sprague-Dawley rats were purchased from Envigo, housed on a 12/12h light/dark cycle, and given food *ad libitum*. Animal experiments were approved by the Animal Care and Use Committee at the University of Virginia and conformed to the National Institutes of Health guidelines for the use of animals in research.

4.5.2 6-OHDA Lesions

Partial striatal lesioning with 6-OHDA was performed as previously described (2, 3). Female Sprague-Dawley rats (~160-180 g) were anesthetized and maintained with 2-2.5% isofluorane in oxygen. The top of the animals' heads were shaved and depilated before being secured prone in a stereotaxic frame (Stoelting, Wood Dale, IL). Buprenorphine (0.03 mg/kg, Reckitt Benckiser Healthcare, Hull, UK) was administered to achieve local anesthesia. A midline scalp incision was made, and the skull was exposed. A total of 12 µg 6-OHDA (Sigma-Aldrich, St. Louis, MO) dissolved in 2µl 0.02% ascorbic acid/0.9% saline was injected in two sites in the right striatum at the coordinates: AP: +0.5, ML: +2.1, DV: -5 and AP: -0.5, ML: +3.8, DV: -5 mm at 0.5 µl/min.

4.5.3 Plasmid Design

The GDNF plasmid (~4 kB) was constructed as previously described(266, 270) using standard molecular biology techniques and kindly donated to us by Dr. Mark Cooper (Copernicus Therapeutics) and Dr. David Yurek for use in this study. In brief, human GDNF was placed downstream of the ubiquitously active and long-lasting polyubiquitin C promoter and first exon and intron sequences. GDNF was codon-optimized and prokaryotic elements were CpG depleted to reduce potential methylation sites known to increase likelihood of gene silencing.

The pBAL plasmid was produced by Copernicus Therapeutics Inc. (Cleveland, OH) and is described elsewhere(265). Briefly, this plasmid contains the luciferase reporter gene driven by the ubiquitously active β -actin promoter.

4.5.4 DNA-BPN Fabrication and Characterization

DNA-BPN were fabricated and characterized as previously described(186, 265). Briefly, PEG_{5k}-PEI copolymer was synthesized by conjugating molar excess of 5kDa methoxy-PEG-N-hydrosuccinimide (mPEG-NHS, 5 kDa, Sigma-Aldrich, St. Louis, MO) to primary amine groups of 25 kDa branched PEI (Sigma-Aldrich, St. Louis, MO). The resulting PEI-PEG conjugate possessed a high degree of PEG conjugation (average of 41 PEG chains per PEI molecule). The final product was extensively dialyzed against ultrapure water and the conjugation was confirmed by nuclear magnetic resonance. DNA-BPN were formulated by drop-wise addition of 10 volumes of plasmid DNA to 1 volume of polymer mixture solution of PEI and PEG_{5k}-PEI. DNA-BPN were purified with 3 volumes of ultrapure water to eliminate free polymers, and concentrated to 1mg/ml using Amicon Ultra Centrifugal Filters (100,000 MWCO; Millipore Corp., Billerica, MA). The DNA concentration of DNA-BPN was confirmed using a NanoDrop 2000 spectrophotometer (Thermo Scientific, Waltham, MA). Hydrodynamic diameter, ζ -potential, and polydispersity index of DNA-BPN were measured using Zetasizer Nano ZS (Malvern Instruments, Southborough, MA). Colloidal stability of DNA-BPN was observed with transmission electron microscopy (TEM, Hitachi H7600, Japan) after incubating DNA-BPN in aCSF (Harvard Apparatus, Holliston, MA) at 37 °C for 6 hours.

4.5.5 Microbubble Fabrication and Characterization

MBs used in the current study have a formulation similar to Optison (GE Healthcare, Little Chalfont, Buckinghamshire, UK). A 1% solution of serum albumin in saline was sonicated (20

kHz, 30 s) with an ultrasound disintegrator (XL2020; Misonix, Farmingdale, NY) with an extended ½-inch titanium probe. The flask containing the solution had its headspace filled with octafluoropropane gas prior to sonication. MBs were sized and counted using a Coulter Counter (Multisizer 3, Beckman Coulter, Fullerton, CA).

4.5.6 FUS-Mediated DNA-BPN Delivery

Female Sprague-Dawley rats were anesthetized with an intraperitoneal injection of ketamine (40 mg/kg, Zoetis, Fort Dodge, IA) and dexdomitor (0.2 mg/kg, Pfizer, New York, NY) in sterilized 0.9% saline. A tail vein catheter was inserted to allow intravenous injections of DNA-BPN and microbubbles. In a previous study by our group(6), BPN with a similar size and surface chemistry were found to be circulating 24 hours after i.v. administration into rats. Rat heads were shaved and depilated before being secured supine in a degassed water bath coupled to the FUS system (RK-100, FUS Instruments, Toronto) and the entire system was placed in the 3T MR scanner (Magnetom Trio, Siemens Medical Solutions, Malvern, PA). A homebuilt 2-inch cylindrical transmit-receive RF coil was placed around the rat's head to maximize imaging SNR. Baseline T2-weighted and T2*-weighted images were acquired using turbo spin-echo and spoiled gradient-echo pulse sequences, respectively. T2-weighted imaging parameters included: TR/TE = 3600/46 ms, flip angle = 90°/150°, readout bandwidth = 219 Hz/pixel, 9 slices, thickness = 1 mm, field of view = 50 mm, matrix = 192 × 192, turbo factor = 18, 100% phase oversampling, 4 averages, total time = 5:22. T2*-weighted imaging parameters included: TR/TE = 101/9 ms, flip angle = 50°, readout bandwidth = 320 Hz/pixel, 7 slices, thickness = 2 mm, field of view = 64 mm, matrix = 192 × 192, 100% phase oversampling, 4 averages, total time = 2:37. T2-weighted images were used to select 4 evenly spaced target locations within the right striatum and 5 mm from the top of the skull.

Rats received a co-injection of GDNF-BPN (100 µg/200g body weight) and MBs (3x10⁵ MBs/g body weight) followed by 0.3 ml of 2% heparinized saline to clear the catheter. Sonication began immediately after clearance of the catheter. Sonications were performed at 0.6 MPa (not accounting for skull/tissue attenuation) using a 1.15 MHz single element focused transducer (FUS Instruments, Toronto, Canada) operating in 10 ms bursts, 0.5 Hz pulse repetition frequency and 2 min total duration. Immediately following BBB opening, post-treatment T2*-weighted images were acquired followed by intravenous administration of MRI contrast agent (0.5 µl/g body weight, Magnevist, Bayer Health Care, PA) and T1-weighted contrast-enhanced images were acquired to verify BBB opening. T1-weighted imaging parameters were identical to those used for the T2*-weighted images, except: TE = 3.1 ms, 2 averages, total time = 1:19. Animals were removed from the MRI table and placed on a warm pad for 30 minutes prior to reversal of the anesthetic with antisedan (2 mg/kg, Orion Pharma, Espoo, Finland)

4.5.7 Behavioral Testing

Assessment of behavioral function was performed 1-3 days before and 2,4,6,8,10 and 12 weeks after injection of 6-OHDA (Figure S4).

1) Cylinder Test of Spontaneous Forelimb Use: Cylinder tests were performed similar to those previously described(25). In a dark testing room, rats were placed a 20-cm diameter glass cylinder and their activity was recorded from above. Left and right weight-bearing forepaw contacts with the wall were quantified by a trained and blinded observer. A minimum of 20 contacts were required to complete the test. Data are presented as percentage of contacts with the contralateral (left) forepaw.

2) Apomorphine-induced Rotational Activity

Rotational tests were performed similar to those previously described (2). Rotational analysis was performed with automated bowls (Med Associates, St. Albans, VT) and the RotoRat software. Rats received a subcutaneous injection of apomorphine (0.4 mg/kg, Sigma-Aldrich, St. Louis, MO). Left (contralateral) and right (ipsilateral) rotations were recorded over 40 minutes. Data are expressed as net full body rotations per minute, with contralateral turns assigned a positive value.

4.5.8 Histological Processing

Immediately following euthanasia, animals were perfused via the left and right carotid arteries with 20 ml of 2% heparinized 0.9% saline followed by 10 ml of 4% formalin. Brains were suffusion-fixed in 4% formalin for 72h at 4°C. Brains were then placed in a brain matrix (Stoelting, Wood Dale, IL). The first coronal slice containing the striatum was prepared by cutting 3 and 6 mm anterior to the front of the brain. The second coronal slide containing the SNpc was prepared by cutting 9 and 12 mm anterior to the front of the brain. Each slice was embedded in paraffin and serially cut in 8 µm coronal sections. Slices were cut in either 6 sections, 240 µm apart, or 8 sections, 120 µm apart, for the striatum-containing and SNpc-containing slices, respectively. Sections were immunolabeled against tyrosine hydroxylase.

4.5.9 Immunohistochemistry

Mounted sections were deparaffinized in xylene and rehydrated in decreasing concentrations of ethanol (100%-70%). Slides were heated to ~95°C for 20 minutes in 10 mM sodium citrate buffer (pH 6.0) to unmask antigens. Endogenous peroxidase activity was blocked using 3% hydrogen peroxide. Sections were washed in PBS and blocked with blocking solution (Vector Labs, Burlingame, CA). Next, sections were incubated overnight at 4 °C with rabbit anti-TH primary antibody (1:250, Millipore, Temecula, CA). Sections were rinsed in PBS and incubated

with goat anti-Rabbit HRP conjugated secondary antibody (1:250, Abcam, Cambridge, MA) for 1 h at room temperature. After washing in PBS, sections were incubated with DAB-peroxidase substrate solution (IHC-Tek, Ellicott City, MD) and mounted with permanent mounting medium (Vector Labs, Burlingame, CA). Sections were imaged on a macroscope (Wild, Heerbrugg, Switzerland) equipped with a CCD camera (Olympus, Center Valley, NJ) at either 16X (striatal sections) or 35X (SNpc sections).

4.5.10 Quantitative Morphology

Images of striatal and SNpc sections were analyzed with in-house written software using MATLAB (Mathworks, Natick, MA). In order to assess inverse staining intensity in the striatum, images were inverted and averaged background was subtracted. Striatal regions were manually selected from the image and the pixel intensity was averaged throughout the entire striatum. Average pixel intensity was then averaged across all six striatal sections. Data are presented as a ratio of average pixel intensity on the ipsilateral side compared to the contralateral side. In order to assess TH⁺ cell bodies in the SNpc, averaged background was subtracted using a Gaussian averaging function. SNpc regions were manually selected from the image and converted to binary images using Otsu's method. Images were then used to create linear structuring elements and individual cell bodies were counted automatically. Cell body counts were averaged across all SNpc sections. Data are presented as a ratio of the average cell body number on the ipsilateral side compared to the contralateral side.

4.5.11 Sample Preparation for Biochemical Analysis

Striatum, SNpc, liver, spleen, heart, kidneys and lungs were rapidly collected on ice and stored at -80°C until further processing. Organs were pulverized in liquid nitrogen and separated into equal fractions for further analysis.

4.5.12 Measurement of Striatal Catecholamines

Striatal samples were lysed with 50 µl of 0.1 M perchloric acid per milligram of tissue using a tissue homogenizer (Omni International, Kennesaw, GA) and centrifuged at 13000 x g for 10 min at 4°C. The supernatant was passed through a 0.22 PVDF Filter (Merck-Millipore, Cork, Ireland), and analyzed by HPLC, a modification of conditions from previously published methods(287). Samples were separated on a C18 reverse-phase HPLC column (Thermo-Scientific, BDS Hypersil, 100 x 2.1 mm). Dopamine, 3,4-dihydroxyphenylacetic acid (DOPAC) and homovanillic acid (HVA) were quantified by electrochemical detection (Antec, Decade) in a mobile phase consisting of 50 mM citrate/acetate, pH 4.5, 1 mM decyl sulfonic acid, 0.1 mM EDTA, and 7% acetonitrile modifying agent. Flow rate was 0.35 ml/min and the detector potential was 0.7 mV relative to a Ag/AgCl reference electrode.

4.5.13 GDNF Protein Levels Measured by ELISA

Striatal, SNpc, liver, spleen, lung, heart and kidney samples were lysed with 10 µl of Lysis Buffer (137 mM NaCl, 20 mM Tris pH 8.0, 1% NP-40, 10% Glycerol) supplemented with 1 mM PMSF, 0.5 mM Sodium Orthovanadate and 10 µl Protease Inhibitor Cocktail (Sigma-Aldrich, cat. nr.: 8340) per ml of Lysis Buffer with a tissue homogenizer (Omni International, Kennesaw, GA). The GDNF ELISA was performed according to the instructions provided by the manufacturer (Promega, cat. nr., G7621). Total protein was measured using a BCA protein assay (Thermo Scientific, Rockford, IL) and GDNF protein was compared to the total amount of protein in the sample.

4.5.14 Statistical Analysis

Sample sizes for all groups were determined empirically. Animals which exhibited severe (>9 rotations/min) or inadequate (<5 rotations/min) apomorphine-induced rotational behavior two

weeks following 6-OHDA administration were excluded. All statistics were conducted using SigmaPlot software (Version 13.0), which automatically suggests parametric or non-parametric tests depending on the results of normality testing. Group comparisons were performed using either three-way ANOVA (locomotor bias tests, body weight comparisons) or two-way ANOVA followed by Mann-Whitney rank sum tests or Holm-Sidak methods. Repeated measures models were used to estimate the effects in the ipsilateral and contralateral sides of the brain. Statistical significance was set at $p < 0.05$. All values are presented as mean \pm SEM.

4.5.15 Data Availability

The data supporting the findings in the current study are available upon request from the corresponding authors.

4.6 Acknowledgements

Supported by the Focused Ultrasound Foundation, NIH R01 CA164789, R01 CA197111, R01 EB020147, and R03 EB016784. BPM was supported by the NHLBI-sponsored Basic Cardiovascular Research Training Grant (5 T32 HL007284) and the Wagner Fellowship. JH is supported by NIH R01GM084128. We are grateful to Dr. David Yurek and Dr. Mark Cooper for donating the GDNF plasmid used in this study.

4.7 Author Contributions

BPM, JSS, JH and RJP conceived of the experiments. BPM conducted animal surgeries and behavioral experiments and *ex vivo* analysis. GWM designed MR imaging sequences and, with BPM, performed MR-Image guided FUS procedures. BPM and DH performed immunohistochemistry and quantitative morphology. NK and PM fabricated and characterized BPN. ALK designed and fabricated microbubbles. JWM assessed H&E stained sections for

safety analysis. JH designed HPLC parameters. All authors contributed to writing the manuscript.

4.8 Chapter 4 Figures

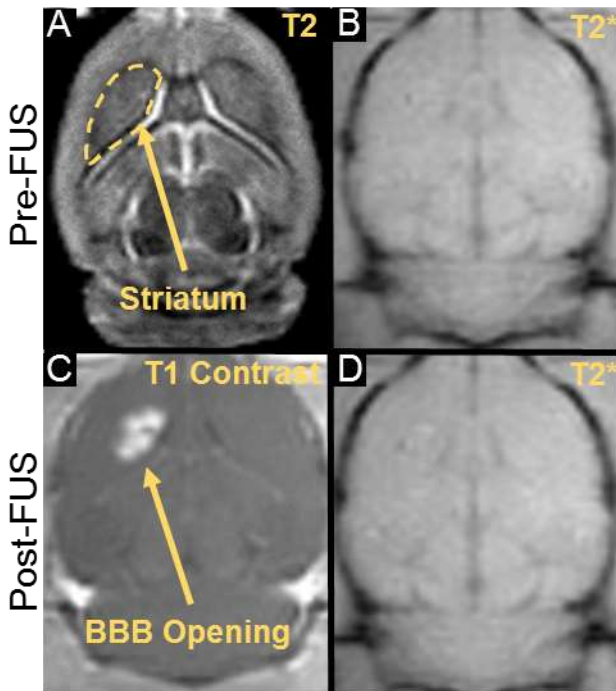


Figure 4.1. MR imaging for guidance, confirmation, and safety evaluation of FUS treatments. A) The treatment site (i.e. 6-OHDA lesioned striatum) was targeted with T2 pre-FUS images. C) BBB opening in the striatum was confirmed with post-FUS contrast-enhanced T1 imaging. B, D) Treatment safety was assessed by comparing pre- and post-FUS T2* images. Hypointensities in T2* images, indicating red-blood cell accumulation, were never observed in FUS-treated animals (n = 32).

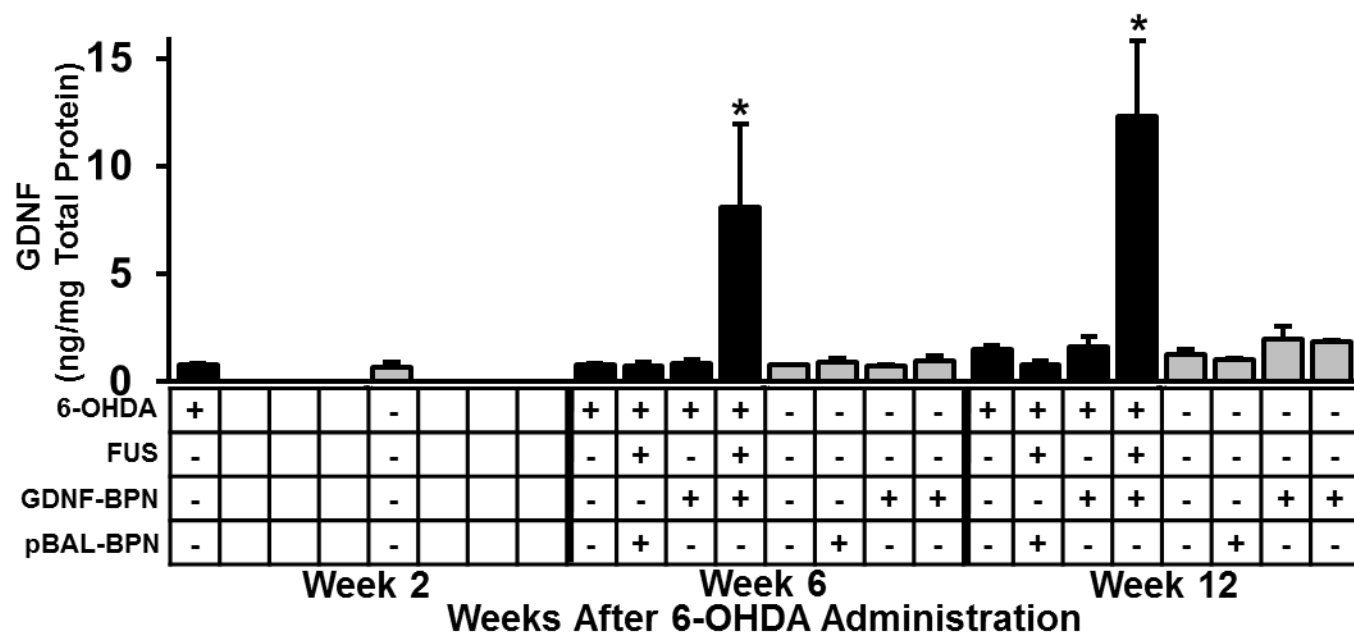


Figure 4.2. FUS-mediated delivery of GDNF-BPN to the striatum of PD rats leads to a significant increase in GDNF protein levels in the striatum. Bar graphs show GDNF protein levels in the ipsilateral (black) and contralateral (gray) striatum. $n = 5$ (6-OHDA +FUS +GDNF-BPN), $n = 4$ or $n = 3$ (6-OHDA +GDNF-BPN) in each group at each time point. *Significantly different from all groups at the same time point ($p < 0.05$).

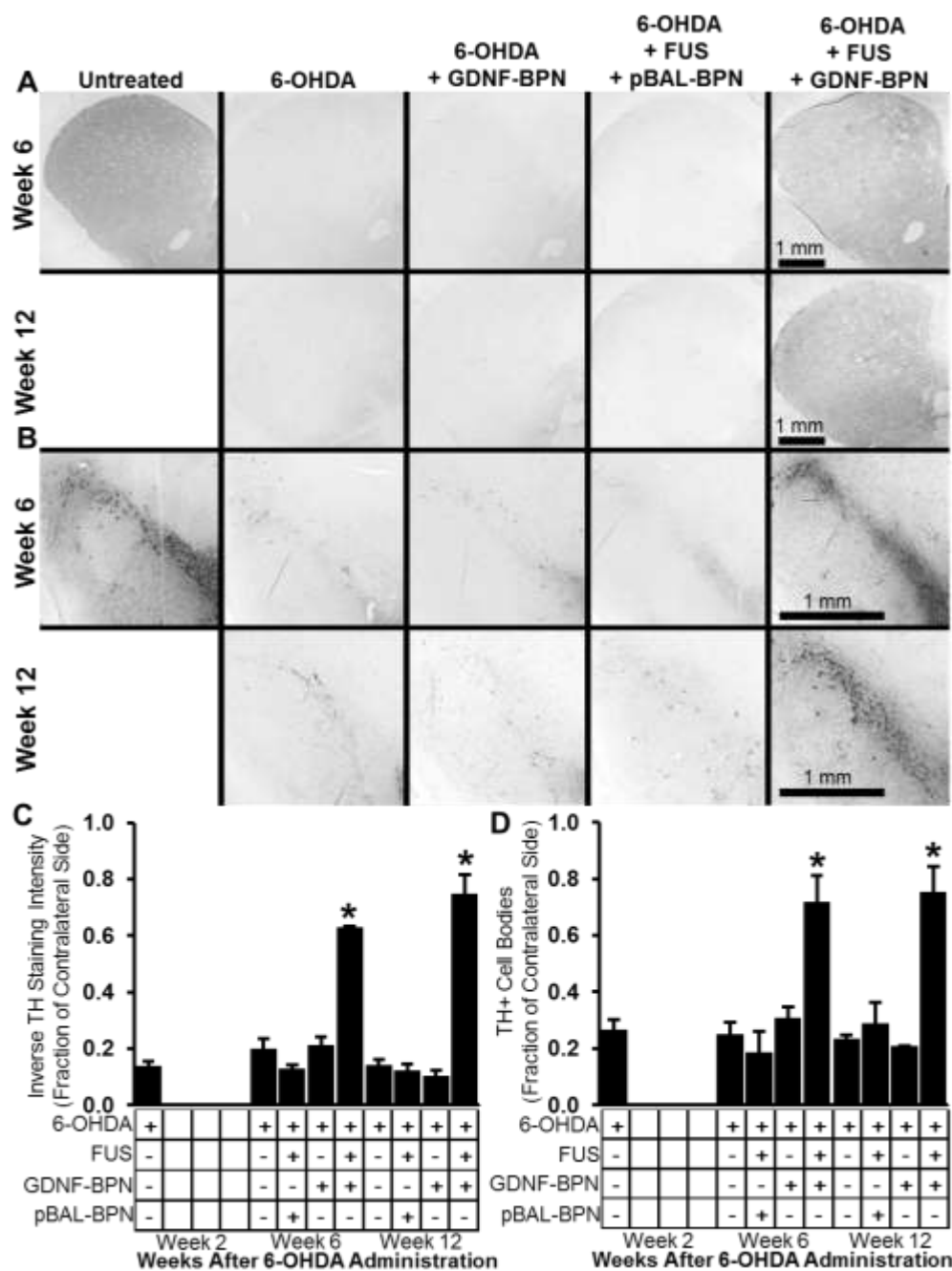


Figure 4.4. Delivery of GDNF-BPN to the striatum with FUS increases dopaminergic neuron density in the striatum and SNpc. Representative images of TH-stained coronal sections through the striatum (A) or SNpc (B) at either week 6 (top row) or week 12 (bottom row) after 6-OHDA administration. Bar graphs show inverse TH staining intensity (C) or TH⁺ cell number (D) normalized to contralateral. $n = 5$ (6-OHDA + FUS + GDNF-BPN) or $n = 4$ in each group and time point. * $p < 0.05$ vs. all groups at same time point.

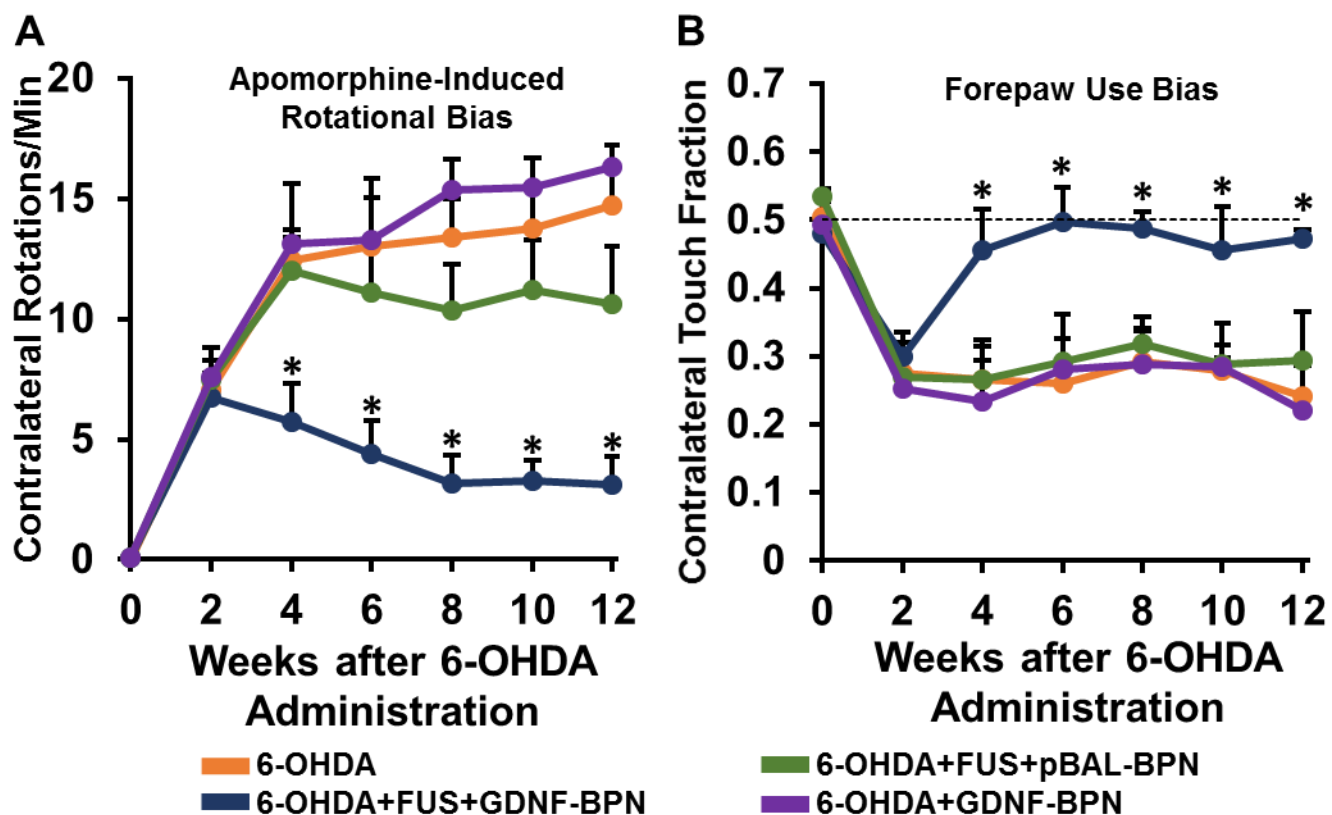


Figure 4.5. Delivery of GDNF-BPN with FUS restores locomotor function in PD rats. (A) Line graph of average contralateral rotations per minute after apomorphine administration. (B) Line graph of contralateral touch fraction in the forepaw use bias test. $n > 14$ in each group at Weeks 0 through 6; $n > 7$ in each group at Weeks 8 through 12. * Significantly different than all other groups at the same time point ($p < 0.01$).

4.9 Chapter 4 Supplemental Figures

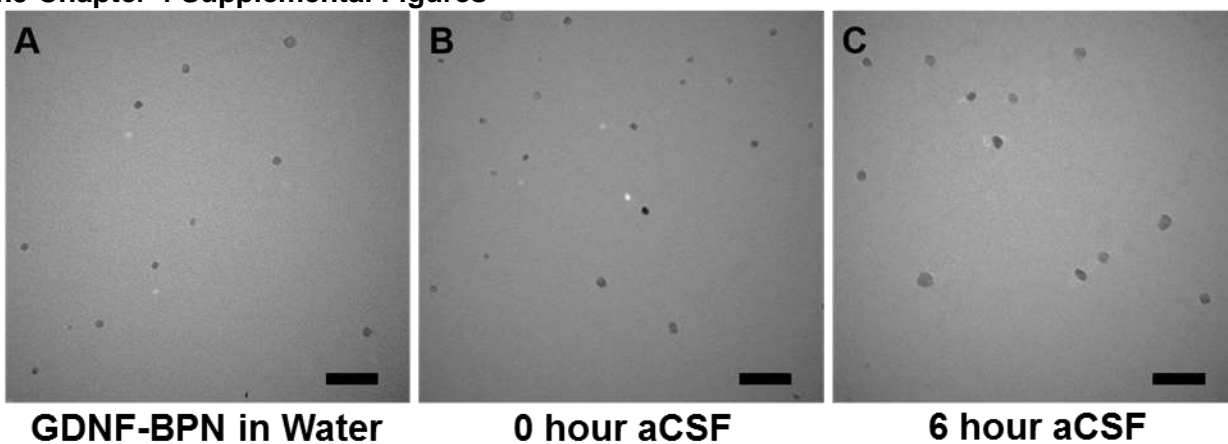


Figure 4.S1. GDNF-BPN are colloiddally stable when incubated in water or artificial cerebrospinal fluid (aCSF). Representative transmission electron microscope images of GDNF-BPN in (A) ultrapure water, (B) immediately after mixing in aCSF, or (C) after 6 hours of incubation in aCSF. Scale bar = 200 nm.

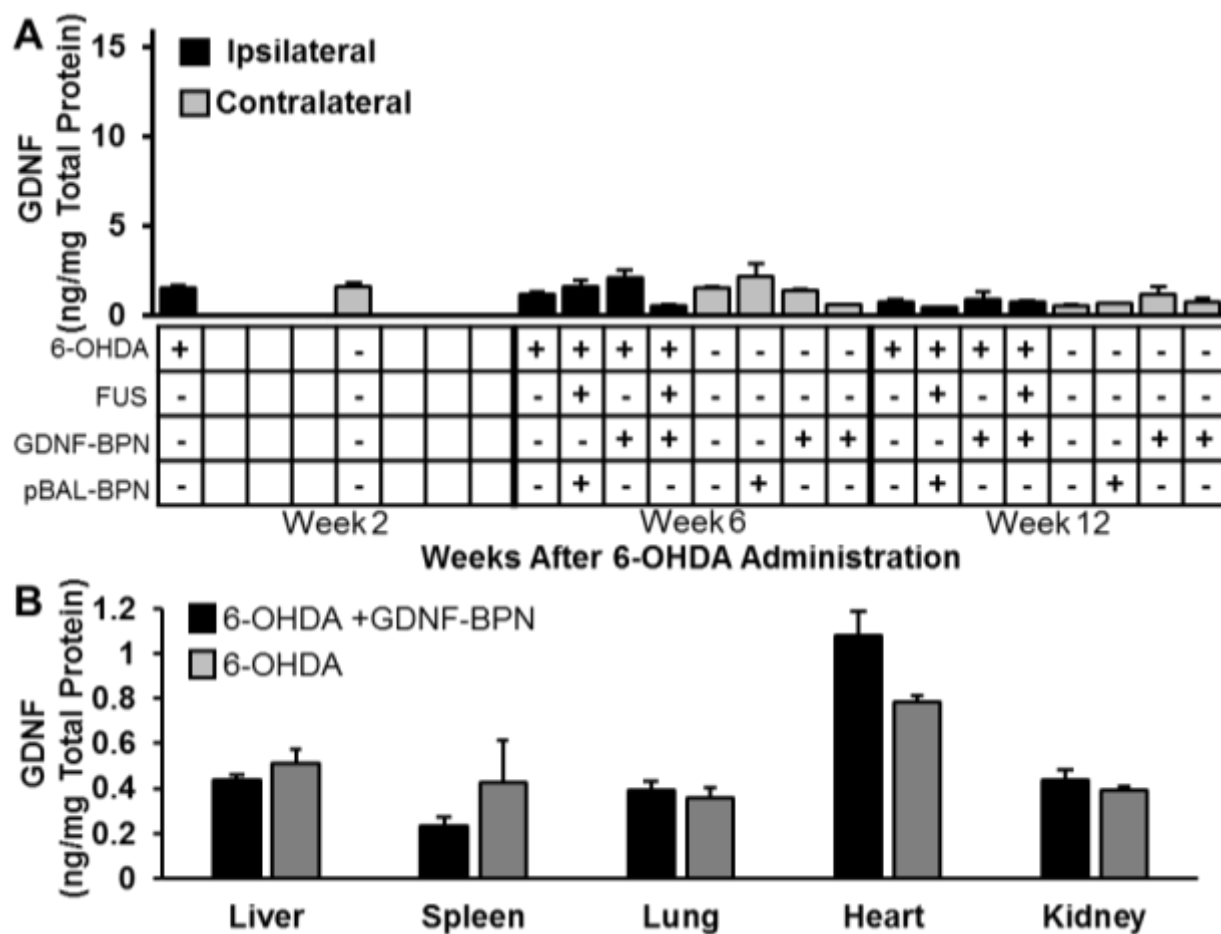


Figure 4.S2. FUS-mediated delivery of GDNF-BPN to the striatum of PD rats does not change GDNF protein levels in the SNpc or other major organs. (A) Bar graphs show GDNF protein levels in the ipsilateral (black) and contralateral (gray) SNpc. $n = 5$ (6-OHDA +FUS +GDNF-BPN), $n = 4$ (6-OHDA only) or $n = 3$ in each group at each time point. (B) Bar graph shows GDNF protein levels in animals 6-OHDA treated (gray) or 6-OHDA + GDNF-BPN treated (black) animals. $n = 3$ (6-OHDA) or $n = 5$ (6-OHDA + GDNF-BPN).

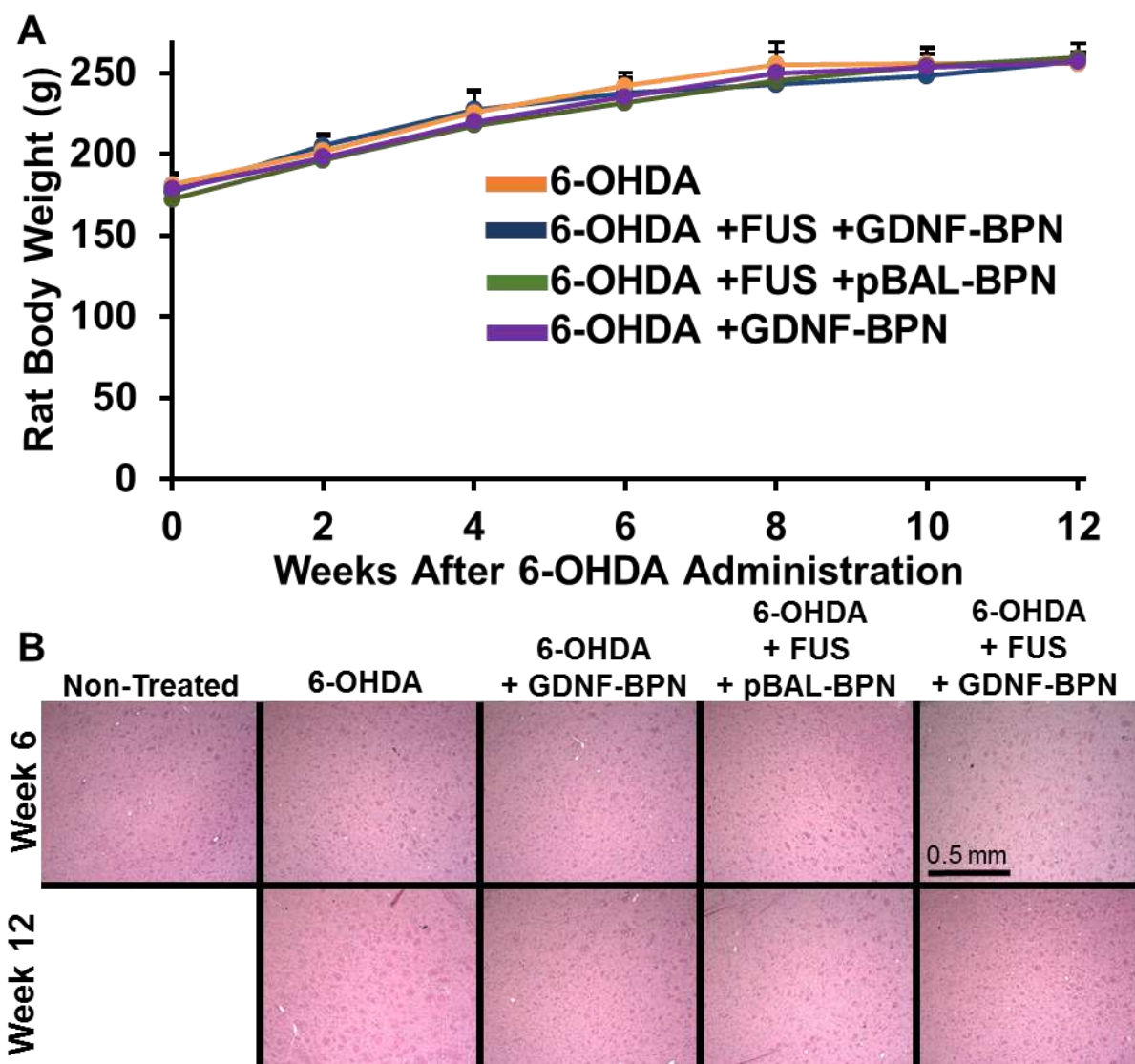


Figure 4.S3. FUS-mediated delivery of GDNF-BPN to the striatum of PD rats does not lead to systemic or local toxicity. (A) Line graph shows animal weights for all animals used in the study. $n > 14$ at each group at Week 0 through 6; $n > 7$ at each group at Week 8 through 12. (B) Representative images from H&E stained sections through the striatum 6 or 12 weeks after 6-OHDA administration. No signs of toxicity beyond the needle injection tract were found.

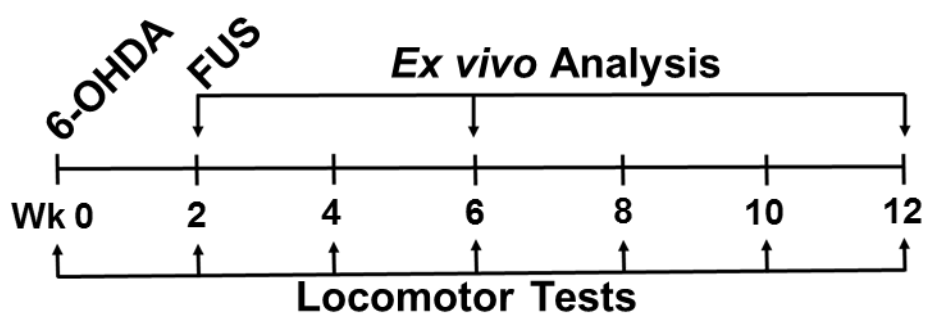


Figure 4.S4. Time schedule of study. Rats received intrastriatal 6-OHDA at week 0 and locomotor function was examined 1-3 days prior to 6-OHDA administration and biweekly with apomorphine-induced rotational behavior and cylinder forepaw use bias tests. Animals were sacrificed at week 2, 6 or 12 and brains were either homogenized or fixed/sectioned for further *ex vivo* analysis.

4.10 Chapter 4 Tables:

Table 4.S1. Dopamine Metabolites in the Ipsilateral Striatum

DOPAC (ng/mg tissue)	6-OHDA	6-OHDA + GDNF-BPN	6-OHDA + FUS + pBAL-BPN	6-OHDA + FUS + GDNF-BPN
Week 2	Not Detected			
Week 6	0.194 ± 0.083	0.109 ± 0.047	0.309 ± 0.128	2.140 ± 0.200*
Week 12	0.887 ± 0.107	0.272 ± 0.088	0.393 ± 0.043	3.343 ± 0.657*

HVA (ng/mg tissue)	6-OHDA	6-OHDA + GDNF-BPN	6-OHDA + FUS + pBAL-BPN	6-OHDA + FUS + GDNF-BPN
Week 2	0.071 ± 0.011			
Week 6	0.349 ± 0.072	0.080 ± 0.015	0.087 ± 0.034	0.375 ± 0.023‡
Week 12	0.289 ± 0.050	0.132 ± 0.028	0.104 ± 0.019	1.24 ± 0.351*

* P < 0.05 vs all other groups at the same time point. ‡ p < 0.05 vs 6-OHDA + FUS + pBAL-BPN and 6-OHDA + GDNF-BPN groups at the same time point.

Chapter 5:**Mechanisms and Applications of Augmented Brain-Penetrating Nanoparticle Dispersion and Non-Viral Transfection via Brain Tissue Pre-Treatment with Pulsed Focused Ultrasound**

5.1 Abstract

Microbubble activation with focused ultrasound (FUS) remains uniquely capable of non-invasive, image-guided, and spatially targeted delivery of systemically administered gene vectors to the CNS; however, we postulate that therapeutic efficacy can be further improved by enhancing delivery and/or uptake through modulation of the targeted tissue. Toward that end, we tested a series of pulsed ~1 MHz FUS “pre-treatment” regimens for their ability to enhance dispersion of reporter gene vector brain-penetrating nanoparticles through healthy CNS and brain tumor (U87 glioma) tissue and improve uptake/expression after delivery across the blood-brain barrier (BBB) with FUS and microbubbles. Pre-treatment with 1 MHz pulsed FUS, both in the presence and absence of intravascular microbubbles, led to significant increases (>76% in both normal brain tissue and U87 tumors) in transfection volume after convection enhanced delivery of BPN. Importantly, the FUS pre-treatment effect was largely attenuated in transient receptor potential ankyrin type 1 (TrpA1) knockout mice, but not in transient receptor potential vanilloidin type 1 (TrpV1) knockouts, thereby identifying TrpA1 as a requisite mechanosensor in this response. Pre-treating brain tissue with pulsed FUS prior to systemic administration of luciferase gene-bearing BPN and opening of the BBB with FUS and microbubbles led to a significant (up to 5-fold) increase in bioluminescence compared to non-pre-treated controls. Pre-treatment did not affect subsequent stable and inertial cavitation doses during BBB opening, and detailed histological and immunohistochemical analyses revealed no evidence of neural damage, ischemic injury, astrogliosis or microgliosis. We conclude that FUS pre-treatment of brain tissue is a safe adjunct approach that is capable of markedly augmenting nanoparticle-mediated dispersion and transfection via activation of mechanosensitive TrpA1 channels.

5.2 Introduction

Gene therapy has the potential to slow or reverse pathology in numerous neurological diseases including Parkinson's disease, Alzheimer's disease and brain tumors (226). However, homogenous and widespread gene vector distribution in the brain is hampered by the presence of a dense and nanoporous extracellular matrix (ECM) (8) as well as the blood-brain barrier (BBB), which prevents nearly 100% of systemically circulating molecules larger than ~400 Da from entering the brain (5). Indeed, despite the promise of viral and non-viral gene vectors to reverse pathology in small animal models of neurological diseases (252, 253, 288), gene therapy trials have had limited success in clinical trials. It has been hypothesized that therapeutic outcomes of these studies, which largely have relied on direct injection strategies, can be improved by enhancing delivery efficiency (145) and transfection volume (289) as well as treating patients at an earlier (or prodromal) stage prior to the onset of irreversible pathology (284).

In order for macromolecules to disperse widely in the brain parenchyma, they must traverse the brain's ECM. Consisting of a dense lattice of electrostatically charged molecules including proteoglycans, hyaluronan, and tenascins, the ECM hampers diffusion of gene vectors via steric and/or adhesive interactions. Moreover, tumors like glioblastoma multiforme (GBM) contain dense and heterogeneous networks of collagen and high interstitial pressures that further limit macromolecule diffusion. As a result, until recently, it was thought that the upper size limit to diffusion in healthy brain was as small as 64 nm (197). While recent studies using non-adhesive nanoparticles coated with dense coats of polyethylene glycol in a "brain-penetrating" nanoparticle (BPN) formulation have revised the upper size limit to ~115 nm (8), treatments of large volumes of diseased tissue remains a significant hurdle.

It is now well established that focused ultrasound (FUS) and microbubbles (MBs) is uniquely capable of temporary, targeted, and spatially localized disruption of the BBB, allowing agents as large as ~100 nm in size to extravasate into the CNS (7). Intravascularly circulating ultrasound contrast agent MBs, when exposed to FUS, exert mechanical shear forces as well as circumferential strain on the capillary endothelium. Barrier function to small (<1 nm) magnetic resonance (MR)-contrast agents is fully restored within 4-6 hours(61). Importantly, under guidance of MR-imaging, FUS systems are capable of exquisite spatial targeting, peri-operative treatment monitoring and post-operative confirmation of success. Use of MR-image guided FUS and MBs to open the BBB is in early stages of human clinical trials for GBM (NCT02986932) and Alzheimer's disease (NCT02986932) and high intensity FUS is now FDA approved for use in humans with Essential Tremor(259) and is in clinical trials for numerous other neurological conditions.

In addition to its ability to target delivery of therapeutic agents across the BBB, FUS may also enhance distribution and/or transfection of therapeutic agents even after they cross the BBB. Ultrasound treatments are now being explored preclinically to enhance dispersion of therapeutic agents when applied simultaneously during direct injection of small molecule tracers(217, 218) or liposomes(219) into rodent or non-human primate brain. More recently studies have suggested that exposure of rodent brain to FUS and MBs prior to direct infusion of adeno-associated viral vectors enhanced transduction volume(220), and ultrasound exposure of *ex vivo* brain slices revealed increases in perivascular and extracellular spaces of the brain(221). Pulsed FUS has also been shown to increase squamous cell carcinoma flank tumor porosity and decrease intratumoral interstitial fluid pressure(222). Indeed, while the mechanism has been hypothesized to be primarily non-thermal(221), additional investigation is required to better understand cellular and tissue-level responses to FUS.

Transient receptor potential ankyrin type 1 (TrpA1) and transient receptor potential vanilloidin type 1 (TrpV1) are calcium channels widely expressed in the brain parenchyma, including in astrocytes(290–293) and endothelial cells(294), and known be activated by mechanical(295) or thermal (>42°C) stimuli(296), respectively. While calcium mediated gliotransmission in the CNS remains controversial(297), it has been hypothesized that calcium waves in astrocytes could constitute an extra-neuronal signaling system in the brain.

In the current study, we investigate how pre-treatment of rodent brain with FUS can a) enhance dispersion of ZsGreen-BPN in both healthy rodent brain, as well as the U87 model of human glioma both in the presence and absence of ultrasound contrast agent MBs, b) identify a role for mechanically activated TrpA1 channels in this increased transport and c) demonstrate how FUS pre-treatment can enhance delivery and/or transgene expression after delivery of Luc-BPN across the BBB with FUS and MBs in a clinically relevant strategy to enhance FUS mediated delivery of gene vectors to the brain.

5.3 Results

5.3.1 Characterization of gene vector BPN

ZsGreen and Luciferase (Luc) bearing plasmids were engineered as previously described(186, 265, 288). ZsGreen and luciferase are driven by the ubiquitously active CMV or β -actin promoter, respectively. ZsGreen or Luc plasmids were condensed with a blend of polyethylenimine (PEI) and PEI-PEG to yield ZsGreen-BPN or Luc-BPN, respectively. The high density of PEG in these systems has been shown to greatly reduce, if not eliminate, *in vivo* toxicity caused by the cationic nature of PEI(148, 186, 265). Both ZsGreen-BPN and Luc-BPN were small (hydrodynamic diameter ≤ 45 nm) and near neutrally charged (ζ -potential ≤ 1 mV), (Table 1). Nanoparticles containing similar size and charge characteristics penetrate rapidly through brain tissue when infused with CED and provide widespread and uniform reporter gene expression(298). Previous studies showed that BPN with similar physiochemical characteristics were stable for at least 6 hours after being incubated in artificial cerebrospinal fluid at 37°C(288).

5.3.2 Pre-exposure of rodent brain to pulsed FUS prior to convection enhanced delivery of ZsGreen-BPN, both with and without MBs, improves volume of distribution.

Sprague-Dawley rats were pre-treated in the right striatum with (i) FUS (1 MHz, 1.2 MPa, 1% duty cycle, 4 minutes), (ii) FUS at low PNP (1 MHz, 0.4 MPa, 5% duty cycle, 10 minutes) or (iii) FUS + MBs (1 MHz, 0.6 MPa, 0.5% duty cycle, 2 minutes, 1×10^5 MB/g) immediately prior to CED infusion of ZsGreen-BPN. Listed PNPs are measured in water, so they do not account for attenuation caused by the skull and other tissue. ZsGreen-BPN transfected tissue volume was assessed at the 48-hour time point, corresponding to the approximate time of maximum transgene expression (Figure 1A). Application of low PNP

FUS had no significant effect on ZsGreen-BPN transfection volume and FUS + MBs without infusion of ZsGreen BPN did not lead to any increase in tissue fluorescence (Figure 1B and 1C). ZsGreen expression was not found in the contralateral left striatum in any animal. Importantly, FUS and FUS + MBs led to, respectively, 44% and 142% increases in transfection volume compared to animals receiving a CED infusion of ZsGreen-BPN without FUS pre-treatment (Figure 1B and 1C). Moreover, pre-treatment with FUS + MB led to a 67% increase in transfection volume compared to rats pre-treated with FUS.

5.3.3 Pulsed FUS enhances transfection volume by activating TrpA1 channels, but not TrpV1 channels.

C57BL/6, TrpA1^{-/-}, and TrpV1^{-/-} mice were pretreated in the right striatum with FUS (1 MHz, 1.2 MPa, 1% duty cycle, 4 minutes) or FUS+ MB (1 MHz, 0.45 MPa, 0.5% duty cycle, 2 minutes, 1x10⁵ MB/g) immediately prior to CED. As previously noted, PNPs were measured in water. PNPs were reduced in the FUS + MB group in the mice compared to the rats to account for differences in attenuation caused by skull thickness differences. In C57BL6 mice pre-treated with FUS or FUS + MB, transfection volume increased by 77% and 74%, respectively (Fig 2A). In a similar fashion, transfection volume increased in TrpV1^{-/-} mice by 54% and 88%, respectively, in the FUS and FUS + MB groups when compared to animals receiving CED infusion of ZsGreen-BPN without FUS pre-treatment FUS (Figure 2). However, transfection volume in TrpA1^{-/-} mice was not significantly augmented by pre-treatment with FUS or FUS + MB. When compared to wild-type C57BL/6 mice, this constitutes 87% and 68% attenuations in the FUS and FUS + MB mediated increases in transfection volume, respectively.

5.3.4 Pulsed FUS enhances transfection volume after CED administration of ZsGreen-BPN into the U87 model of human GBM.

Athymic nude mice were inoculated in the right striatum with intracranial U87mg glioma xenograft stably expressing mCherry (Figure 3a). Tumors were imaged with T1 contrast MRI to determine precise tumor location on day 15. On day 16, tumors were pre-treated with FUS or FUS + MB immediately prior to CED infusion of ZsGreen-BPN. FUS and FUS + MB led to, respectively, 113% and 112% increases in the volume of U87 tumor transfection compared to animals receiving a CED infusion of ZsGreen-BPN, but no FUS pretreatment (Figures 3B and C).

5.3.5 Application of pulsed FUS to brain tissue before trans-BBB delivery of Luc-BPN markedly enhances transfection.

FUS mediated BBB opening and Luc-BPN delivery treatments in rats were operated under the guidance of peri-operative MRI. Pre-FUS T2-weighted MR images were acquired and used to plan 3 equally spaced sites in the right or left striatum to be pre-treated with FUS and, after pre-treatment, used to plan 3 equally spaced sites in both the left and right striatum to be treated with FUS + MB (Figure 4a). Pre-treatment FUS was operated at either 2 or 4 MPa PNP (1.11 MHz, 2.25% duty cycle; 10 min duration). BBB opening was then generated after i.v. MB injection using FUS (0.55 MPa PNP, 1.11 MHz, 0.5% duty cycle, 1e5 MB/g, 2 min duration). PNPs were measured in water and do not account for attenuation caused by skull and other tissue. *In vivo* and *ex vivo* bioluminescence images were acquired at day 2 or 3 after FUS treatments, respectively, corresponding to the approximate days of peak transgene expression (Figure 4B). Bioluminescence was localized to the approximate volume treated with FUS + MBs in both *in vivo* and *ex vivo* imaging (Fig 4B). Importantly, pre-treatment with 2 MPa (Fig 4C) or 4 MPa (Fig 4D) pulsed-

FUS led to 1.46- and 5.74-fold increases in bioluminescence (Fig 4E), respectively, compared to the contralateral striatum which did not receive FUS pre-conditioning.

5.3.6 Passive cavitation detection reveals no change in cavitation detected during BBB opening.

Acoustic emissions were collected via a listening hydrophone during all Luc-BPN delivery procedures. Stable cavitation dose (SCD) and inertial cavitation dose (ICD) were calculated during FUS + MB treatment to open the BBB. SCD and ICD were not statistically different in the pre-treated striatum compared to the contralateral striatum, which received FUS + MB, but not pre-treatment FUS (Fig 6).

5.3.7 Histology

Three days after FUS treatment, immediately after *ex vivo* imaging for transgene expression, brains were fixed and sectioned. Sections from animals pre-treated with FUS prior to BBB-opening and delivery of Luc-BPN with FUS were acquired at 300 μm spacing, representing the entire depth of the striatum. Sections were stained with H&E or immunolabeled for astrocytic [glial fibrillary acidic protein (GFAP)] and microglial markers of inflammation/toxicity (Iba1) (Figure 7). H&E, GFAP, Iba1 stained sections were scored for signs of toxicity by a board certified neuropathologist (JWM) blinded to the treatment conditions. No evidence of neural damage, ischemic injury, astrogliosis or microgliosis was found. A minority (4/10 at 4 MPa and 1/7 at 2 MPa) of the sections were found to have small focal parenchymal microhemorrhages; although these may have been caused by handling of non-perfused tissue during *ex vivo* bioluminescence imaging. Comparisons of grayscale intensity of GFAP stained images acquired through the depth of the left and right

striatum revealed no changes in GFAP staining intensity amongst any group, including naïve, non-treated animals.

5.4 Discussion

Despite success in pre-clinical models, clinical gene therapy studies have largely failed to meet primary outcomes due to incomplete or heterogeneous delivery to targeted structures or invasive surgical strategies that preclude treatment of early stage patients(254, 255). Here, we demonstrate the ability of FUS to increase brain tissue pore spaces in a TrpA1 dependent manner, thereby markedly expanding volume of transfection when applied before CED infusion of ZsGreen-BPN. Next, in a clinically relevant treatment paradigm, we show that FUS pre-treatment can lead to up to ~5-fold enhancement in bioluminescence after delivery of Luc-BPN to the rodent striatum with FUS and MBs without signs of toxicity. The non-invasive and spatially-targeted nature of FUS as a strategy for homogenous and robust CNS gene delivery makes it an attractive approach that may eventually be translated to the clinic.

5.4.1 Rationale for Testing Pulsed FUS as a Means for Enhancing Transfection in the CNS

In vivo gene therapy is finally reaching FDA approvals (299–301), including for use in the CNS(301). The restrictive nature of the BBB has so far precluded widespread application of systemically administered gene vectors. For this reason, intraparenchymal infusions have remained the gold standard. Unfortunately, intraparenchymal injection strategies are hampered by low volumes of distribution(302), as well as by risk and invasiveness (144, 255). Volumes of distribution can be enhanced with convection enhanced delivery (CED) strategies, where convective flow away from infusion catheters

can enhance infusate dispersion; however, clinical results have remained largely unsuccessful(303). Volumes can be enhanced even further using multi-port catheters, however, additional catheters increases invasiveness as well as risk of damage including significant edema(144) from the catheter placement. In order to avoid these complications, novel viral (304, 305) and non-viral vectors engineered with BBB-targeting ligands(306, 307) capable of crossing the BBB after systemic administration have each shown promise in animal disease models. However, in order to achieve efficacy after systemic administration, large doses are required(308), leading to concerns about systemic toxicity and side effects resulting from off-target delivery. Additional hurdles, including limited packaging capacity and difficulty in scale-up(172), also remain. Less invasive strategies capable of homogenous and widespread gene vector delivery are required.

5.4.2 Improving Transfection Volume in the CNS by Combining Ultrasound and Direct Injection

In this study, we demonstrate how FUS can augment volume of transfection of non-adhesive gene-bearing BPN when applied prior to CED infusion in rats, mice, and the U87 model of human glioma. FUS has recently been explored as an adjunct strategy to enhance dispersion in CNS tissue. Toward this end, numerous studies aimed at increasing agent dispersion in the brain have applied ultrasound during infusion with cannulas equipped with ultrasound transducers(217, 218, 309). While these studies showed an increased volume of distribution in animals treated with ultrasound, this effect has been attributed to the acoustic radiation force driving infusate through the brain tissue. More recently, application of high-duty cycle (~0.36 MPa, 10% duty cycle) pulsed ultrasound was shown to increase ECM pore spaces and perivascular spaces(221). In the current study, we found that application of FUS at a similar frequency and pressure (1 MHz, 0.4 MPa, 5% duty cycle) did not significantly affect the volume

of transfection when applied before CED infusion of ZsGreen-BPN. However, when FUS pretreatment was applied at a greater PNP (1 MHz, 1.2 MPa, 1% duty cycle), we found that pretreatment with FUS increased volume of transfection robustly across multiple species, including 1.77-fold in mice, 1.44-fold in rats, 1.77-fold in mice and 2.13-fold in U87 human tumors implanted into mice. Another study used intravascularly circulating MBs to enhance transfection volume, wherein application of FUS and MBs (1.5 MHz, 0.72 MPa, 5% duty cycle, $\sim 2.5 \times 10^6$ MB/g) prior to direct injection of reporter gene-bearing adeno-associated virus (AAV) into a mouse brain, enhanced transduction volume by ~ 3 -fold(220). The current study found a 2.41-fold increase in rats pre-treated with FUS and MBs (0.6 MPa, 0.5% duty cycle, 1×10^5 MB/g), 1.76-fold increase in mice (1 MHz, 0.45 MPa, 0.5% duty cycle), as well as a 2.11-fold increase U87 human glioma tumors implanted in mice (0.45 MPa, 0.5% duty cycle).

MBs are typically used for FUS-mediated BBB-opening due to their ability to reduce acoustic energy required to open the BBB and, importantly, largely confine the mechanical effects of FUS to the vasculature(46). MBs, when exposed to FUS, expand during rarefaction and contract during compression creating mechanical forces on the vascular wall including shear forces(47) and microstreaming(48). For this reason, BBB opening protocols with FUS and MBs are typically operated at relatively low FUS pressures and duty cycles and are not typically associated with thermal effects. Indeed, despite limiting most mechanical effects to the vasculature during the FUS + MB pretreatment, our study found that this pretreatment increased ZsGreen-BPN volume of transfection after infusion into the parenchyma, suggesting that the physiological response not restricted to the vasculature. Moreover, even in the absence of MBs, FUS can transfer momentum to the propagating medium(310), creating an acoustic radiation force capable of causing small tissue displacements on the order of hundreds of microns(311) that are not confined to the vasculature(312). Tissue deformations during FUS pulses and restoration to its normal state after the end of the pulse can each occur in as little as 6-8 ms

(312). It has been postulated that mechanical shear forces created by the acoustic radiation force can disrupt ECM components and enlarge perivascular and ECM pore spaces(221).

5.4.3 Increased volume of transfection after FUS Pre-treatment is attenuated in TrpA1 knockout mice.

Our FUS pre-treatment strategies yielded 1.77-fold and 1.74-fold increases in volume of transfection in C57BL6 mice pre-treated with FUS (1.2 MPa, 1% duty cycle) and FUS + MB (0.45 MPa, 0.5% duty cycle, 1×10^5 MB/g), respectively, compared to animals receiving CED infusion of ZsGreen-BPN, but no FUS. However, in TrpA1^{-/-} animals, transfection volumes were not significantly augmented with FUS pre-treatment and, when considered as a function of fold-increase over CED transfection volume, TrpA1^{-/-} mice exhibited significantly diminished transfection volumes when compared to wild-type controls. Calcium signaling in the brain has been shown to control a variety of cellular and tissue level functions(294). TrpA1 and TrpV1, two calcium channels known to be expressed on astrocytes(290–293), are activated by mechanical (295) and thermal (313) stimuli, respectively, causing calcium transients that can propagate through astrocytes and into neighboring astrocytes that are connected through gap junctions(314). Astrocytic calcium transients have been linked to numerous changes in the brain, including a) changes in blood flow via signaling through astrocytic end foot processing surround the BBB (315–317), b) changes in astrocyte morphology (318, 319), c) alteration of extracellular homeostasis(320), and d) alteration of neuronal activity through gliotransmitters including glutamate (321, 322), ATP (323), D-serine (324), and GABA(325).

Increased agent dispersion after FUS pre-treatment has been hypothesized to have a non-thermal mechanism(221, 311). This is due mainly due to observation of increased ECM pore spaces and perivascular spaces following a pulsed FUS regimen that, similar to the pulsed FUS regimens of the current study, is not typically associated with heating.

Application of FUS with short pulses and relatively long off-times minimizes heat accumulation and, importantly, repeated pulsing can cause cyclic tissue deformation and relaxation caused by the acoustic radiation force. Consistent with this paradigm, the current study demonstrated that animals lacking the mechanosensitive TrpA1 channel attenuated the FUS pre-treatment augmented ZsGreen-BPN dispersion compared to animals lacking the thermosensitive TrpV1 channel and wild-type C57BL6 controls.

5.4.4 FUS Pre-treatment as a Strategy to Enhance Glioma Transfection

In addition to enhancing volume of transfection in healthy tissue, FUS pre-treatment also augmented volume of transfection by 2.13- and 2.11-fold in the FUS + MBs (0.45 MPa, 0.5% duty cycle, 1×10^5 MBs/g) and FUS (1.2 MPa, 1% duty cycle) groups, respectively. Limited drug penetration into tumors remains a major obstacle for treatment of brain tumors(192) including GBM(326), due to a dense and heterogeneous ECM as well as high interstitial fluid pressures. Extremely dense collagen can obstruct transport of macromolecules known to diffuse readily through healthy tissue(327). Interestingly, one recent study using acoustic radiation force imaging showed that pulsed FUS exposure reduced tissue elasticity and interstitial fluid pressures and increased penetration of fluorescent tracer nanoparticles(222), however, this study used FUS PNP of 8.95 MPa and a duty cycle of 5%, more than 7-fold greater than the PNPs used in the current study. Unfortunately, while this study did not assess thermal changes, temperature rise with similar FUS intensities was shown in a previous study to be $<5^\circ\text{C}$ (328). Nonetheless, It has been postulated that the increase fluid conductivity of the tumor after FUS pre-treatment results in more rapid fluid flow away from the high pressure tumor core to the relatively lower pressure tumor periphery(329). High interstitial fluid pressures remain a major barrier to uptake of intravascularly circulating therapeutic agents into tumors(330), which is typically dependent on differences in capillary hydrostatic pressure and tumor interstitial fluid

pressure(331). The current study demonstrates increased penetration of non-adhesive ZsGreen-BPN at with FUS operated at lower 0.45 MPa PNP and 1% duty cycle. Importantly, a similar increase in transfection volume was achieved with FUS + MB treatments with similar treatment parameters (0.45 MPa, 0.5% duty cycle, 1×10^5 MB/g) to BBB-opening procedures.

FUS is also being explored clinically to enhance delivery of systemically administered therapeutic agents to tumors(7, 332). Recent studies using pre-treatment FUS have demonstrated increased nanoparticle uptake(333) and penetration(334) into tumors via the enhanced permeability and retention effect after systemic administration. FUS pre-treatment, therefore, may be able to enhance FUS + MB delivery strategies.

5.4.5 Pretreatment of CNS tissue with FUS to enhance delivery of systemically administered agents with FUS and MBs.

MB activation with FUS constitutes a non-invasive and spatially localized delivery strategy capable of temporary opening of the BBB to agents as large as 100 nm. This strategy has been shown to be safe and BBB barrier function to MR contrast agents is typically restored within 4-6 hours after treatments. FUS and MBs has been used by other investigators to deliver naked plasmid(156, 157) and AAV(155, 163) across the BBB, leading to significant transgene expression in the CNS. We have previously demonstrated the ability of FUS and MBs to target the delivery of Luc-BPN or BPN bearing the mCherry reporter gene into the brains of healthy rats, leading to exceptionally homogenous transgene expression limited to the site of FUS application, without signs of toxicity or astrocyte activation(265). Importantly, this strategy was able to restore multiple indicators of neurodegeneration in a rat model of Parkinson's disease after delivery of BPN bearing a gene for the glial cell-derived neurotrophic factor(288).

Despite the success of FUS and MBs to deliver therapeutic gene vectors into the CNS in pre-clinical models, delivery efficiency remains low(335). This study has demonstrated the

ability of FUS pre-treatment to enhance dispersion of non-adhesive gene vector BPN after CED infusion in the CNS. Moreover, FUS has previously been shown to increase blood flow(333, 336) as well as increase expression of negatively charged heparan sulfate proteoglycans(165), which are known to facilitate PEI based gene vector nanoparticles (337) or AAV(168) entry into cells.

Pre-treatment of the rat striatum with FUS at either 4 MPa or 2 MPa (1.1 MHz, 2.25% duty cycle) immediately prior to opening of the BBB with FUS and MBs (1.1 MHz, 0.5% duty cycle, 1×10^5 MB/g) and delivery of systemically administered Luc-BPN (0.5 μ g/g) led to a 5.74- or 1.46-fold increase in *in vivo* bioluminescence compared to the contralateral hemisphere, in which the BBB was opened with FUS and MBs, but not pre-treated. Consistent with these results, a previous study showed that bioluminescence following systemic administration of Luc-BPN and delivery into skeletal muscle with FUS and MBs was ~10-fold higher than in skeletal muscle receiving a direct injection of the same dose of BPN into 5 evenly spaced sites(148). Another study demonstrated that animals pre-treated with FUS (8.95 MPa, 5% duty cycle) in the hind limb led to a significant (>10-fold) increase in intravascular fluorescent nanoparticle concentration compared to non-pre-treated tissue and that the most extensive effects were seen when nanoparticles were administered immediately after FUS pre-treatment(312). This study did not observe extravascular nanoparticles after FUS pre-treatment, consistent with a pulsing regimen that is predominated by mechanical effects and not thermal effects, which are capable of enhancing nanoparticle extravasation(338).

In the current study, we demonstrate a novel strategy to use FUS pre-treatment to enhance delivery of gene bearing BPN into the CNS that leads to significantly more robust delivery compared to FUS and MB treatment alone. In addition to its non-invasive nature which obviates risks associated with traditional surgery, FUS is capable of exceptionally homogenous and spatially localized delivery over a large volume in the CNS.

5.5 Materials and Methods

5.5.1 Animals

Female Sprague-Dawley rats were purchased from Envigo. Male C57Bl6 as well as the TrpA1 (JAX Stock# 006401) and TrpV1 (JAX Stock# 003770) knockout mice were purchased from Jackson and were originally developed elsewhere (339, 340). Male athymic nude mice were purchased from Charles River. Animals were housed on a 12/12h light/dark cycle, and given food *ad libitum*. Rats were ~180 – 220 g at the time of treatment and mice were ~25 g. Animal experiments were approved by the Animal Care and Use Committee at the University of Virginia and conformed to the National Institutes of Health guidelines for the use of animals in research.

5.5.2 Plasmid Design

The Luc and ZsGreen plasmids (~4 kB) were constructed as previously described using standard molecular biology by Copernicus Therapeutics Inc. (Cleveland, OH) and is described elsewhere (265, 288, 341) (265). Briefly, the Luc plasmid contains the luciferase reporter gene driven by the ubiquitously active β -actin promoter. The ZsGreen plasmid contains the ZsGreen reporter gene driven by the ubiquitously active CMV promoter.

5.5.3 DNA-BPN Fabrication and Characterization

DNA-BPN were fabricated and characterized as previously described (186, 265). Briefly, PEG_{5k}-PEI copolymer was synthesized by conjugating molar excess of 5kDa methoxy-PEG-N-hydrosuccinimide (mPEG-NHS, 5 kDa, Sigma-Aldrich, St. Louis, MO) to primary amine groups of 25 kDa branched PEI (Sigma-Aldrich, St. Louis, MO). The resulting PEI-PEG conjugate possessed a high degree of PEG conjugation (average of 50 PEG chains per PEI molecule). The final product was extensively dialyzed against ultrapure water and the conjugation was confirmed by nuclear magnetic resonance. DNA-BPN were formulated by drop-wise addition of

10 volumes of plasmid DNA to 1 volume of polymer mixture solution of PEI and PEG_{5k}-PEI. DNA-BPN were purified with 3 volumes of ultrapure water to eliminate free polymers, and concentrated to 1mg/ml using Amicon Ultra Centrifugal Filters (100,000 MWCO; Millipore Corp., Billerica, MA). The DNA concentration of DNA-BPN was confirmed using a NanoDrop 2000 spectrophotometer (Thermo Scientific, Waltham, MA). Hydrodynamic diameter, ζ -potential, and polydispersity index of DNA-BPN were measured using Zetasizer Nano ZS (Malvern Instruments, Southborough, MA). Colloidal stability of DNA-BPN was observed with transmission electron microscopy (TEM, Hitachi H7600, Japan) after incubating DNA-BPN in aCSF (Harvard Apparatus, Holliston, MA) at 37 °C for 6 hours.

5.5.4 Microbubble Fabrication and Characterization

Microbubbles used in this study have a similar formulation to Optison (GE Healthcare, Little Chalfont, Buckinghamshire, UK) and its fabrication is described elsewhere(6, 265). In brief, saline containing 1% serum albumin was sonicated (20 kHz, 30 s) with an ultrasound disintegrator (XL2020; Misonix, Farmingdale, NY) with an extended ½-inch titanium probe. The headspace of the vial containing the solution was filled with octafluoropropane gas prior to sonication. Microbubbles were sized and counted using a Coulter Counter (Multisizer 3, Beckman Coulter, Fullerton, CA) and contained an average mean size of 2.5 – 3 microns.

5.5.5 FUS Pre-exposure and Convection Enhanced Delivery

Female Sprague-Dawley rats (180-220 g), male C57Bl6 mice, male TrpA1^{-/-} mice, male TrpV1^{-/-} mice or male athymic nude mice (~25 g) were anesthetized with an intraperitoneal injection of ketamine (40 mg/kg, rats or 80 mg/kg, mice; Fort Dodge, IA) and dexdomitor (0.2 mg/kg, Pfizer, New York, NY) in sterilized 0.9% saline. A tail vein catheter was inserted to allow intravenous injections of microbubbles. Animal heads were shaved and depilated before being secured

prone in a stereotaxic frame (Stoelting, Wood Dale, IL). Rodent heads were ultrasonically coupled to a single element FUS transducer (1 MHz, Olympus, Center Valley, NJ) and positioned such that the ultrasound focus was localized in the right striatum. Animals received an injection microbubbles (1×10^5 MBs/g body weight) followed by 0.1 ml of 2% heparinized saline to clear the catheter. Sonication began immediately after clearance of the catheter.

Sonications in animals pre-treated with FUS with high PNP proceeded at 1 MHz, 1.2 MPa, 1% duty cycle, 10 ms bursts for 4 minutes, and animals pre-treated with FUS with low PNP proceeded at 1 MHz, 0.4 MPa 5% duty cycle, 45 ms bursts for 10 minutes. Sonications in rats pre-treated with FUS and MBs proceeded at 1 MHz, 0.6 MPa, 0.5% duty cycle, 10 ms bursts for 2 minutes and in mice pre-treated with FUS and MBs proceeded at 1 MHz, 0.45 MPa, 0.5% duty cycle, 10 ms bursts, for 2 minutes. Peak negative pressures Peak negative pressure listed are non-derated and do not account for attenuation caused by the skull or other tissue.

Immediately following FUS treatment, animals' heads were cleaned, sanitized and prepared for convection enhanced delivery (CED) surgery. Buprenorphine (0.03 mg/kg, Reckitt Benckiser Healthcare, Hull, UK) was administered to achieve local anesthesia. A midline scalp incision was made, and the skull was exposed. A Neuros syringe (Neuros 1705, Hamilton, Reno, NV) containing a 33g needle and a 1mm step was inserted at 1 mm/min into the injection site in either rats (AP +0.5, ML: +2.8, DV: -3.5), healthy mice (AP: +0.5, ML: +2.0, DV: -2.0) or GBM-bearing mice (coordinates determined based off T1 contrast MRI on the day prior to CED infusion). The rate of infusion was set to 0.33 μ l/min using a frame-mounted syringe pump (UMP3, World Precision Instruments, Sarasota, USA). A total of 19 μ g ZsGreen-BPN in 20 μ l 0.9% NaCl was injected. Five minutes following the completion of the CED, the needle was slowly removed at 1 mm/min and the burr hole filled with sterile bone wax.

5.5.6 Histological Processing and Imaging after Convection Enhanced Delivery

To evaluate volume of distribution of BPN following CED administration, animals were sacrificed 48 hours after CED administration, at the day of approximate peak expression. Rats were perfused via the left and right carotid arteries with 20 mls of 2% heparinized 0.9% saline or mice were perfused via transcardial perfusion with 10 mls of 2% heparinized 0.9% saline followed by 10 mls of Tris-Buffered Saline containing 0.1 g/L calcium chloride. Brains were carefully removed, rapid frozen and stored at -80°C until sectioning. Freshly frozen brains were sectioned coronally into 100 µm sections using a cryostat (1905, Leica, Buffalo Grove, IL). Every other section within 2-3 mm of the injection site was collected on a slide and mounted with permanent mounting medium (P36970, Invitrogen, Carlsbad, USA).

Freshly cut sections were imaged using a Nikon Eclipse TE2000 confocal microscope (Nikon, Melville, NY) under 4x magnification. In order to capture the entire ZsGreen+ site, multiple images were taken and stitched together in montages. Settings, including pinhole size, pixel dwell, digital gain, were carefully selected and maintained through the entire study.

Volume of distribution was quantified using a MATLAB script similar to previously studies(186). Briefly, this script subtracted background fluorescence and thresholded images at 5% of the maximum intensity. The area of distribution on each slice was then multiplied by the slice thickness, and summed to calculate the total volume of vector distribution.

5.5.7 U87mg-mCherry Tumor Inoculation

U87mg-mcherry cells were generated by stably transfecting U87mg cells with a plasmid to express the mCherry fluorescent reporter gene under control of the CMV promoter and were kindly donated by Roger Abounader. Mice were anesthetized with a mixture of ketamine (40 mg/kg, Fort Dodge, IA) and dexdomitor (0.2 mg/kg, Pfizer, New York, NY). The top of the mouse heads were depilated, and the mice were secured prone on a stereotaxic frame (Stoelting, Wood Dale, IL) and the heads were cleans and sanitized for surgery. An incision was

made at the midline of the scalp and the skull exposed. A 10 μ l Hamilton syringe with a 26-gauge needle was loaded with tumor cells (1.5×10^8 cells per ml) and inserted into the injection site (AP: +0.5, ML: +2.0, DV: -3 mm). A total volume of 2 μ l (3×10^5 cells) was injected over 4 minutes. After 1 additional minute the needle was slowly removed from the brain, the burr hole was filled with bone wax, and the incision was closed with sutures.

5.5.8 MRI-guided FUS Delivery of Luc-BPN

Female Sprague-Dawley rats were anesthetized with an intraperitoneal injection of ketamine (40 mg/kg, Zoetis, Fort Dodge, IA) and dexdomitor (0.2 mg/kg, Pfizer, New York, NY) in sterilized 0.9% saline. A tail vein catheter was inserted to allow intravenous injections of Luc-BPN and microbubbles. In a previous study by our group(6), BPN with a similar size and surface chemistry were found to be circulating 24 hours after i.v. administration into rats. Rat heads were shaved and depilated before being secured supine in a degassed water bath coupled to a FUS system (RK-100, FUS Instruments, Toronto, Canada) containing a 10 cm diameter 1.11 MHz single-element annular FUS transducer with a 2.5 mm listening hydrophone mounted at the center. The entire system was placed in a 3T MR scanner (Magnetom Trio, Siemens Medical Solutions, Malvern, PA). A homebuilt 2-inch cylindrical transmit-receive RF coil was placed around the rat's head to maximize imaging SNR. Baseline T2-weighted images were acquired using turbo spin-echo pulse sequences. T2-weighted imaging parameters included: TR/TE = 3600/46 ms, flip angle = $90^\circ/150^\circ$, readout bandwidth = 219 Hz/pixel, 9 slices, thickness = 1 mm, field of view = 50 mm, matrix = 192×192 , turbo factor = 18, 100% phase oversampling, 4 averages, total time = 5:22.

Three evenly spaced targets for the preconditioning FUS treatment were selected in either the left or right striatum from T2-weighted images. Target locations were approximately 5 mm ventral from the top of the skull. Preconditioning FUS sonications were performed at 4 MPa or 2

MPa, 45 ms bursts, 0.5 Hz pulse repetition frequency for 10 minutes. During preconditioning sonications, MR-thermometry was acquired to detect possible changes in temperature.

Immediately following preconditioning FUS sonications, rats were given a co-injection of Luc-BPN (0.5 $\mu\text{g/g}$ body weight) and MBs (1×10^5 MBs/g body weight) followed by 0.3 ml of 2% heparinized saline to clear the catheter. Sonication began immediately after clearance of the catheter. Sonications were performed at 0.55 MPa (not accounting for skull/tissue attenuation) operating in 10 ms bursts, 0.5 Hz pulse repetition frequency and 2 min total duration. Immediately following BBB opening, DCE-MRI was performed to assess changes in gadolinium uptake kinetics. Gadolinium (Magnevist, Bayer Health Care, PA) was injected intravenously at 0.5 $\mu\text{l/g}$ body weight. Animals were removed from the MRI table and placed on a warm pad for 30 minutes prior to reversal of the anesthetic with antisedan (2 mg/kg, Orion Pharma, Espoo, Finland)

5.5.9 Passive Cavitation Detection

Acoustic emissions were detected with a 2.5 mm wideband unfocused hydrophone mounted in the center of the transducer. Acoustic signal was captured using a scope card (ATS460, Alazar, Pointe-Claire, Canada) and processed using an in-house built MATLAB algorithm. To assess inertial cavitation at each burst, frequencies produced by stable cavitation including 300 kHz bandwidth around the fundamental frequency as well as 100 kHz bandwidth surround the harmonics (2f, 3f, 4f), sub-harmonics (0.5f), and ultra-harmonics (1.5f, 2.5f, 3.5f) were filtered and the root mean square of the spectral amplitude was obtained. Stable cavitation was assessed by taking the root mean square of the peak spectral amplitude (V_{rms}) in the frequency bands filtered out for the inertial cavitation calculation. Inertial cavitation dose (ICD) and stable cavitation dose (SCD) were obtained by multiplying V_{rms} values, respectively, by the total sonication time and integrated over the duration of the sonication.

5.5.10 *In Vivo* Bioluminescence Imaging

Two days following FUS-delivery of Luc-BPN, animals were anesthetized and maintained on 2-2.5% isoflurane in oxygen. D-Luciferin (Gold Biotechnology, St. Louis, MO) was administered by intraperitoneal injection at 150 mg/kg. Animals were serially imaged using an IVIS100 imaging system (Xenogen, Alameda, CA, USA). Photons were collected and integrated for a period of 1 minute. Images were processed using Xenogen's Living Image software. Total flux intensities were measured from a region of interest over the FUS targeted region.

5.5.11 *Ex Vivo* Bioluminescence Imaging

Three days following delivery of Luc-BPN, rats were anesthetized and maintained on 2-2.5% isoflurane in oxygen. D-Luciferin (Gold Biotechnology, St. Louis, MO) was administered by intraperitoneal injection at 150 mg/kg. Five minutes after administering D-luciferin, rats euthanized and decapitated. The brains were quickly harvested, dipped in 1 mg/ml D-luciferin and imaged using the IVIS100 imaging system. Photons emitted were collected over 3 min.

5.5.12 Histological Processing for Safety Analysis

Following *ex vivo* bioluminescence imaging, brains were placed in a brain matrix (Stoelting, Wood Dale, IL) and a slice containing the FUS-treated striatum was dissected by cutting two coronal slices 2 and 10 mm from the anterior front of the brain, and fixed in 4% PFA for 48 hours. The striatum were rapidly frozen in OCT and sectioned in a cryostat (Leica, Buffalo Grove, IL). 10-micron thick sections were cut in 30 sections, 100 μ m apart. Every third section was stained with hematoxylin and eosin or immunolabeled against the astrocyte marker, GFAP, or the microglial marker, Iba1. Iba1 slides were scored by a neuropathologist (JWM) blinded to experimental conditions. Grayscale intensity of GFAP images for each section was assessed

with an in-house built MATLAB program and averaged across all sections for both the left and right striatum.

Hematoxylin and Eosin staining was performed on mounted sections according to standard protocols. Tissues were imaged on a bright field microscope (Zeiss, Jena, Germany) equipped with a color CCD Camera (Olympus, Center Valley, NJ). Slides were scored by a neuropathologist (JWM) blinded to experimental conditions.

5.5.13 Immunolabeling and Histology for Safety Analysis

Freshly mounted sections were rinsed in PBS + 0.1% Tween-20 and blocked with 10% horse serum for 1 hour. Sections were incubated overnight with goat anti-Iba1 antibody (Ab5076, 1:500, Abcam, Cambridge, UK) or goat anti-GFAP antibody (Ab53554, 1:500, Abcam) in a humidified chamber at 4°C. Sections were washed in PBS + 0.1% Tween-20 and incubated with Alexa-fluor-647 conjugated donkey anti-goat secondary antibody (Thermo21447, Thermo, Waltham, USA) for one hour and mounted with permanent mounting medium (P36970, Invitrogen, Carlsbad, USA). Sections were imaged on a Nikon Eclipse TE2000 confocal microscope (Nikon, Melville, NY).

5.5.14 Statistical Analysis

Sample sizes for all groups were determined empirically. All statistics were conducted using SigmaPlot software (Version 13.0), which automatically suggests parametric or non-parametric tests depending on the results of normality testing. Statistical significance was set at $p < 0.05$. All values are presented as mean \pm SEM.

5.5.15 Data Availability

The data supporting the findings in the current study are available upon request from the corresponding authors.

5.6 Acknowledgements

Supported by the Focused Ultrasound Foundation, NIH R01 Ca164789, R01 CA197111, R01 EB020147 and R03 EB016784. BPM was supported by F31 EB023090, NHLBI-sponsored Basic Cardiovascular Research Training Grant 5 T32 HL007284 and the Wagner Fellowship. The authors are grateful to Roger Abounader for donating the U87mg-mCherry cell line used in this study.

5.7 Chapter 5 Figures

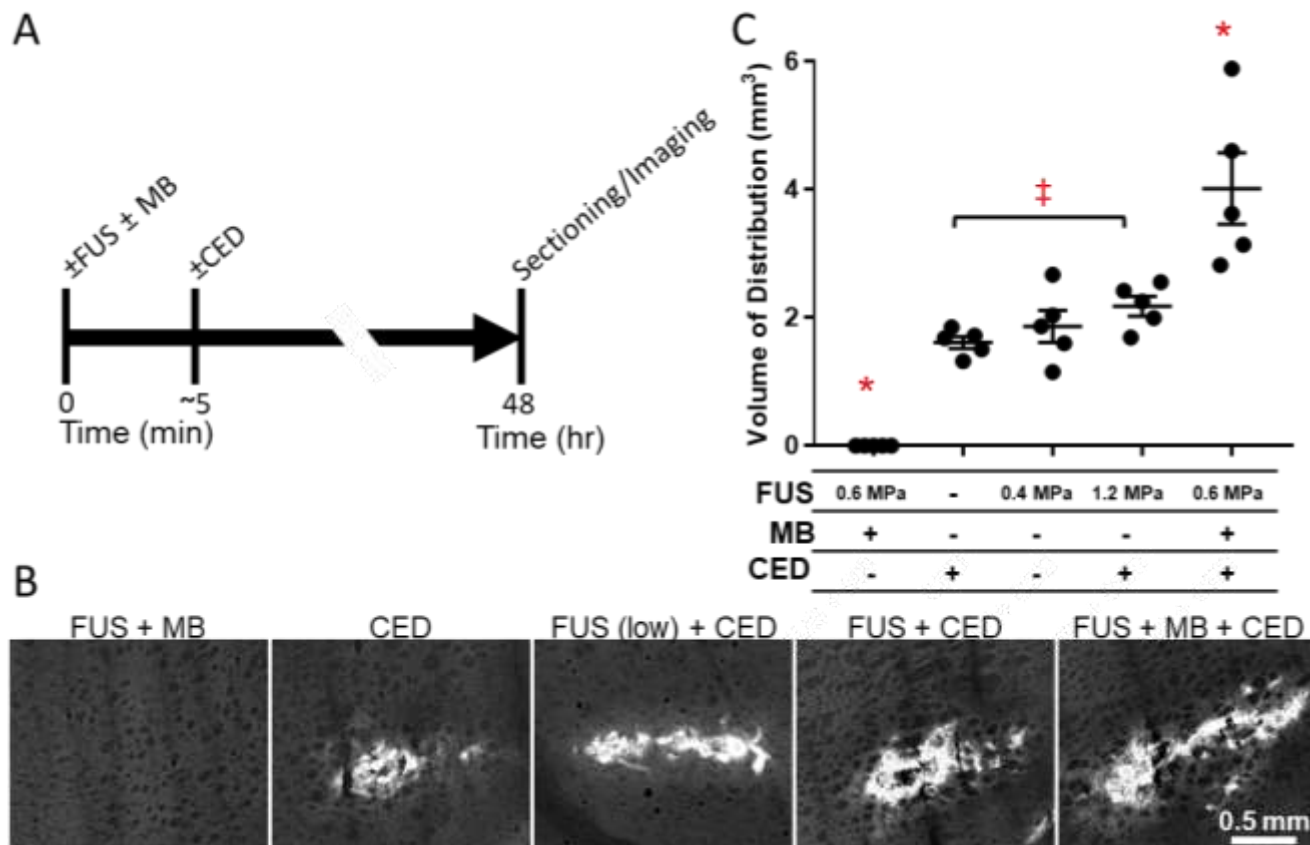


Figure 5.1. Pre-exposure of rat brain to 1.2 MPa FUS or 0.6 MPa FUS with MBs increases volume of distribution after CED administration of ZsGreen-BPN. (A) Timeline of study. Rats received FUS \pm MB just prior to the start of the CED. Animals were sacrificed at 48 hours and their brains sectioned to analyze volume of distribution. (B) Representative images from sections through the striatum after CED administration of ZsGreen-BPN. (C) Bar graph of volume of distribution of ZsGreen-BPN in the striatum after CED administration. $n = 5$ in each group. $*p < 0.05$ vs all groups, one-way ANOVA. $\ddagger p < 0.05$.

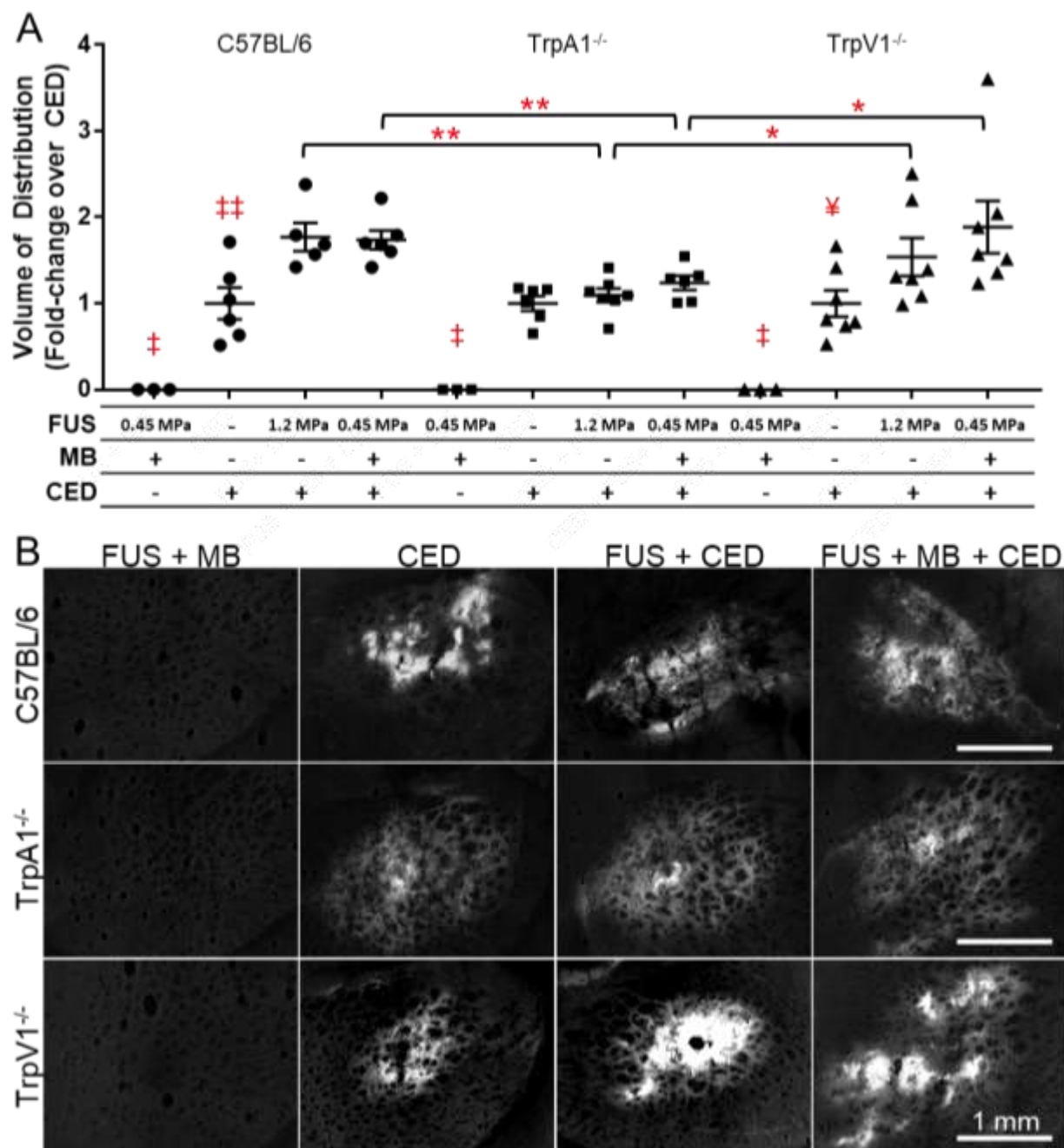


Figure 5.2. Enhancement of ZsGreen-BPN volume of distribution with FUS is attenuated in TrpA1^{-/-} mice but not in TrpV1^{-/-} mice. Bar graphs show volume of distribution fold change compared to CED control after CED administration of ZsGreen-BPN into the striatum of (A) C57BL/6, (B) TrpA1^{-/-} and (C) TrpV1^{-/-} mice. (D) Representative images from sections through the mouse striatum after CED administration of ZsGreen-BPN in C57BL/6 (top row), TrpA1^{-/-} (middle row) and TrpV1^{-/-} (bottom row). n = 6, n = 7 (CED + FUS) or n = 3 (FUS + MB) in each group. * = p < 0.05, ** = p < 0.01, ‡ = p < 0.05 vs all groups in same genotype, ‡‡ = p < 0.01 vs all groups in same genotype, ‡‡‡ = p < 0.05 vs FUS + MB + CED.

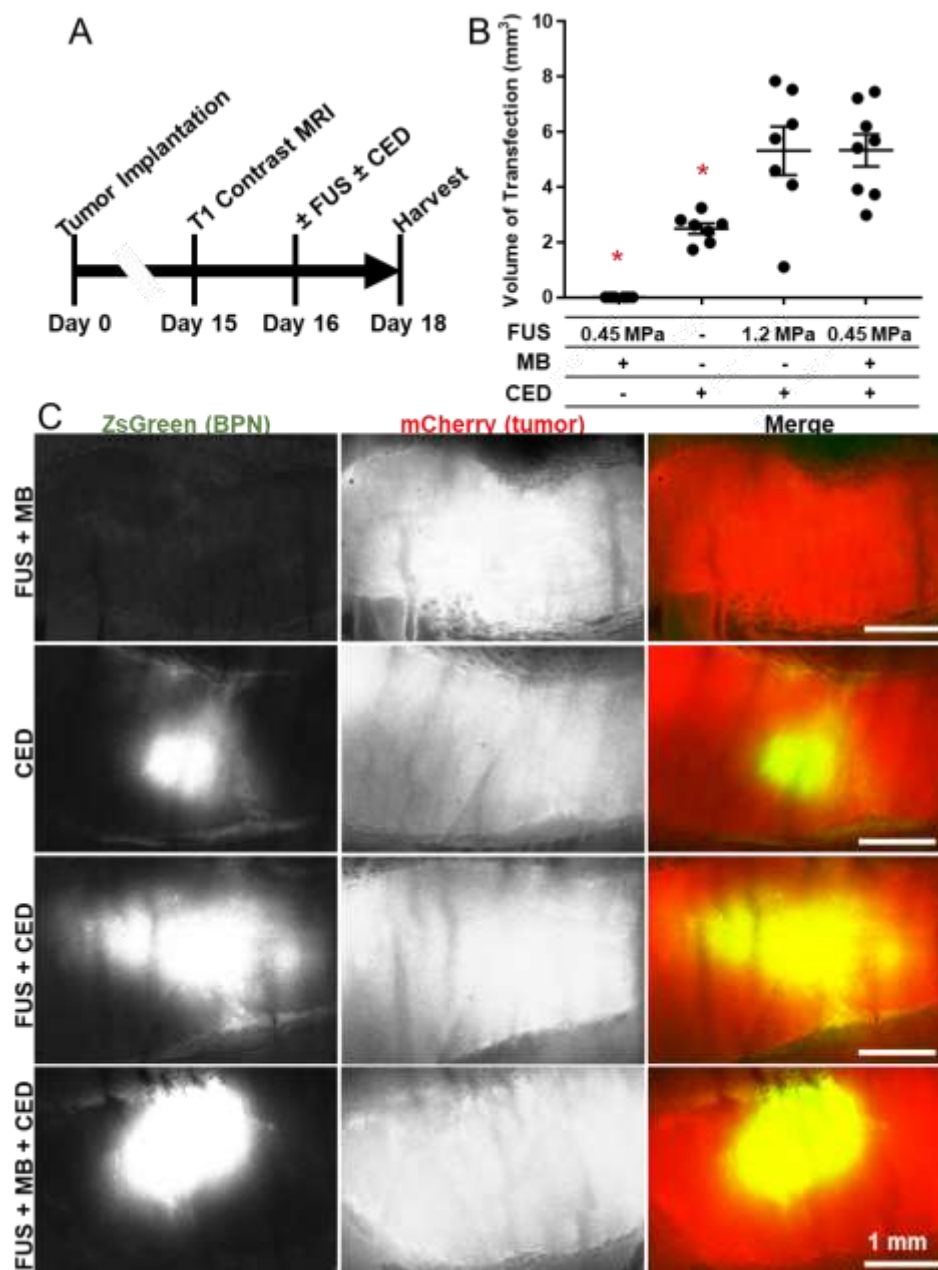


Figure 5.3. Pre-treatment of an intracranial mCherry-expressing U87 human glioma tumor in a mouse increases volume of distribution after CED administration of ZsGreen-BPN. (A) Timeline of study. Tumors were imaged 15 days after inoculation, treated with FUS and/or CED on day 16 and their brains harvested on day 18. (B) Bar graph of volume of distribution of ZsGreen-BPN in the tumor after CED administration. (C) Representative images from sections through the tumor after CED administration of ZsGreen-BPN showing the ZsGreen distribution (left column), mCherry-expressing tumor (middle column) and merge. $n = 7$ or $n = 3$ (FUS + MB) in each group. * $p < 0.05$ vs all groups, one-way ANOVA.

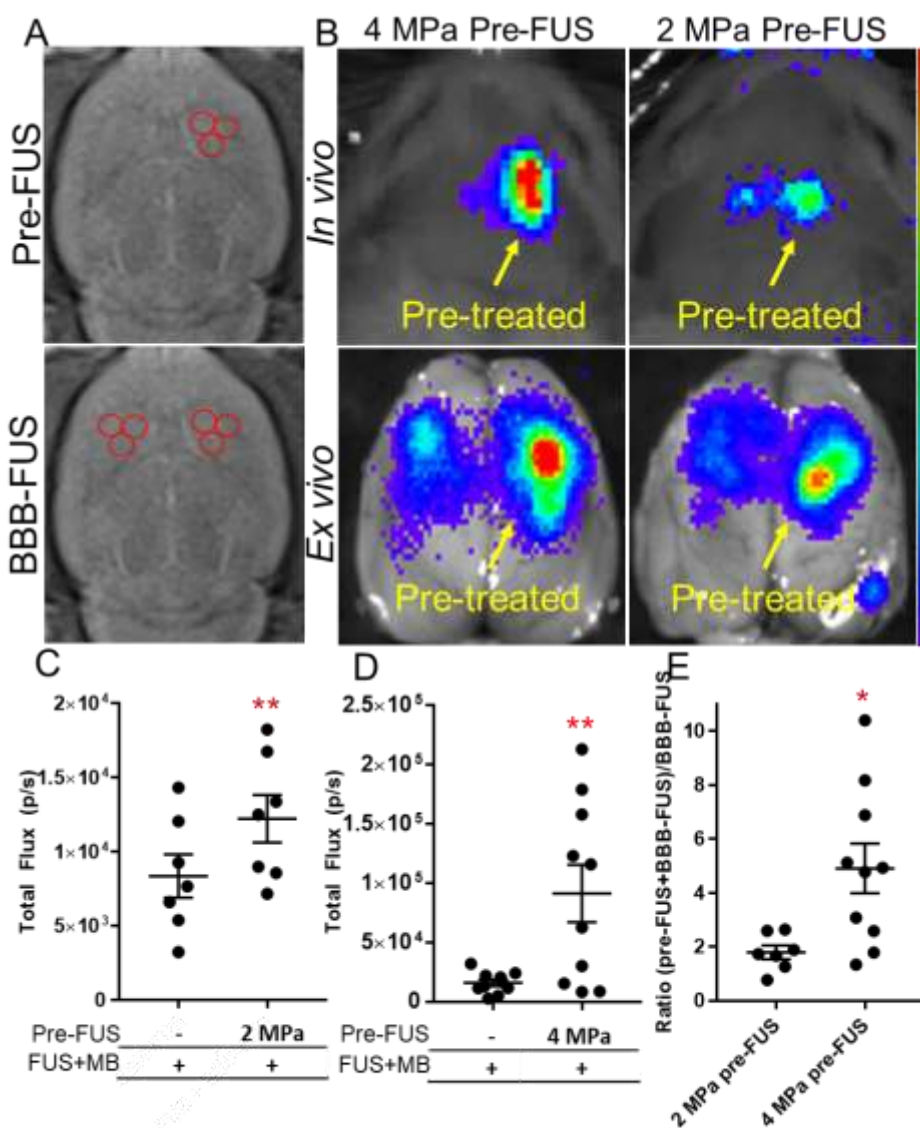


Figure 5.4. Pre-exposure of rat brain to 4 MPa or 2 MPa FUS (2.25% duty cycle, 10 mins) without MBs increases bioluminescence after delivery of Luc-BPN with FUS compared to non-pre-treated controls. (A) Representative pre-treatment T2 MRI images showing treatment planning locations in the striatum of the rats. The striatum of one hemisphere was pre-treated and the BBB of both hemispheres was opened with FUS + MB. (B) Representative *in vivo* (top) and *ex vivo* (bottom) bioluminescence images taken two days after application of FUS + MB treatment. The right striatum was pre-treated. (C – E) Bar graphs showing *in vivo* bioluminescence total flux in animals pre-treated with either 2 MPa (C) or 4 MPa (D) or ratio of the bioluminescence on the pre-treated side. $n = 7$ (2 MPa) or $n = 10$ (4 MPa). * $p < 0.05$ vs all groups, t-test. ** $p < 0.01$, paired t-test.

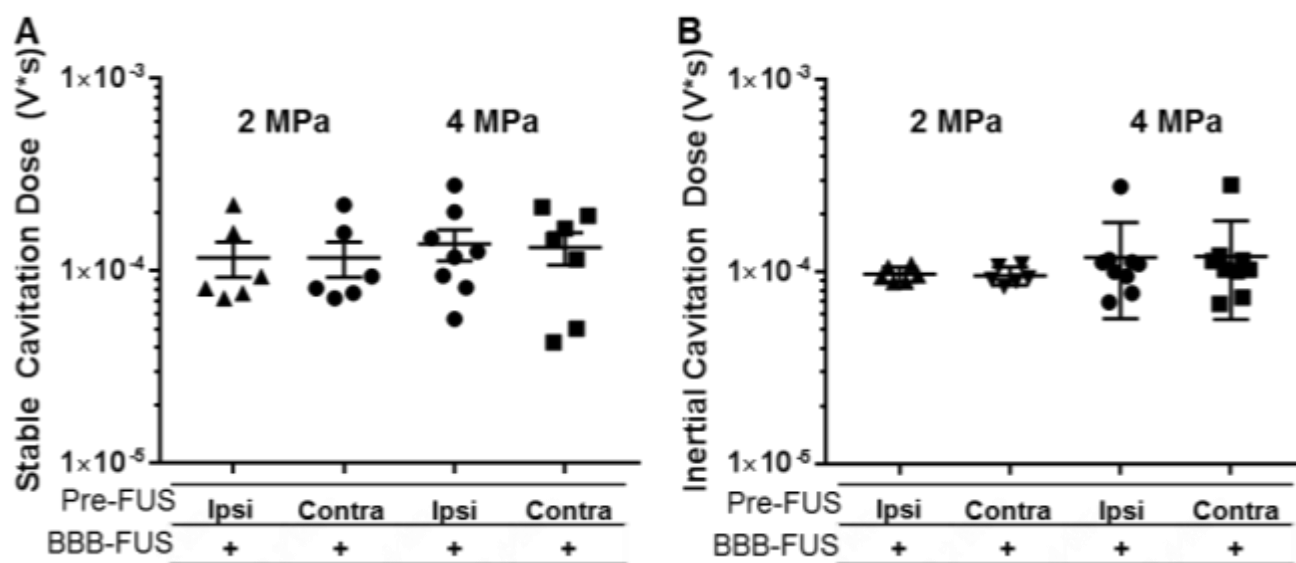


Figure 5.5. Pretreatment with 4 MPa or 2 MPa FUS does not alter SCD and ICD during BBB-opening. Bar graph of stable cavitation dose (A) and inertial cavitation dose (B) collected during FUS + MB treatment to open the BBB on the pre-treated ipsilateral striatum and the contralateral non-pre-treated striatum. No statistical differences were found.

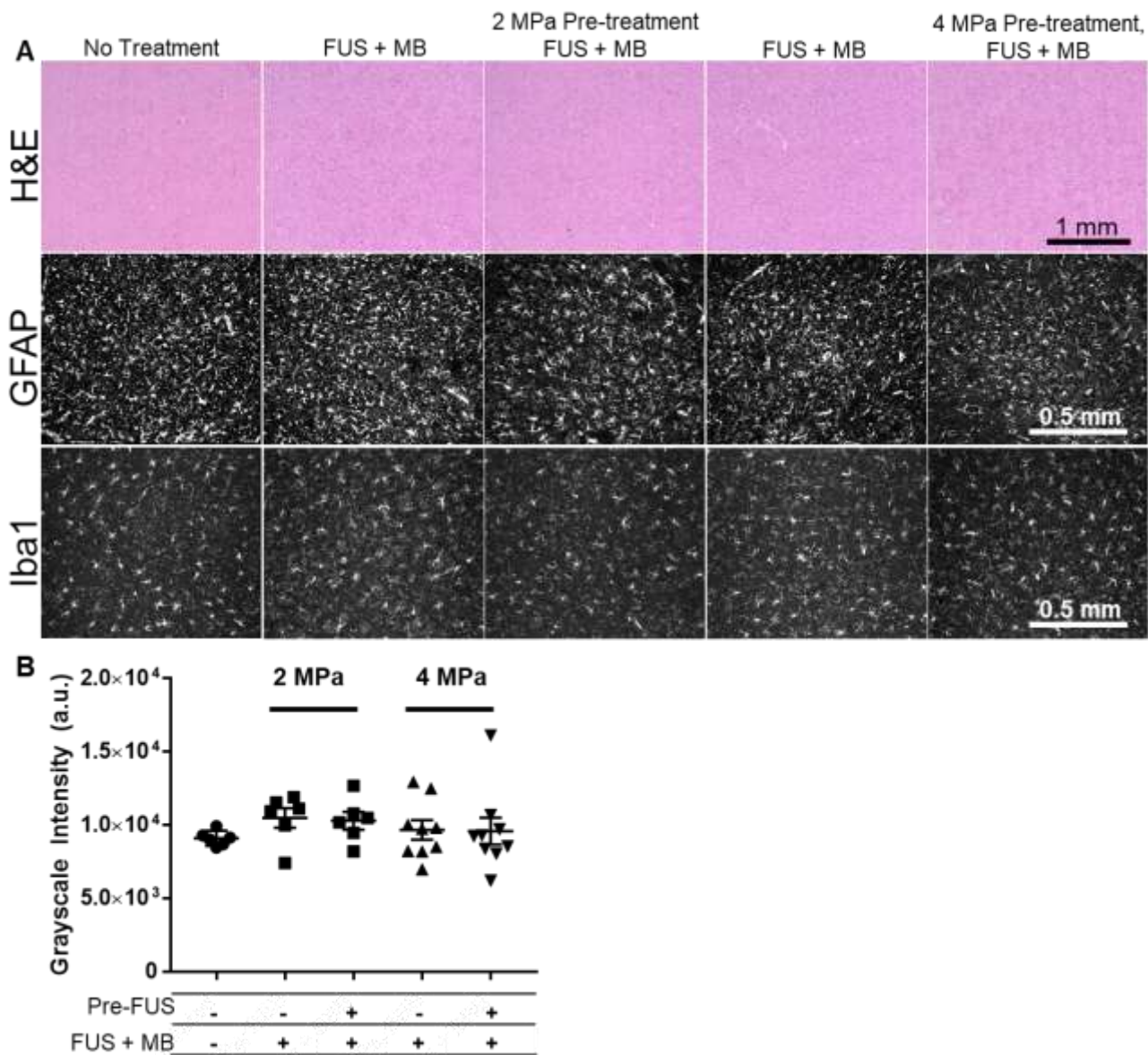


Figure 5.6. Pre-treatment with FUS at either 4 MPa or 2 MPa does not lead to signs of damage, ischemic injury, astrogliosis, or microgliosis. (A) Representative images of H&E (top) stained and GFAP (middle) or Iba1 (bottom) immunostained sections through ipsilateral pre-treated and FUS + MB treated as well as contralateral FUS + MB treated striatum. (B) Bar graph showing GFAP grayscale intensity in all groups including pre-treated and FUS + MB treated and contralateral FUS + MB treated striatum at both 4 and 2 MPa as well as control non-treated striatum. No statistical differences were found.

5.8 Chapter 5 Tables**Table 1.** Physiochemical properties of BPN

	ZsGreen-BPN	Luc-BPN
Size	44.8 ± 7.3	42.2 ± 5
Zeta	0.4 ± 4.5	0.93 ± 4.6
PDI	0.26	0.24

^a Size and polydispersity index (PDI) were measured by dynamic light scattering in 10 mM NaCl at pH 7.0. Data are presented as the average of all BPN preps ± SEM

^b ζ-potential was measured by laser Doppler anemometry. Data are presented as the average of all BPN preps ± SEM.

Chapter 6: Thoughts on the Direction of Future Research Projects

6.1 Focused Ultrasound as a Strategy for Treating Brain Disease

Focused ultrasound (FUS) has now been well established as a treatment strategy for numerous brain diseases. High intensity FUS has been FDA approved for treatment of Essential Tremor (259), and clinical trials for other CNS disorders including tremor dominant Parkinson's disease (PD) (NCT01772693), Parkinson's dyskinesia (NCT02263885), OCD (NCT03156335) and Huntington's disease (NCT02252380) and others are being planned. Moreover, use of lower intensity pulsed FUS, in conjunction with MBs, to temporarily open the blood-brain barrier (BBB) is now beginning clinical trials in glioblastoma multiforme (GBM, MCT02343991) and Alzheimer's disease (NCT02986932). However, despite its immense promise, additional investigation is required to improve delivery efficiency, reduce off-target uptake, and better understand how different types of ultrasound regimes (i.e. ablation, hyperthermia, mechanical tissue disruption, etc.) can work in combination to reduce barriers to treatment of disease.

6.2 Integrating Alternative Nanoparticle Formulations into Focused Ultrasound Treatment Paradigms

In chapter 2, we demonstrated that delivery of reporter gene-bearing nanoparticles across the BBB leads to localized and robust transgene expression in the brain parenchyma. We showed that this strategy is safe, with no significant activation of astrocytes or signs of toxicity under H&E staining.

Our long term goal is to pre-clinically test and translate novel gene delivery approaches for treatment of PD. While numerous cationic polymer backbone candidates for non-viral gene delivery have demonstrated promise for efficient and non-toxic gene transfer *in vitro*, PEI(342, 343) and poly (β -amino) esters (PBAE)(344, 345) have shown particular promise for *in vivo*

applications due to their ability to overcome harsh physiological environments and numerous cellular barriers to gene delivery. The delivery of PEI based DNA-BPN with FUS did not show signs of local or systemic toxicity at low or moderate doses (<200 µg); however, higher doses (>350 µg) led to signs of local toxicity in the ipsilateral striatum including gliosis and pyknotic nuclei. PBAE may have improved efficiency and a better safety profile *in vivo* compared to PEI(344–346), as well as an ability to rapidly degrade into biocompatible products over several hours. Therefore, a key component to translation of strategies involving delivery of nanoparticles with FUS will be to determine if the FUS-targeted delivery of PBAE based DNA-BPN can surpass the safety and/or efficacy profile of PEI based DNA-BPN delivery. Broadly speaking, the improvements in gene delivery achieved will represent an improved platform for gene therapies for other brain diseases.

Future studies could also seek to limit off-target gene expression obtained after systemic administration of gene vector BPN. Toward this end, advances in genetic tools including promoter design and inclusion of miRNA target sites(347) can limit expression to specific cell types or knock down expression in off-target organs, respectively. Limiting expression to targeted structures could obviate risks associated with off-target expression.

6.3 Development of GDNF-BPN delivery with FUS as a Clinical Treatment Strategy for Parkinson's Disease

In chapter 3, we used the unique delivery capabilities of FUS and MBs to deliver a BPN bearing the plasmid for a neurotrophic factor, GDNF, to restore locomotor function in a rat model of PD. We determined that delivery of GDNF-BPN with FUS led to an ~10-fold enhancement in GDNF protein levels that was sustained for at least 10 weeks after delivery and was sufficient to improve behavioral, histological and biochemical markers of disease in this model. Indeed, we postulate that the non-invasive nature of FUS to deliver GDNF-

BPN makes this strategy enticing for the treatment of early stage human PD, where treatment strategies are most likely to produce a significant effect.

In order to maximize treatment efficacy, it may be worthwhile to test whether the FUS pre-treatment strategies demonstrated in chapter 4 can enhance delivery and therapeutic response to GDNF-BPN delivery. Indeed, by improving delivery and expression of transgenes to the targeted striatum, doses of systemically administered GDNF-BPN may be reduced which may ultimately mitigate concerns about side effects associated with off-target delivery and expression.

Next, prior to translating FUS-delivery of GDNF-BPN as treatment strategy in humans, further studies could seek additional testing in alternative models of PD including the rodent α -synuclein overexpression model and the toxin based MPTP model in non-human primates. It is important to note that α -synuclein-based PD models have previously demonstrated lack of efficacy of GDNF gene therapies(280), presumably due to GDNF receptor (Ret) downregulation(281). Indeed, improved homogeneity of delivery as well as FUS-mediated modulation of immune cell activation could improve outcomes. Non-human primates represent much more complex models capable of better predictions of clinical success and translation.

Ultimately, one critical question for determining the efficacy of FUS delivery of GDNF-BPN to treat human PD clinically is the integrity of the cerebral vasculature in older patients who are most likely to suffer to neurodegenerative diseases like PD. Most pre-clinical studies using FUS and MBs to open the BBB and deliver therapeutic agents have done so in young and naïve mice. However, the vasculature in a human PD brain is known to be disrupted, and dysfunctional BBB has been observed post-mortem substantia nigra and the striatum of PD patients(348). Moreover, activated microglia are more abundant in the SN of PD patients compared to age-matched healthy controls(349). Notably, opening of the BBB

appears to be required for extravasation of leukocytes into the brain parenchyma (350) and immune activation has been associated with an increased risk of PD (351). In light of this cerebrovascular dysfunction, translation of BBB opening strategies including FUS and MBs, which is known to activate microglia (110, 225), should be approached with caution. For this reason, future studies in aged rodents or more sophisticated models of PD are required.

6.4 Secondary Mechanisms of Focused Ultrasound to Enhance Nanoparticle-based treatment strategies

In chapter 4, we demonstrated the ability of FUS pre-treatment to a) enhance BPN volume of distribution when administered via CED into healthy rodent brain and in a glioma-bearing mouse. We further suggested a role for the TrpA1 calcium channel in altering ECM properties after mechanical activation. In addition, we demonstrated that FUS pre-treatment led to increased uptake and/or expression after delivery of BPN with FUS and MBs.

Future studies could seek to determine whether this approach could improve delivery of BPN into either a U87 human glioma tumor model or a B16F10 melanoma brain metastasis model. Indeed, while our studies demonstrated increased penetration of BPN through FUS pre-treated U87 tumor tissue, FUS pre-treatment has also been shown by other groups to decrease intratumoral interstitial fluid pressure (222) and penetration after uptake via the enhanced permeability and retention effect (334), suggesting that FUS pre-treatment can reduce several major barriers to therapeutic delivery into tumors. To test this, U87 tumor-bearing athymic nude mice or melanoma bearing C57Bl6 mice could be pre-treated in both the tumor as well as the surrounding healthy tissue with a FUS pre-treatment regime followed by systemic administration of Luc-BPN and opening of the BBB with FUS and MBs. Tumors could be harvested, isolated, and imaged with *ex vivo* bioluminescence imaging or homogenized and

luciferase expression could be assessed through luciferase assays. Increased drug penetration and homogeneity of BPN distribution could be assessed by sectioning and staining treated brain tissue. Changes in interstitial fluid flow after pre-treatment could be assessed with serial T1 imaging, in a technique being developed by the Munson Lab. Ultimately, if successful, this strategy could be used to test whether FUS pre-treatment followed by delivery of therapeutic-bearing BPN with FUS and MBs could lead to significant growth control.

Additional future studies could also look at strategies to improve the increased uptake via FUS pre-conditioning. In chapter 4, we demonstrated the role of mechano-sensitive channels in regulation of ECM permeability and others have postulated that the mechanism of increased tissue permeability after FUS pre-treatment is non-thermal(221). In contrast, however, mild tissue hyperthermia with FUS has been shown to lead to vasodilation and increased blood flow(336). In order to maximize the effect of pre-treatment, multiple FUS pre-treatment protocols including regimes known to a) cause sustained mild hyperthermia (~5°C temperature rise), b) produce significant mechanical tissue strain but negligible heating (< 2°C temperature rise) could be tested alongside the FUS regime demonstrated in chapter 4.

Finally, further studies into cellular responses to FUS could include live imaging of astrocytes and microglia seeded into 3D matrices housed in acoustically transparent cell culture chambers. Toward this end, we could use astrocytes or microglia that fluoresce when intracellular calcium levels rise. By confocally aligning a FUS transducer and a fluorescence-capable optical objective, it would be possible to live image astrocytes and microglia in a brain-like environment. This would allow evaluation of the extent of mechanical strain that is required to activate mechano-sensitive channels including TrpA1 and evaluate changes in astrocyte or microglial morphology following FUS pre-treatment.

6.5 Promise for Therapeutic Genome and Transcriptome Engineering strategies with Focused Ultrasound

This dissertation has described the development of a non-invasive delivery paradigm wherein nucleic-acid bearing nanoparticles can be delivered to spatially-localized sites within the brain. Non-viral delivery of CRISPR/Cas9 components (i.e. mRNA and sgRNA) was recently described for the first time in adult animals(352) and hold immense potential for site specific and long-term *in vivo* gene editing. Programmable CRISPR systems with RNA-targeting Cas9 capable of visualizing and eliminating toxic RNAs have been shown to be effective in treatment of poly-glutamine disorders like Huntington's disease and a common form of amyotrophic lateral sclerosis(353). Delivery strategies like FUS and MBs could allow for exciting opportunities for transcriptome and/or genome engineering in numerous models of brain disease.

6.6 Pre-treatment with Focused Ultrasound as a Strategy to Enhance Immune Infiltration and Activation

In addition to enhancing permeability of healthy brain and tumor tissue, FUS pre-treatment has been shown to reduce intratumoral interstitial fluid pressure (222) and it has been hypothesized that the mechanism includes increasing fluid flow from the core of the tumor to the tumor periphery, where the pressure is known to be lower(354). Numerous studies have argued that opening of the BBB with FUS and MBs can activate microglia(355, 356), and disruption of the BBB with FUS and MBs is currently being explored for its potential to increase trafficking of immune cells into the tumor(202). Indeed, future studies could investigate how increases in tissue permeability and/or interstitial fluid flow out of the tumor may increase exposure of tumor antigen via increased drainage to the meningeal lymphatics and ultimately the cervical lymph nodes, which are known to have roles in immune cell trafficking and

activation (357). Moreover, it has recently been demonstrated that dense tumor ECM can prohibit T-cell migration and reduce antitumor immunity(358). Increased permeability of the tumor ECM with pre-treatment FUS regimens may allow increased immune cell activation and surveillance. When used in combination with FUS and MBs to increase drug and/or gene delivery, this multi-pronged approach has the potential to elicit strong and lasting tumor growth control.

It is important to note that the immune system in the CNS has roles in both health and disease. Activation of immune cells in the parenchyma, including microglia, or in the meninges, including dendritic cells can lead to neuroprotective and/or neurorestorative responses(359, 360). Consistent with this, stimulation of immune in the brain system has also shown promise for the treatment of neurodegenerative diseases(361, 362). Moreover, aged brain is associated with decreased glymphatic flux and, importantly, decreased amyloid- β clearance in a mouse model of Alzheimer's disease(363, 364). FUS has been used by several groups as a strategy to increase antibody delivery across the BBB and enhance immune cell activation (79, 110) and has been shown to decrease amyloid- β plaque burden(110, 225) in rodent models of Alzheimer's disease. Further studies could explore the use of a pre-treatment FUS regime to enhance antibody delivery, immune cell infiltration and, indeed, increase fluid conductivity and ISF flux to enhance amyloid- β clearance from the aged brain.

6.7 Summary

Taken collectively, these chapters prompt numerous questions that ultimately could drive novel and exciting research pathways. FUS is poised, through a variety of mechanisms, to fundamentally alter how diseases in both the brain as well as the periphery are treated.

References

1. R. T. Bartus, M. S. Weinberg, R. J. Samulski, Parkinson's disease gene therapy: success by design meets failure by efficacy., *Mol. Ther.* **22**, 487–97 (2014).
2. J. Tereshchenko, A. Maddalena, M. Bähr, S. Kügler, Pharmacologically controlled, discontinuous GDNF gene therapy restores motor function in a rat model of Parkinson's disease., *Neurobiol. Dis.* **65**, 35–42 (2014).
3. A. Drinkut, Y. Tereshchenko, J. B. Schulz, M. Bähr, S. Kügler, Efficient gene therapy for Parkinson's disease using astrocytes as hosts for localized neurotrophic factor delivery., *Mol. Ther.* **20**, 534–43 (2012).
4. J. L. Eberling, A. P. Kells, P. Pivrotto, J. Beyer, J. Bringas, H. J. Federoff, J. Forsayeth, K. S. Bankiewicz, Functional effects of AAV2-GDNF on the dopaminergic nigrostriatal pathway in parkinsonian rhesus monkeys., *Hum. Gene Ther.* **20**, 511–8 (2009).
5. W. M. Pardridge, The blood-brain barrier: bottleneck in brain drug development., *NeuroRx* **2**, 3–14 (2005).
6. E. Nance, K. Timbie, G. W. Miller, J. Song, C. Louttit, A. L. Klibanov, T.-Y. Shih, G. Swaminathan, R. J. Tamargo, G. F. Woodworth, J. Hanes, R. J. Price, Non-invasive delivery of stealth, brain-penetrating nanoparticles across the blood-brain barrier using MRI-guided focused ultrasound., *J. Control. Release* **189**, 123–32 (2014).
7. K. Timbie, B. P. . Mead, R. J. Price, Drug and Gene Delivery Across the Blood-Brain Barrier with Focused Ultrasound, *J. Control. Release* **219**, 71–75 (2015).
8. E. A. Nance, G. F. Woodworth, K. A. Sailor, T.-Y. Shih, Q. Xu, G. Swaminathan, D. Xiang, C. Eberhart, J. Hanes, A dense poly(ethylene glycol) coating improves penetration of large polymeric nanoparticles within brain tissue., *Sci. Transl. Med.* **4**, 149ra119 (2012).
9. P. Mastorakos, C. Zhang, S. Berry, Y. Oh, S. Lee, C. G. Eberhart, G. F. Woodworth, J. S. Suk, J. Hanes, P. Mastorakos, C. Zhang, S. Berry, Y. Oh, S. Lee, J. S. Suk, P. J. Hanes,

- Manuscript Highly PEGylated DNA Nanoparticles Provide Uniform and Widespread Gene Transfer in the Brain, *Adv. Healthc. Mater.* , 1–32 (2015).
10. F. C. Pérez-Martínez, J. Guerra, I. Posadas, V. Ceña, Barriers to non-viral vector-mediated gene delivery in the nervous system., *Pharm. Res.* **28**, 1843–58 (2011).
 11. S. Puhalla, W. Elmquist, D. Freyer, L. Kleinberg, C. Adkins, P. Lockman, J. McGregor, L. Muldoon, G. Nesbit, D. Peereboom, Q. Smith, S. Walker, E. Neuwelt, Unsantifying the sanctuary: challenges and opportunities with brain metastases., *Neuro. Oncol.* **17**, 639–651 (2015).
 12. M. D. Prados, S. A. Byron, N. L. Tran, J. J. Phillips, A. M. Molinaro, K. L. Ligon, P. Y. Wen, J. G. Kuhn, I. K. Mellinghoff, J. F. de Groot, H. Colman, T. F. Cloughesy, S. M. Chang, T. C. Ryken, W. D. Tembe, J. A. Kiefer, M. E. Berens, D. W. Craig, J. D. Carpten, J. M. Trent, Toward precision medicine in glioblastoma: the promise and the challenges., *Neuro. Oncol.* (2015), doi:10.1093/neuonc/nov031.
 13. *Neurological Disorders: public health challenges.* (2006).
 14. Substance Abuse and Mental Health Services Administration, *Results from the 2012 National Survey on Drug Use and Health : Summary of National Findings* (2013).
 15. W. F. Stewart, J. A. Ricci, E. Chee, S. R. Hahn, D. Morganstein, Cost of lost productive work time among US workers with depression., *JAMA* **289**, 3135–44 (2003).
 16. H.-C. Bauer, I. A. Krizbai, H. Bauer, A. Traweger, “You Shall Not Pass”-tight junctions of the blood brain barrier., *Front. Neurosci.* **8**, 392 (2014).
 17. W. M. Pardridge, R. J. Boado, *Reengineering biopharmaceuticals for targeted delivery across the blood-brain barrier* (Elsevier Inc., ed. 1, 2012; <http://dx.doi.org/10.1016/B978-0-12-396962-0.00011-2>).
 18. D. Deleu, M. G. Northway, Y. Hanssens, Clinical pharmacokinetic and pharmacodynamic properties of drugs used in the treatment of Parkinson’s disease., *Clin. Pharmacokinet.* **41**, 261–

309 (2002).

19. R. R. Lonser, M. Sarntinoranont, P. F. Morrison, E. H. Oldfield, Convection-enhanced delivery to the central nervous system, *J Neurosurg* **122**, 697–706 (2015).

20. P. F. Morrison, in *Principles of Clinical Pharmacology*, (2007), pp. 107–128.

21. R. H. Bobo, D. W. Laske, A. Akbasak, P. F. Morrisont, R. L. Dedrickt, E. H. Oldfield, Convection-enhanced delivery of macromolecules in the brain, *Proc. Natl. Acad. Sci.* **91**, 2076–2080 (1994).

22. W. J. Marks, R. T. Bartus, J. Siffert, C. S. Davis, A. Lozano, N. Boulis, J. Vitek, M. Stacy, D. Turner, L. Verhagen, R. Bakay, R. Watts, B. Guthrie, J. Jankovic, R. Simpson, M. Tagliati, R. Alterman, M. Stern, G. Baltuch, P. a Starr, P. S. Larson, J. L. Ostrem, J. Nutt, K. Kieburzt, J. H. Kordower, C. W. Olanow, Gene delivery of AAV2-neurturin for Parkinson's disease: a double-blind, randomised, controlled trial., *Lancet. Neurol.* **9**, 1164–72 (2010).

23. W. J. Marks, J. L. Ostrem, L. Verhagen, P. a Starr, P. S. Larson, R. A. Bakay, R. Taylor, D. a. Cahn-Weiner, a. J. Stoessl, C. W. Olanow, R. T. Bartus, Safety and tolerability of intraputaminial delivery of CERE-120 (adeno-associated virus serotype 2-neurturin) to patients with idiopathic Parkinson's disease: an open-label, phase I trial, *Lancet Neurol.* **7**, 400–408 (2008).

24. S. Ramaswamy, J. L. McBride, I. Han, E. M. Berry-Kravis, L. Zhou, C. D. Herzog, M. Gasmi, R. T. Bartus, J. H. Kordower, Intrastratial CERE-120 (AAV-Neurturin) protects striatal and cortical neurons and delays motor deficits in a transgenic mouse model of Huntington's disease., *Neurobiol. Dis.* **34**, 40–50 (2009).

25. M. Gasmi, E. P. Brandon, C. D. Herzog, A. Wilson, K. M. Bishop, E. K. Hofer, J. J. Cunningham, M. A. Printz, J. H. Kordower, R. T. Bartus, AAV2-mediated delivery of human neurturin to the rat nigrostriatal system: long-term efficacy and tolerability of CERE-120 for Parkinson's disease., *Neurobiol. Dis.* **27**, 67–76 (2007).

26. X. Ren, T. Zhang, X. Gong, G. Hu, W. Ding, X. Wang, AAV2-mediated striatum delivery of human CDFN prevents the deterioration of midbrain dopamine neurons in a 6-hydroxydopamine induced parkinsonian rat model, *Exp. Neurol.* **248**, 148–156 (2013).
27. G. S. Gonzales-Portillo, P. R. Sanberg, M. Franzblau, C. Gonzales-Portillo, T. Diamandis, M. Staples, C. D. Sanberg, C. V. Borlongan, Mannitol-enhanced delivery of stem cells and their growth factors across the blood-brain barrier, *Cell Transplant.* **23**, 531–539 (2014).
28. H. J. Lee, Y. Zhang, W. M. Pardridge, Blood-brain barrier disruption following the internal carotid arterial perfusion of alkyl glycerols., *J. Drug Target.* **10**, 463–467 (2002).
29. A. K. Bhattacharjee, T. Kondoh, T. Nagashima, M. Ikeda, K. Ehara, N. Tamaki, Quantitative analysis of papaverine-mediated blood-brain barrier disruption in rats., *Biochem. Biophys. Res. Commun.* **289**, 548–552 (2001).
30. K. L. Black, T. Cloughesy, S. C. Huang, Y. P. Gobin, Y. Zhou, J. Grous, G. Nelson, K. Farahani, C. K. Hoh, M. Phelps, *Intracarotid infusion of RMP-7, a bradykinin analog, and transport of gallium-68 ethylenediamine tetraacetic acid into human gliomas.* (1997).
31. J. J. Lochhead, R. G. Thorne, Intranasal delivery of biologics to the central nervous system, *Adv. Drug Deliv. Rev.* **64**, 614–628 (2012).
32. H. R. Costantino, L. Illum, G. Brandt, P. H. Johnson, S. C. Quay, Intranasal delivery: Physicochemical and therapeutic aspects, *Int. J. Pharm.* **337**, 1–24 (2007).
33. M. Ikeda, A. K. Bhattacharjee, T. Kondoh, T. Nagashima, N. Tamaki, Synergistic effect of cold mannitol and Na(+)/Ca(2+) exchange blocker on blood-brain barrier opening., *Biochem. Biophys. Res. Commun.* **291**, 669–674 (2002).
34. E. Zylber-Katz, J. M. Gormori, A. Schwartz, A. Lossos, F. Bokstein, T. Siegal, Pharmacokinetics of methotrexate in cerebrospinal fluid and serum after osmotic blood-brain barrier disruption in patients with brain lymphoma., *Clin. Pharmacol. Ther.* **67**, 631–641 (2000).
35. N. Lipsman, M. L. Schwartz, Y. Huang, L. Lee, T. Sankar, M. Chapman, K. Hynynen, A. M.

- Lozano, MR-guided focused ultrasound thalamotomy for essential tremor: a proof-of-concept study, *Lancet Neurol.* **12**, 462–468 (2013).
36. W. J. Elias, D. Huss, T. Voss, J. Loomba, M. Khaled, E. Zadicario, R. C. Frysjinger, S. a Sperling, S. Wylie, S. J. Monteith, J. Druzgal, B. B. Shah, M. Harrison, M. Wintermark, A pilot study of focused ultrasound thalamotomy for essential tremor., *N. Engl. J. Med.* **369**, 640–8 (2013).
37. R. Dallapiazza, M. S. McKisic, B. Shah, W. J. Elias, Neuromodulation for movement disorders., *Neurosurg. Clin. N. Am.* **25**, 47–58 (2014).
38. P. P. Dobrakowski, A. K. Machowska-Majchrzak, B. Labuz-Roszak, K. G. Majchrzak, E. Kluczewska, K. B. Pierzchała, MR-guided focused ultrasound: a new generation treatment of Parkinson's disease, essential tremor and neuropathic pain., *Interv. Neuroradiol.* **20**, 275–82.
39. K. Hynynen, N. J. McDannold, Noninvasive MR Imaging-guided Focal Opening of the Blood-Brain Barrier in Rabbits, *Radiology* **220**, 640–646 (2001).
40. K. Hynynen, N. J. McDannold, N. I. Vykhodtseva, F. A. Jolesz, Non-invasive opening of BBB by focused ultrasound., *Acta Neurochir. Suppl.* **86**, 555–558 (2003).
41. N. J. McDannold, N. I. Vykhodtseva, S. Raymond, F. A. Jolesz, K. Hynynen, MRI-guided targeted blood-brain barrier disruption with focused ultrasound: Histological findings in rabbits, *Ultrasound Med. Biol.* **31**, 1527–1537 (2005).
42. V. M. Runge, J. A. Clanton, A. C. Price, C. J. Wehr, W. A. Herzer, C. L. Partain, A. E. James, The use of Gd DTPA as a perfusion agent and marker of blood-brain barrier disruption., *Magn. Reson. Imaging* **3**, 43–55 (1985).
43. H. L. Liu, Y. Y. Wai, W. S. Chen, J. C. Chen, P. H. Hsu, X. Y. Wu, W. C. Huang, T. C. Yen, J. J. Wang, Hemorrhage Detection During Focused-Ultrasound Induced Blood-Brain-Barrier Opening by Using Susceptibility-Weighted Magnetic Resonance Imaging, *Ultrasound Med. Biol.* **34**, 598–606 (2008).

44. A. L. Cheng, S. Batool, C. R. McCreary, M. L. Lauzon, R. Frayne, M. Goyal, E. E. Smith, Susceptibility-weighted imaging is more reliable than T2*-weighted gradient-recalled echo mri for detecting microbleeds, *Stroke* **44**, 2782–2786 (2013).
45. W. Fry, F. Fry, R. Meyers, R. C. Eggleton, in *The Third International Conference on Medical Electronics*, (1960).
46. K. Hynynen, F. a. Jolesz, Demonstration of potential noninvasive ultrasound brain therapy through an intact skull, *Ultrasound Med. Biol.* **24**, 275–283 (1998).
47. J. Rooney, Shear as a mechanism for sonically induced biological effects., *J. Acoust. Soc. Am.* **52**, 1718–24 (1972).
48. B. J. Davidson, N. Riley, Cavitation Microstreaming, *J. Sound Vib.* **15**, 217–233 (1971).
49. H. Chen, W. Kreider, A. A. Brayman, M. R. Bailey, T. J. Matula, Blood vessel deformations on microsecond time scales by ultrasonic cavitation., *Phys. Rev. Lett.* **106**, 34301 (2011).
50. J. Wu, J. P. Ross, J.-F. Chiu, Reparable sonoporation generated by microstreaming, *J. Acoust. Soc. Am.* **111**, 1460 (2002).
51. L. J. M. Juffermans, A. van Dijk, C. A. M. Jongenelen, B. Drukarch, A. Reijerkerk, H. E. de Vries, O. Kamp, R. J. P. Musters, Ultrasound and microbubble-induced intra- and intercellular bioeffects in primary endothelial cells., *Ultrasound Med. Biol.* **35**, 1917–27 (2009).
52. N. Sheikov, N. J. McDannold, S. Sharma, K. Hynynen, Effect of focused ultrasound applied with an ultrasound contrast agent on the tight junctional integrity of the brain microvascular endothelium., *Ultrasound Med. Biol.* **34**, 1093–104 (2008).
53. J. Deng, Q. Huang, F. Wang, Y. Liu, Z. Wang, Z. Wang, Q. Zhang, B. Lei, Y. Cheng, The role of caveolin-1 in blood-brain barrier disruption induced by focused ultrasound combined with microbubbles., *J. Mol. Neurosci.* **46**, 677–87 (2012).
54. C. Xia, Z. Zhang, Y. Xue, P. Wang, Y. Liu, Mechanisms of the increase in the permeability of the blood-tumor barrier obtained by combining low-frequency ultrasound irradiation with small-

- dose bradykinin., *J. Neurooncol.* **94**, 41–50 (2009).
55. B. D. M. Meijering, L. J. M. Juffermans, A. van Wamel, R. H. Henning, I. S. Zuhorn, M. Emmer, A. M. G. Versteilen, W. J. Paulus, W. H. van Gilst, K. Kooiman, N. de Jong, R. J. P. Musters, L. E. Deelman, O. Kamp, Ultrasound and microbubble-targeted delivery of macromolecules is regulated by induction of endocytosis and pore formation., *Circ. Res.* **104**, 679–87 (2009).
56. T. Nhan, A. Burgess, E. E. Cho, B. Stefanovic, L. Lilge, K. Hynynen, Drug delivery to the brain by focused ultrasound induced blood-brain barrier disruption: Quantitative evaluation of enhanced permeability of cerebral vasculature using two-photon microscopy., *J. Control. Release* **172**, 274–280 (2013).
57. H. Chen, E. E. Konofagou, The size of blood-brain barrier opening induced by focused ultrasound is dictated by the acoustic pressure., *J. Cereb. Blood Flow Metab.* **34**, 1197–1204 (2014).
58. E. E. Cho, J. Drazic, M. Ganguly, B. Stefanovic, K. Hynynen, Two-photon fluorescence microscopy study of cerebrovascular dynamics in ultrasound-induced blood-brain barrier opening., *J. Cereb. Blood Flow Metab.* **31**, 1852–1862 (2011).
59. N. J. McDannold, N. I. Vykhodtseva, K. Hynynen, Targeted disruption of the blood-brain barrier with focused ultrasound: association with cavitation activity., *Phys. Med. Biol.* **51**, 793–807 (2006).
60. G. Samiotaki, F. Vlachos, Y. S. Tung, J. Feshitan, M. Borden, E. E. Konofagou, Pressure and microbubble size dependence study of focused ultrasound-induced blood-brain barrier opening reversibility in vivo, *AIP Conf. Proc.* **1481**, 300–306 (2012).
61. J. Park, Y. Zhang, N. I. Vykhodtseva, F. A. Jolesz, N. J. McDannold, The kinetics of blood brain barrier permeability and targeted doxorubicin delivery into brain induced by focused ultrasound., *J. Control. Release* **162**, 134–42 (2012).

62. G. P. Howles, K. F. Bing, Y. Qi, S. J. Rosenzweig, K. R. Nightingale, G. A. Johnson, Contrast-enhanced in vivo magnetic resonance microscopy of the mouse brain enabled by noninvasive opening of the blood-brain barrier with ultrasound, *Magn. Reson. Med.* **64**, 995–1004 (2010).
63. N. J. McDannold, C. D. D. Arvanitis, N. I. Vykhodtseva, M. S. S. Livingstone, Temporary disruption of the blood-brain barrier by use of ultrasound and microbubbles: safety and efficacy evaluation in rhesus macaques., *Cancer Res.* **72**, 3652–63 (2012).
64. M. E. Downs, A. Buch, C. Sierra, M. E. Karakatsani, S. Chen, E. E. Konofagou, V. P. Ferrera, Long-Term Safety of Repeated Blood-Brain Barrier Opening via Focused Ultrasound with Microbubbles in Non-Human Primates Performing a Cognitive Task, *PLoS One* **10**, e0125911 (2015).
65. K. Hynynen, N. J. McDannold, N. Sheikov, F. A. Jolesz, N. I. Vykhodtseva, Local and reversible blood-brain barrier disruption by noninvasive focused ultrasound at frequencies suitable for trans-skull sonications., *Neuroimage* **24**, 12–20 (2005).
66. P. J. Rauch, H. S. Park, J. P. S. Knisely, V. L. Chiang, A. O. Vortmeyer, Delayed radiation-induced vasculitic leukoencephalopathy, *Int. J. Radiat. Oncol. Biol. Phys.* **83**, 369–375 (2012).
67. B. C. Oh, P. G. Pagnini, M. Y. Wang, C. Y. Liu, P. E. Kim, C. Yu, M. L. J. Apuzzo, Stereotactic radiosurgery: Adjacent tissue injury and response after high-dose single fraction radiation: Part I - Histology, imaging, and molecular events *Neurosurgery* **60**, 31–44 (2007).
68. M. a. O'Reilly, K. Hynynen, Blood-Brain Barrier: Real-time Feedback-controlled Focused Ultrasound Disruption by Using an Acoustic Emissions-based Controller, *Radiology* **263**, 96–106 (2012).
69. Y.-S. Tung, F. Vlachos, J. J. Choi, T. Deffieux, K. Selert, E. E. Konofagou, In vivo transcranial cavitation threshold detection during ultrasound-induced blood-brain barrier opening in mice., *Phys. Med. Biol.* **55**, 6141–6155 (2010).

70. S. Samuel, M. a Cooper, J. L. Bull, J. B. Fowlkes, D. L. Miller, An ex vivo study of the correlation between acoustic emission and microvascular damage., *Ultrasound Med. Biol.* **35**, 1574–1586 (2009).
71. S. I. Madanshetty, R. A. Roy, R. E. Apfel, Acoustic microcavitation: its active and passive acoustic detection., *J. Acoust. Soc. Am.* **90**, 1515–1526 (1991).
72. V. I. Ilyichev, V. L. Koretz, N. P. Melnikov, Spectral characteristics of acoustic cavitation., *Ultrasonics* **27**, 357–361 (1989).
73. T. G. Leighton, The Acoustic Bubble *J. Acoust. Soc. Am.* **96**, 2616 (1994).
74. C. D. Arvanitis, M. S. Livingstone, N. I. Vykhodtseva, N. J. McDannold, Controlled Ultrasound-Induced Blood-Brain Barrier Disruption Using Passive Acoustic Emissions Monitoring, *PLoS One* **7** (2012), doi:10.1371/journal.pone.0045783.
75. S. Y. Wu, Y. S. Tung, F. Marquet, M. Downs, C. Sanchez, C. Chen, V. Ferrera, E. E. Konofagou, Transcranial cavitation detection in primates during blood-brain barrier opening-a performance assessment study, *IEEE Trans. Ultrason. Ferroelectr. Freq. Control* **61**, 966–978 (2014).
76. W. Y. Chai, P. C. Chu, M. Y. Tsai, Y. C. Lin, J. J. Wang, K. C. Wei, Y. Y. Wai, H. L. Liu, Magnetic-resonance imaging for kinetic analysis of permeability changes during focused ultrasound-induced blood-brain barrier opening and brain drug delivery, *J. Control. Release* **192**, 1–9 (2014).
77. H.-L. Liu, C.-Y. Huang, J.-Y. Chen, H.-Y. J. Wang, P.-Y. Chen, K.-C. Wei, Pharmacodynamic and therapeutic investigation of focused ultrasound-induced blood-brain barrier opening for enhanced temozolomide delivery in glioma treatment., *PLoS One* **9**, e114311 (2014).
78. L. H. Treat, N. J. McDannold, N. I. Vykhodtseva, Y. Zhang, K. Tam, K. Hynynen, Targeted delivery of doxorubicin to the rat brain at therapeutic levels using MRI-guided focused

ultrasound., *Int. J. Cancer* **121**, 901–7 (2007).

79. J. F. Jordão, C. a Ayala-Grosso, K. Markham, Y. Huang, R. Chopra, J. McLaurin, K. Hynynen, I. Aubert, Antibodies targeted to the brain with image-guided focused ultrasound reduces amyloid-beta plaque load in the TgCRND8 mouse model of Alzheimer's disease., *PLoS One* **5**, e10549 (2010).

80. G. Samiotaki, C. Acosta, S. Wang, E. E. Konofagou, Enhanced delivery and bioactivity of the neurturin neurotrophic factor through focused ultrasound-mediated blood-brain barrier opening in vivo., *J. Cereb. Blood Flow Metab.* **35**, 611–22 (2015).

81. M. Aryal, J. Park, N. I. Vykhodtseva, Y.-Z. Zhang, N. J. McDannold, Enhancement in blood-tumor barrier permeability and delivery of liposomal doxorubicin using focused ultrasound and microbubbles: evaluation during tumor progression in a rat glioma model., *Phys. Med. Biol.* **60**, 2511–27 (2015).

82. M. Aryal, N. I. Vykhodtseva, Y.-Z. Zhang, J. Park, N. J. McDannold, Multiple treatments with liposomal doxorubicin and ultrasound-induced disruption of blood–tumor and blood–brain barriers improve outcomes in a rat glioma model, *J. Control. Release* **169**, 103–111 (2013).

83. C.-H. Fan, C.-Y. Ting, H.-L. Liu, C.-Y. Huang, H.-Y. Hsieh, T.-C. Yen, K.-C. Wei, C.-K. Yeh, Antiangiogenic-targeting drug-loaded microbubbles combined with focused ultrasound for glioma treatment., *Biomaterials* **34**, 2142–55 (2013).

84. F.-Y. Yang, T.-T. Wong, M.-C. Teng, R.-S. Liu, M. Lu, H.-F. Liang, M.-C. Wei, Focused ultrasound and interleukin-4 receptor-targeted liposomal doxorubicin for enhanced targeted drug delivery and antitumor effect in glioblastoma multiforme., *J. Control. Release* **160**, 652–8 (2012).

85. R. D. Alkins, P. M. Brodersen, R. N. S. Sodhi, K. Hynynen, Enhancing drug delivery for boron neutron capture therapy of brain tumors with focused ultrasound., *Neuro. Oncol.* **15**, 1225–35 (2013).

86. A. Malmström, B. H. Grønberg, C. Marosi, R. Stupp, D. Frappaz, H. Schultz, U. Abacioglu,

- B. Tavelin, B. Lhermitte, M. E. Hegi, J. Rosell, R. Henriksson, Temozolomide versus standard 6-week radiotherapy versus hypofractionated radiotherapy in patients older than 60 years with glioblastoma: the Nordic randomised, phase 3 trial., *Lancet. Oncol.* **13**, 916–26 (2012).
87. A. Darlix, C. Baumann, V. Lorgis, F. Ghiringhelli, M. Blonski, B. Chauffert, S. Zouaoui, C. Pinelli, F. Rech, P. Beauchesne, L. Taillandier, Prolonged administration of adjuvant temozolomide improves survival in adult patients with glioblastoma., *Anticancer Res.* **33**, 3467–74 (2013).
88. M. R. Gilbert, M. Wang, K. D. Aldape, R. Stupp, M. E. Hegi, K. A. Jaeckle, T. S. Armstrong, J. S. Wefel, M. Won, D. T. Blumenthal, A. Mahajan, C. J. Schultz, S. Erridge, B. Baumert, K. I. Hopkins, T. Tzuk-Shina, P. D. Brown, A. Chakravarti, W. J. Curran, M. P. Mehta, Dose-dense temozolomide for newly diagnosed glioblastoma: a randomized phase III clinical trial., *J. Clin. Oncol.* **31**, 4085–91 (2013).
89. A. D. Norden, G. J. Lesser, J. Drappatz, K. L. Ligon, S. N. Hammond, E. Q. Lee, D. R. Reardon, C. E. Fadul, S. R. Plotkin, T. T. Batchelor, J.-J. Zhu, R. Beroukhi, A. Muzikansky, L. Doherty, D. Lafrankie, K. Smith, V. Tafoya, R. Lis, E. C. Stack, M. R. Rosenfeld, P. Y. Wen, Phase 2 study of dose-intense temozolomide in recurrent glioblastoma., *Neuro. Oncol.* **15**, 930–5 (2013).
90. K.-C. Wei, P.-C. Chu, H.-Y. J. Wang, C.-Y. Huang, P.-Y. Chen, H.-C. Tsai, Y.-J. Lu, P.-Y. Lee, I.-C. Tseng, L.-Y. Feng, P.-W. Hsu, T.-C. Yen, H.-L. Liu, Focused ultrasound-induced blood-brain barrier opening to enhance temozolomide delivery for glioblastoma treatment: a preclinical study., *PLoS One* **8**, e58995 (2013).
91. M. Westphal, D. C. Hilt, E. Bortey, P. Delavault, R. Olivares, P. C. Warnke, I. R. Whittle, J. Jääskeläinen, Z. Ram, A phase 3 trial of local chemotherapy with biodegradable carmustine (BCNU) wafers (Gliadel wafers) in patients with primary malignant glioma., *Neuro. Oncol.* **5**, 79–88 (2003).

92. S. Gururangan, L. Cokgor, J. N. Rich, S. Edwards, M. L. Affronti, J. A. Quinn, J. E. Herndon, J. M. Provenzale, R. E. McLendon, S. Tourt-Uhlig, J. H. Sampson, V. Stafford-Fox, S. Zaknoen, M. Early, A. H. Friedman, H. S. Friedman, Phase I study of Gliadel wafers plus temozolomide in adults with recurrent supratentorial high-grade gliomas., *Neuro. Oncol.* **3**, 246–50 (2001).
93. M. Westphal, Z. Ram, V. Riddle, D. Hilt, E. Bortey, Gliadel wafer in initial surgery for malignant glioma: long-term follow-up of a multicenter controlled trial., *Acta Neurochir. (Wien)*. **148**, 269–75; discussion 275 (2006).
94. F. J. Attenello, D. Mukherjee, G. Datto, M. J. McGirt, E. Bohan, J. D. Weingart, A. Olivi, A. Quinones-Hinojosa, H. Brem, Use of Gliadel (BCNU) wafer in the surgical treatment of malignant glioma: a 10-year institutional experience., *Ann. Surg. Oncol.* **15**, 2887–93 (2008).
95. H.-L. Liu, M.-Y. Hua, P.-Y. Chen, P.-C. Chu, C.-H. Pan, H.-W. Yang, C.-Y. Huang, J.-J. Wang, T.-C. Yen, K.-C. Wei, Blood-brain barrier disruption with focused ultrasound enhances delivery of chemotherapeutic drugs for glioblastoma treatment., *Radiology* **255**, 415–425 (2010).
96. P. Hau, K. Fabel, U. Baumgart, P. Rümmele, O. Grauer, A. Bock, C. Dietmaier, W. Dietmaier, J. Dietrich, C. Dudel, F. Hübner, T. Jauch, E. Drechsel, I. Kleiter, C. Wismeth, A. Zellner, A. Brawanski, A. Steinbrecher, J. Marienhagen, U. Bogdahn, Pegylated liposomal doxorubicin-efficacy in patients with recurrent high-grade glioma, *Cancer* **100**, 1199–1207 (2004).
97. K. Fabel, J. Dietrich, P. Hau, C. Wismeth, B. Winner, S. Przywara, A. Steinbrecher, W. Ullrich, U. Bogdahn, Long-term stabilization in patients with malignant glioma after treatment with liposomal doxorubicin., *Cancer* **92**, 1936–42 (2001).
98. S. Ananda, A. K. Nowak, L. Cher, A. Dowling, C. Brown, J. Simes, M. A. Rosenthal, Phase 2 trial of temozolomide and pegylated liposomal doxorubicin in the treatment of patients with glioblastoma multiforme following concurrent radiotherapy and chemotherapy., *J. Clin. Neurosci.* **18**, 1444–8 (2011).

99. Z. Kovacs, B. Werner, A. Rassi, J. O. Sass, E. Martin-Fiori, M. Bernasconi, Prolonged survival upon ultrasound-enhanced doxorubicin delivery in two syngenic glioblastoma mouse models., *J. Control. Release* (2014), doi:10.1016/j.jconrel.2014.05.033.
100. S. Savolainen, M. Kortnesniemi, M. Timonen, V. Reijonen, L. Kuusela, J. Uusi-Simola, E. Salli, H. Koivunoro, T. Seppälä, N. Lönnroth, P. Välimäki, H. Hyvönen, P. Kotiluoto, T. Serén, A. Kuronen, S. Heikkinen, A. Kosunen, I. Auterinen, Boron neutron capture therapy (BNCT) in Finland: technological and physical prospects after 20 years of experiences., *Phys. Med.* **29**, 233–48 (2013).
101. L. Kankaanranta, T. Seppälä, H. Koivunoro, K. Saarilahti, T. Atula, J. Collan, E. Salli, M. Kortnesniemi, J. Uusi-Simola, P. Välimäki, A. Mäkitie, M. Seppänen, H. Minn, H. Revitzer, M. Kouri, P. Kotiluoto, T. Seren, I. Auterinen, S. Savolainen, H. Joensuu, Boron neutron capture therapy in the treatment of locally recurred head-and-neck cancer: final analysis of a phase I/II trial., *Int. J. Radiat. Oncol. Biol. Phys.* **82**, e67-75 (2012).
102. S.-I. Miyatake, S. Kawabata, K. Yokoyama, T. Kuroiwa, H. Michiue, Y. Sakurai, H. Kumada, M. Suzuki, A. Maruhashi, M. Kirihata, K. Onoc, Survival benefit of boron neutron capture therapy for recurrent malignant gliomas., *Appl. Radiat. Isot.* **67**, S22-4 (2009).
103. J. W. Hopewell, T. Gorlia, L. Pellettieri, V. Giusti, B. H-Stenstam, K. Sköld, Boron neutron capture therapy for newly diagnosed glioblastoma multiforme: an assessment of clinical potential., *Appl. Radiat. Isot.* **69**, 1737–40 (2011).
104. F.-Y. Yang, Y.-W. Chen, F.-I. Chou, S.-H. Yen, Y.-L. Lin, T.-T. Wong, Boron neutron capture therapy for glioblastoma multiforme: enhanced drug delivery and antitumor effect following blood-brain barrier disruption induced by focused ultrasound., *Future Oncol.* **8**, 1361–9 (2012).
105. F.-Y. Yang, Y.-L. Lin, F.-I. Chou, Y.-C. Lin, Y.-W. Hsueh Liu, L.-W. Chang, Y.-L. Hsieh, Pharmacokinetics of BPA in Gliomas with Ultrasound Induced Blood-Brain Barrier Disruption as

Measured by Microdialysis., *PLoS One* **9**, e100104 (2014).

106. P. Kawalec, S. Łopuch, A. Mikrut, Effectiveness of Targeted Therapy in Patients With Previously Untreated Metastatic Breast Cancer: A Systematic Review and Meta-Analysis., *Clin. Breast Cancer* **15**, 90–100.e1 (2015).

107. B. Spencer, E. Masliah, Immunotherapy for Alzheimer's disease: past, present and future., *Front. Aging Neurosci.* **6**, 114 (2014).

108. N. Sheikov, N. J. McDannold, N. I. Vykhodtseva, F. A. Jolesz, K. Hynynen, Cellular mechanisms of the blood-brain barrier opening induced by ultrasound in presence of microbubbles., *Ultrasound Med. Biol.* **30**, 979–89 (2004).

109. M. Kinoshita, N. J. McDannold, F. A. Jolesz, K. Hynynen, Targeted delivery of antibodies through the blood-brain barrier by MRI-guided focused ultrasound., *Biochem. Biophys. Res. Commun.* **340**, 1085–90 (2006).

110. J. F. Jordão, E. Thévenot, K. Markham-Coultes, T. Scarcelli, Y.-Q. Weng, K. Xhima, M. O'Reilly, Y. Huang, J. McLaurin, K. Hynynen, I. Aubert, Amyloid- β plaque reduction, endogenous antibody delivery and glial activation by brain-targeted, transcranial focused ultrasound., *Exp. Neurol.* **248**, 16–29 (2013).

111. S. B. Raymond, L. H. Treat, J. D. Dewey, N. J. McDannold, K. Hynynen, B. J. Bacskai, Ultrasound enhanced delivery of molecular imaging and therapeutic agents in Alzheimer's disease mouse models., *PLoS One* **3**, e2175 (2008).

112. M. Kinoshita, N. J. McDannold, F. A. Jolesz, K. Hynynen, Noninvasive localized delivery of Herceptin to the mouse brain by MRI-guided focused ultrasound-induced blood-brain barrier disruption., *Proc. Natl. Acad. Sci. U. S. A.* **103**, 11719–23 (2006).

113. A. O. Ahmed, A. M. Mantini, D. J. Fridberg, P. F. Buckley, Brain-derived neurotrophic factor (BDNF) and neurocognitive deficits in people with schizophrenia: A meta-analysis., *Psychiatry Res.* **226**, 1–13 (2015).

114. M. Kalia, J. Costa E Silva, Biomarkers of psychiatric diseases: current status and future prospects., *Metabolism*. **64**, S11-5 (2015).
115. T. C. Theoharides, M. Athanassiou, S. Panagiotidou, R. Doyle, Dysregulated brain immunity and neurotrophin signaling in Rett syndrome and autism spectrum disorders., *J. Neuroimmunol.* **279**, 33–8 (2015).
116. S. V Hegarty, G. W. O’Keeffe, A. M. Sullivan, Neurotrophic factors: from neurodevelopmental regulators to novel therapies for Parkinson’s disease., *Neural Regen. Res.* **9**, 1708–11 (2014).
117. B. Baseri, J. J. Choi, T. Deffieux, G. Samiotaki, Y.-S. Tung, O. Olumolade, S. a Small, B. Morrison, E. E. Konofagou, Activation of signaling pathways following localized delivery of systemically administered neurotrophic factors across the blood-brain barrier using focused ultrasound and microbubbles., *Phys. Med. Biol.* **57**, N65-81 (2012).
118. F. Wang, Y. Shi, L. Lu, L. Liu, Y. Cai, H. Zheng, X. Liu, F. Yan, C. Zou, C. Sun, J. Shi, S. Lu, Y. Chen, Targeted delivery of GDNF through the blood-brain barrier by MRI-guided focused ultrasound., *PLoS One* **7**, e52925 (2012).
119. A. A. Thomas, C. W. Brennan, L. M. DeAngelis, A. M. Omuro, Emerging therapies for glioblastoma., *JAMA Neurol.* **71**, 1437–44 (2014).
120. L. Ampie, E. C. Woolf, C. Dardis, Immunotherapeutic advancements for glioblastoma., *Front. Oncol.* **5**, 12 (2015).
121. P.-Y. Chen, H.-Y. Hsieh, C.-Y. Huang, C.-Y. Lin, K.-C. Wei, H.-L. Liu, Focused ultrasound-induced blood-brain barrier opening to enhance interleukin-12 delivery for brain tumor immunotherapy: a preclinical feasibility study., *J. Transl. Med.* **13**, 451 (2015).
122. G. Bozzuto, A. Molinari, Liposomes as nanomedical devices., *Int. J. Nanomedicine* **10**, 975–99 (2015).
123. A. Mohan, S. Narayanan, S. Sethuraman, U. M. Krishnan, Novel resveratrol and 5-

fluorouracil coencapsulated in PEGylated nanoliposomes improve chemotherapeutic efficacy of combination against head and neck squamous cell carcinoma., *Biomed Res. Int.* **2014**, 424239 (2014).

124. M. L. Immordino, F. Dosio, L. Cattel, Stealth liposomes: review of the basic science, rationale, and clinical applications, existing and potential., *Int. J. Nanomedicine* **1**, 297–315 (2006).

125. B. M. Dicheva, G. A. Koning, Targeted thermosensitive liposomes: an attractive novel approach for increased drug delivery to solid tumors, *Expert Opin. Drug Deliv.* **11**, 83–100 (2014).

126. G. Storm, F. H. Roerdink, P. A. Steerenberg, W. H. de Jong, D. J. Crommelin, Influence of lipid composition on the antitumor activity exerted by doxorubicin-containing liposomes in a rat solid tumor model., *Cancer Res.* **47**, 3366–72 (1987).

127. L. H. Treat, N. J. McDannold, Y. Zhang, N. I. Vykhodtseva, K. Hynynen, Improved anti-tumor effect of liposomal doxorubicin after targeted blood-brain barrier disruption by MRI-guided focused ultrasound in rat glioma., *Ultrasound Med. Biol.* **38**, 1716–25 (2012).

128. F.-Y. Yang, H.-E. Wang, R.-S. Liu, M.-C. Teng, J.-J. Li, M. Lu, M.-C. Wei, T.-T. Wong, D. Heymann, Ed. Pharmacokinetic Analysis of ¹¹¹In-Labeled Liposomal Doxorubicin in Murine Glioblastoma after Blood-Brain Barrier Disruption by Focused Ultrasound, *PLoS One* **7**, e45468 (2012).

129. M. Aryal, N. I. Vykhodtseva, Y.-Z. Zhang, N. J. McDannold, Multiple sessions of liposomal doxorubicin delivery via focused ultrasound mediated blood-brain barrier disruption: A safety study., *J. Control. Release* **204**, 60–9 (2015).

130. N. Nomikou, P. Tiwari, T. Trehan, K. Gulati, A. P. McHale, Studies on neutral, cationic and biotinylated cationic microbubbles in enhancing ultrasound-mediated gene delivery in vitro and in vivo, *Acta Biomater.* **8**, 1273–1280 (2012).

131. C.-H. Fan, H.-L. Liu, C.-Y. Ting, Y.-H. Lee, C.-Y. Huang, Y.-J. Ma, K.-C. Wei, T.-C. Yen, C.-K. Yeh, Submicron-bubble-enhanced focused ultrasound for blood-brain barrier disruption and improved CNS drug delivery., *PLoS One* **9**, e96327 (2014).
132. C.-H. Fan, C.-Y. Ting, Y.-C. Chang, K.-C. Wei, H.-L. Liu, C.-K. Yeh, Drug-loaded bubbles with matched focused ultrasound excitation for concurrent blood-brain barrier opening and brain-tumor drug delivery., *Acta Biomater.* **15**, 89–101 (2015).
133. C.-Y. Ting, C.-H. Fan, H.-L. Liu, C.-Y. Huang, H.-Y. Hsieh, T.-C. Yen, K.-C. Wei, C.-K. Yeh, Concurrent blood-brain barrier opening and local drug delivery using drug-carrying microbubbles and focused ultrasound for brain glioma treatment., *Biomaterials* **33**, 704–12 (2012).
134. C.-H. Fan, C.-Y. Ting, H.-J. Lin, C.-H. Wang, H.-L. Liu, T.-C. Yen, C.-K. Yeh, SPIO-conjugated, doxorubicin-loaded microbubbles for concurrent MRI and focused-ultrasound enhanced brain-tumor drug delivery., *Biomaterials* **34**, 3706–15 (2013).
135. S. Bäck, J. Peränen, E. Galli, P. Pulkila, L. Lonka-Nevalaita, T. Tamminen, M. H. Voutilainen, A. Raasmaja, M. Saarma, P. T. Männistö, R. K. Tuominen, Gene therapy with AAV2-CDNF provides functional benefits in a rat model of Parkinson's disease., *Brain Behav.* **3**, 75–88 (2013).
136. T. Bjorklund, J. H. Kordower, Gene therapy for Parkinson's disease., *Mov. Disord.* **25 Suppl 1**, S161-73 (2010).
137. P. a LeWitt, A. R. Rezai, M. a Leehey, S. G. Ojemann, A. W. Flaherty, E. N. Eskandar, S. K. Kostyk, K. Thomas, A. Sarkar, M. S. Siddiqui, S. B. Tatter, J. M. Schwalb, K. L. Poston, J. M. Henderson, R. M. Kurlan, I. H. Richard, L. Van Meter, C. V Sapan, M. J. Doring, M. G. Kaplitt, A. Feigin, AAV2-GAD gene therapy for advanced Parkinson's disease: a double-blind, sham-surgery controlled, randomised trial., *Lancet Neurol.* **10**, 309–19 (2011).
138. S. R. Murphy, C. C. Y. Chang, G. Dogbevia, E. Y. Bryleva, Z. Bowen, M. T. Hasan, T.

Chang, Acat1 Knockdown Gene Therapy Decreases Amyloid- β in a Mouse Model of Alzheimer's Disease, *Mol. Ther.* **21**, 1497–1506 (2013).

139. R. J. Mandel, CERE-110, an adeno-associated virus-based gene delivery vector expressing human nerve growth factor for the treatment of Alzheimer's disease., *Curr. Opin. Mol. Ther.* **12**, 240–247 (2010).

140. V. J. Mccurdy, H. E. Rockwell, J. R. Arthur, A. M. Bradbury, A. K. Johnson, A. N. Randle, B. L. Brunson, M. Hwang, H. L. Gray-edwards, Widespread correction of central nervous system disease after intracranial gene therapy in a feline model of Sandhoff disease, *Gene Ther.* **22**, 181–189 (2014).

141. M. Berry, L. Barrett, L. Seymour, A. Baird, A. Logan, Gene therapy for central nervous system repair., *Curr. Opin. Mol. Ther.* **3**, 338–349 (2001).

142. H. Okura, C. A. Smith, J. T. Rutka, Gene therapy for malignant glioma., *Expert Rev. Neurother.* **6**, 479–488 (2006).

143. K. S. Bankiewicz, J. L. Eberling, M. Kohutnicka, W. Jagust, P. Pivrotto, J. Bringas, J. Cunningham, T. F. Budinger, J. Harvey-White, Convection-enhanced delivery of AAV vector in parkinsonian monkeys; in vivo detection of gene expression and restoration of dopaminergic function using pro-drug approach., *Exp. Neurol.* **164**, 2–14 (2000).

144. T. Shahar, Z. Ram, A. a. Kanner, Convection-enhanced delivery catheter placements for high-grade gliomas: Complications and pitfalls, *J. Neurooncol.* **107**, 373–378 (2012).

145. E. Allard, C. Passirani, J.-P. Benoit, Convection-enhanced delivery of nanocarriers for the treatment of brain tumors., *Biomaterials* **30**, 2302–18 (2009).

146. D. Omata, Y. Negishi, S. Hagiwara, S. Yamamura, Y. Endo-Takahashi, R. Suzuki, K. Maruyama, M. Nomizu, Y. Aramaki, Bubble liposomes and ultrasound promoted endosomal escape of TAT-PEG liposomes as gene delivery carriers., *Mol. Pharm.* **8**, 2416–23 (2011).

147. D. Omata, Y. Negishi, R. Suzuki, Y. Oda, *Nonviral Gene Delivery Systems by the*

Combination of Bubble Liposomes and Ultrasound (Elsevier Ltd, 2015;

<http://dx.doi.org/10.1016/bs.adgen.2014.11.001>).

148. C. W. Burke, J. S. Suk, A. J. Kim, Y.-H. J. Hsiang, A. L. Klibanov, J. Hanes, R. J. Price, Markedly Enhanced Skeletal Muscle Transfection Achieved by the Ultrasound-Targeted Delivery of Non-Viral Gene Nanocarriers with Microbubbles, *J. Control. Release* **162**, 414–421 (2012).

149. S. Xenariou, H. D. Liang, U. Griesenbach, J. Zhu, R. Farley, L. Somerton, C. Singh, P. K. Jeffery, R. K. Scheule, S. H. Cheng, D. M. Geddes, M. Blomley, E. W. F. W. Alton, Low-frequency ultrasound increases non-viral gene transfer to the mouse lung, *Acta Biochim. Biophys. Sin. (Shanghai)*. **42**, 45–51 (2010).

150. D. H. Park, B. K. Jung, Y. S. Lee, J. Y. Jang, M. K. Kim, J. K. Lee, H. Park, J. Seo, C. W. Kim, Evaluation of in vivo antitumor effects of ANT2 shRNA delivered using PEI and ultrasound with microbubbles, *Gene Ther.* **22**, 325–332 (2015).

151. W. Xie, S. Liu, H. Su, Z. Wang, Y. Zheng, Y. Fu, Ultrasound microbubbles enhance recombinant adeno-associated virus vector delivery to retinal ganglion cells in vivo, *Acad. Radiol.* **17**, 1242–1248 (2010).

152. A. G. Sorace, J. M. Warram, M. Mahoney, K. R. Zinn, K. Hoyt, Enhancement of Adenovirus Delivery after Ultrasound-Stimulated Therapy in a Cancer Model, *Ultrasound Med. Biol.* **39**, 2374–2381 (2013).

153. M. Konishi, K. Kawamoto, M. Izumikawa, H. Kuriyama, T. Yamashita, Gene transfer into guinea pig cochlea using adeno-associated virus vectors., *J. Gene Med.* **10**, 610–618 (2008).

154. J. P. Christiansen, B. a. French, A. L. Klibanov, S. Kaul, J. R. Lindner, Targeted tissue transfection with ultrasound destruction of plasmid-bearing cationic microbubbles, *Ultrasound Med. Biol.* **29**, 1759–1767 (2003).

155. E. Thévenot, J. F. Jordão, M. a O'Reilly, K. Markham, Y.-Q. Weng, K. D. Foust, B. K.

- Kaspar, K. Hynynen, I. Aubert, Targeted delivery of self-complementary adeno-associated virus serotype 9 to the brain, using magnetic resonance imaging-guided focused ultrasound., *Hum. Gene Ther.* **23**, 1144–55 (2012).
156. Q. Huang, J. Deng, Z. Xie, F. Wang, S. Chen, B. Lei, P. Liao, N. Huang, Z. Wang, Z. Wang, Y. Cheng, Effective Gene Transfer into Central Nervous System Following Ultrasound-Microbubbles-Induced Opening of the Blood-Brain Barrier, *Ultrasound Med. Biol.* **38**, 1234–1243 (2012).
157. Q. Huang, J. Deng, F. Wang, S. Chen, Y. Liu, Z. Z. Wang, Z. Z. Wang, Y. Cheng, Targeted gene delivery to the mouse brain by MRI-guided focused ultrasound-induced blood-brain barrier disruption., *Exp. Neurol.* **233**, 350–6 (2012).
158. D. S. Wang, C. Panje, M. A. Pysz, R. Paulmurugan, J. Rosenberg, S. S. Gambhir, M. Schneider, J. K. Willmann, Cationic versus Neutral Microbubbles for Ultrasound-mediated Gene Delivery in Cancer *Radiology* **264**, 721–732 (2012).
159. C. W. Burke, Y.-H. H. J. H. J. Hsiang, E. Alexander, A. L. Kilbanov, R. J. Price, E. Alexander IV, A. L. Kilbanov, R. J. Price, Covalently linking poly(lactic-co-glycolic acid) nanoparticles to microbubbles before intravenous injection improves their ultrasound-targeted delivery to skeletal muscle., *Small* **7**, 1227–35 (2011).
160. C. W. Burke, E. Alexander, K. Timbie, A. L. Kilbanov, R. J. Price, Ultrasound-activated Agents Comprised of 5FU-bearing Nanoparticles Bonded to Microbubbles Inhibit Solid Tumor Growth and Improve Survival., *Mol. Ther.* **22**, 321–8 (2014).
161. S. Duque, B. Joussemet, C. Riviere, T. Marais, L. Dubreil, A.-M. Douar, J. Fyfe, P. Moullier, M.-A. Colle, M. Barkats, Intravenous administration of self-complementary AAV9 enables transgene delivery to adult motor neurons., *Mol. Ther.* **17**, 1187–1196 (2009).
162. D. Weber-Adrian, E. Thévenot, M. a O'Reilly, W. Oakden, M. K. Akens, N. Ellens, K. Markham-Coultes, A. Burgess, J. Finkelstein, a J. M. Yee, C. M. Whyne, K. D. Foust, B. K.

Kaspar, G. J. Stanisiz, R. Chopra, K. Hynynen, I. Aubert, Gene delivery to the spinal cord using MRI-guided focused ultrasound, *Gene Ther.* (2015), doi:10.1038/gt.2015.25.

163. S. Wang, O. O. Olumolade, T. Sun, G. Samiotaki, E. E. Konofagou, Noninvasive, neuron-specific gene therapy can be facilitated by focused ultrasound and recombinant adeno-associated virus, *Gene Ther.* **22**, 104–110 (2015).

164. A. Alonso, E. Reinz, B. Leuchs, J. Kleinschmidt, M. Fatar, B. Geers, I. Lentacker, M. G. Hennerici, S. C. de Smedt, S. Meairs, Focal Delivery of AAV2/1-transgenes Into the Rat Brain by Localized Ultrasound-induced BBB Opening., *Mol. Ther. Nucleic Acids* **2**, e73 (2013).

165. P.-H. Hsu, K.-C. Wei, C.-Y. Huang, C.-J. Wen, T.-C. Yen, C.-L. Liu, Y.-T. Lin, J.-C. Chen, C.-R. Shen, H.-L. Liu, Noninvasive and targeted gene delivery into the brain using microbubble-facilitated focused ultrasound., *PLoS One* **8**, e57682 (2013).

166. M. G. Kaplitt, P. Leone, R. J. Samulski, X. Xiao, D. W. Pfaff, K. L. O'Malley, M. J. During, Long-term gene expression and phenotypic correction using adeno-associated virus vectors in the mammalian brain., *Nat. Genet.* **8**, 148–154 (1994).

167. T. J. McCown, X. Xiao, J. Li, G. R. Breese, R. J. Samulski, Differential and persistent expression patterns of CNS gene transfer by an adeno-associated virus (AAV) vector, *Brain Res.* **713**, 99–107 (1996).

168. C. Summerford, R. J. Samulski, Membrane-associated heparan sulfate proteoglycan is a receptor for adeno-associated virus type 2 virions., *J. Virol.* **72**, 1438–1445 (1998).

169. F. Properzi, R. Lin, J. Kwok, M. Naidu, T. H. Van Kuppevelt, G. B. Ten Dam, L. M. Camargo, R. Raha-Chowdhury, Y. Furukawa, T. Mikami, K. Sugahara, J. W. Fawcett, Heparan sulphate proteoglycans in glia and in the normal and injured CNS: Expression of sulphotransferases and changes in sulphation, *Eur. J. Neurosci.* **27**, 593–604 (2008).

170. C. S. Peden, C. Burger, N. Muzyczka, R. J. Mandel, Circulating Anti-Wild-Type Adeno-Associated Virus Type 2 (AAV2) Antibodies Inhibit Recombinant AAV2 (rAAV2)-Mediated, but

- Not rAAV5-Mediated, Gene Transfer in the Brain, *J. Virol.* **78**, 6344–6359 (2004).
171. R. Calcedo, J. M. Wilson, Humoral Immune Response to AAV., *Front. Immunol.* **4**, 1–7 (2013).
172. J. Wu, W. Zhao, L. Zhong, Z. Han, B. Li, W. Ma, K. a Weigel-Kelley, K. H. Warrington, A. Srivastava, Self-complementary recombinant adeno-associated viral vectors: packaging capacity and the role of rep proteins in vector purity., *Hum. Gene Ther.* **18**, 171–182 (2007).
173. A. Z. Wilczewska, K. Niemirowicz, K. H. Markiewicz, H. Car, Nanoparticles as drug delivery systems, *Pharmacol. Reports* **64**, 1020–1037 (2012).
174. N. J. Boylan, J. S. Suk, S. K. Lai, R. Jelinek, M. P. Boyle, M. J. Cooper, J. Hanes, Highly compacted DNA nanoparticles with low MW PEG coatings: in vitro, ex vivo and in vivo evaluation., *J. Control. Release* **157**, 72–9 (2012).
175. H. L. Wong, X. Y. Wu, R. Bendayan, Nanotechnological advances for the delivery of CNS therapeutics., *Adv. Drug Deliv. Rev.* (2011), doi:10.1016/j.addr.2011.10.007.
176. J. Suh, K.-L. L. Choy, S. K. Lai, J. S. Suk, B. C. Tang, S. Prabhu, J. Hanes, PEGylation of nanoparticles improves their cytoplasmic transport, *Int. J. Nanomedicine* **2**, 735–741 (2007).
177. F. Danhier, E. Ansorena, J. M. Silva, R. Coco, A. Le Breton, V. Pr eat, PLGA-based nanoparticles: An overview of biomedical applications, *J. Control. Release* **161**, 505–522 (2012).
178. G. Tosi, B. Bortot, B. Ruozi, D. Dolcetta, M. A. Vandelli, F. Forni, G. M. Severini, Potential use of polymeric nanoparticles for drug delivery across the blood-brain barrier., *Curr. Med. Chem.* **20**, 2212–25 (2013).
179. A. Giteau, M. C. Venier-Julienne, A. Aubert-Pou essel, J. P. Benoit, How to achieve sustained and complete protein release from PLGA-based microparticles?, *Int. J. Pharm.* **350**, 14–26 (2008).
180. S. Dufort, L. Sancey, J.-L. Coll, Physico-chemical parameters that govern nanoparticles

- fate also dictate rules for their molecular evolution., *Adv. Drug Deliv. Rev.* **64**, 179–89 (2012).
181. A. Kumari, S. K. Yadav, S. C. Yadav, Biodegradable polymeric nanoparticles based drug delivery systems *Colloids Surfaces B Biointerfaces* **75**, 1–18 (2010).
182. J. C. Chappell, J. Song, C. W. Burke, A. L. Klibanov, R. J. Price, Targeted delivery of nanoparticles bearing fibroblast growth factor-2 by ultrasonic microbubble destruction for therapeutic arteriogenesis., *Small* **4**, 1769–77 (2008).
183. A. V Naumova, M. Modo, A. Moore, C. E. Murry, J. a Frank, Clinical imaging in regenerative medicine., *Nat. Biotechnol.* **32**, 804–818 (2014).
184. F. Chen, E. B. Ehlerding, W. Cai, Theranostic Nanoparticles, *J. Nucl. Med.* **55**, 1919–1922 (2014).
185. S. Walia, A. Acharya, Silica micro/nanospheres for theranostics: from bimodal MRI and fluorescent imaging probes to cancer therapy, *Beilstein J. Nanotechnol.* **6**, 546–558 (2015).
186. P. Mastorakos, C. Zhang, S. Berry, Y. Oh, S. Lee, C. G. Eberhart, G. F. Woodworth, J. S. Suk, J. Hanes, Highly PEGylated DNA Nanoparticles Provide Uniform and Widespread Gene Transfer in the Brain, *Adv. Healthc. Mater.* **4**, 1023–1033 (2015).
187. C. L. Grigsby, K. W. Leong, Balancing protection and release of DNA: tools to address a bottleneck of non-viral gene delivery., *J. R. Soc. Interface* **7 Suppl 1**, S67-82 (2010).
188. D. R. Zimmermann, M. T. Dours-Zimmermann, Extracellular matrix of the central nervous system: From neglect to challenge, *Histochem. Cell Biol.* **130**, 635–653 (2008).
189. C. Sykova, Eva; Nicholson, E. Syková, C. Nicholson, Diffusion in Brain Extracellular Space, *Physiol. Rev.* **88**, 1277–1340 (2009).
190. G. D. Kenny, A. S. Bienemann, A. D. Tagalakis, J. a. Pugh, K. Welser, F. Campbell, A. B. Tabor, H. C. Hailes, S. S. Gill, M. F. Lythgoe, C. W. McLeod, E. a. White, S. L. Hart, Multifunctional receptor-targeted nanocomplexes for the delivery of therapeutic nucleic acids to the Brain, *Biomaterials* **34**, 9190–9200 (2013).

191. P. a Netti, D. a Berk, M. a Swartz, a J. Grodzinsky, R. K. Jain, Role of extracellular matrix assembly in interstitial transport in solid tumors., *Cancer Res.* **60**, 2497–2503 (2000).
192. C.-H. Heldin, K. Rubin, K. Pietras, A. Ostman, High interstitial fluid pressure - an obstacle in cancer therapy., *Nat. Rev. Cancer* **4**, 806–813 (2004).
193. a Pluen, Y. Boucher, S. Ramanujan, T. D. McKee, T. Gohongi, E. di Tomaso, E. B. Brown, Y. Izumi, R. B. Campbell, D. a Berk, R. K. Jain, Role of tumor-host interactions in interstitial diffusion of macromolecules: cranial vs. subcutaneous tumors., *Proc. Natl. Acad. Sci. U. S. A.* **98**, 4628–4633 (2001).
194. R. K. Jain, T. Stylianopoulos, Delivering nanomedicine to solid tumors., *Nat. Rev. Clin. Oncol.* **7**, 653–664 (2010).
195. I. Beyer, Z. Li, J. Persson, Y. Liu, R. van Rensburg, R. Yumul, X.-B. Zhang, M.-C. Hung, A. Lieber, Controlled extracellular matrix degradation in breast cancer tumors improves therapy by trastuzumab., *Mol. Ther.* **19**, 479–489 (2011).
196. T. Stylianopoulos, M. Z. Poh, N. Insin, M. G. Bawendi, D. Fukumura, L. L. Munn, R. K. Jain, Diffusion of particles in the extracellular matrix: The effect of repulsive electrostatic interactions, *Biophys. J.* **99**, 1342–1349 (2010).
197. R. G. Thorne, C. Nicholson, In vivo diffusion analysis with quantum dots and dextrans predicts the width of brain extracellular space., *Proc. Natl. Acad. Sci. U. S. A.* **103**, 5567–5572 (2006).
198. E. Nance, C. Zhang, T.-Y. Shih, Q. Xu, B. S. Schuster, J. Hanes, Brain-penetrating nanoparticles improve paclitaxel efficacy in malignant glioma following local administration., *ACS Nano* **8**, 10655–64 (2014).
199. R. Gref, Y. Minamitake, M. T. Peracchia, V. Trubetskoy, V. Torchilin, R. Langer, Biodegradable long-circulating polymeric nanospheres., *Science* **263**, 1600–1603 (1994).
200. P. Calvo, B. Gouritin, H. Chacun, D. Desmaile, J. D'Angelo, J. P. Noel, D. Geogin, E.

- Fattal, J. P. Andreux, P. Couvreur, Long-circulating pegylated polycyanoacrylate nanoparticles as new drug carrier for brain delivery, *Pharm. Res.* **18**, 1157–1166 (2001).
201. J. Morizet, G. Eve, H. El, Poly (ethylene glycol) -Coated Hexadecylcyanoacrylate Nanospheres Display a Combined Effect for Brain Tumor Targeting, *J. Pharmacol. Exp. Ther.* **303**, 928–936 (2002).
202. C. T. Curley, N. D. Sheybani, T. N. Bullock, R. J. Price, Focused ultrasound immunotherapy for central nervous system pathologies: challenges and opportunities, *Theranostics* **7**, 3608–3623. (2017).
203. Y. Meng, M. Volpini, S. Black, A. M. Lozano, K. Hynynen, N. Lipsman, Focused ultrasound as a novel strategy for Alzheimer disease therapeutics, *Ann. Neurol.* **81**, 611–617 (2017).
204. G. Leinenga, J. Götz, J. Gotz, J. Götz, Scanning ultrasound removes amyloid-b and restores memory in an Alzheimer's disease mouse model, *Sci. Transl. Med.* **7**, 278ra33-278ra33 (2015).
205. R. M. Nisbet, A. Van Der Jeugd, G. Leinenga, H. T. Evans, P. W. Janowicz, J. Götz, Combined effects of scanning ultrasound and a tau-specific single chain antibody in a tau transgenic mouse model, *Brain* **140**, 1220–1230 (2017).
206. C. W. Burke, A. L. Klibanov, J. P. Sheehan, R. J. Price, Inhibition of glioma growth by microbubble activation in a subcutaneous model using low duty cycle ultrasound without significant heating., *J. Neurosurg.* **114**, 1654–1661 (2011).
207. T. Scarcelli, J. F. Jordão, M. a. O'reilly, N. Ellens, K. Hynynen, I. Aubert, Stimulation of hippocampal neurogenesis by transcranial focused ultrasound and microbubbles in adult mice., *Brain Stimul.* **7**, 304–307 (2014).
208. Y. Tufail, A. Matyushov, N. Baldwin, M. L. Tauchmann, J. Georges, A. Yoshihiro, S. I. H. Tillery, W. J. Tyler, Transcranial pulsed ultrasound stimulates intact brain circuits., *Neuron* **66**, 681–94 (2010).

209. S. Jalali, Y. Huang, D. J. Dumont, K. Hynynen, Focused ultrasound-mediated bbb disruption is associated with an increase in activation of AKT: experimental study in rats., *BMC Neurol.* **10**, 114 (2010).
210. S.-J. Tsai, Transcranial focused ultrasound as a possible treatment for major depression, *Med. Hypotheses* **84**, 381–383 (2015).
211. W. J. Tyler, Y. Tufail, M. Finsterwald, M. L. Tauchmann, E. J. Olson, C. Majestic, Remote excitation of neuronal circuits using low-intensity, low-frequency ultrasound., *PLoS One* **3**, e3511 (2008).
212. T. Deffieux, Y. Younan, N. Wattiez, M. Tanter, P. Pouget, J.-F. Aubry, Low-intensity focused ultrasound modulates monkey visuomotor behavior., *Curr. Biol.* **23**, 2430–3 (2013).
213. H. Kim, S. J. Taghados, K. Fischer, L. S. Maeng, S. Park, S. S. Yoo, Noninvasive Transcranial Stimulation of Rat Abducens Nerve by Focused Ultrasound, *Ultrasound Med. Biol.* **38**, 1568–1575 (2012).
214. S. S. Yoo, A. Bystritsky, J. H. Lee, Y. Zhang, K. Fischer, B. K. Min, N. J. McDannold, A. Pascual-Leone, F. a. Jolesz, Focused ultrasound modulates region-specific brain activity, *Neuroimage* **56**, 1267–1275 (2011).
215. W. Legon, A. Rowlands, A. Opitz, T. F. Sato, W. J. Tyler, Pulsed Ultrasound Differentially Stimulates Somatosensory Circuits in Humans as Indicated by EEG and fMRI, *PLoS One* **7** (2012), doi:10.1371/journal.pone.0051177.
216. W. Lee, H. Kim, Y. Jung, I.-U. Song, Y. A. Chung, S.-S. Yoo, Image-Guided Transcranial Focused Ultrasound Stimulates Human Primary Somatosensory Cortex, *Sci. Rep.* **5**, 8743 (2015).
217. G. K. Lewis, Z. R. Schulz, S. C. Pannullo, T. L. Southard, W. L. Olbricht, Ultrasound-assisted Convection-Enhanced Delivery to the Brain in vivo with a Novel Transducer Cannula, *J Neurosurg* **117**, 1128–1140 (2012).

218. Y. Mano, R. Saito, Y. Haga, T. Matsunaga, R. Zhang, M. Chonan, S. Haryu, T. Shoji, A. Sato, Y. Sonoda, N. Tsuruoka, K. Nishiyachi, A. Sumiyoshi, H. Nonaka, R. Kawashima, T. Tominaga, Intraparenchymal ultrasound application and improved distribution of infusate with convection-enhanced delivery in rodent and nonhuman primate brain, *J. Neurosurg.* **124**, 1490–1500 (2016).
219. Y. Liu, S. Paliwal, K. S. Bankiewicz, J. R. Bringas, G. Heart, S. Mitragotri, M. R. Prausnitz, Ultrasound-enhanced drug transport and distribution in the brain., *AAPS PharmSciTech* **11**, 1005–17 (2010).
220. S. Wang, M. E. Karakatsani, C. Fung, T. Sun, C. Acosta, E. Konofagou, Direct brain infusion can be enhanced with focused ultrasound and microbubbles, *J. Cereb. Blood Flow Metab.* , 1–9 (2016).
221. D. S. Hersh, B. A. Nguyen, J. G. Dancy, A. R. Adapa, J. A. Winkles, G. F. Woodworth, A. J. Kim, V. Frenkel, Pulsed ultrasound expands the extracellular and perivascular spaces of the brain, *Brain Res.* **1646**, 543–550 (2016).
222. A. Ziadloo, J. Xie, V. Frenkel, Pulsed focused ultrasound exposures enhance locally administered gene therapy in a murine solid tumor model., *J. Acoust. Soc. Am.* **133**, 1827–34 (2013).
223. A. Burgess, Y. Huang, W. Querbes, D. W. Sah, K. Hynynen, Focused ultrasound for targeted delivery of siRNA and efficient knockdown of Htt expression, *J. Control. Release* **163**, 125–129 (2012).
224. K. Timbie, C. Burke, E. Nance, G. Woodworth, G. W. Miller, J. Hanes, R. J. Price, Ultrasound-targeted delivery of systemically administered therapeutic nanoparticles., *J. Acoust. Soc. Am.* **134**, 4047 (2013).
225. G. Leinenga, J. Gotz, Scanning ultrasound removes amyloid-b and restores memory in an Alzheimer's disease mouse model, *Sci. Transl. Med.* **7**, 278ra33-278ra33 (2015).

226. J. Ning, H. Wakimoto, Oncolytic herpes simplex virus-based strategies: Toward a breakthrough in glioblastoma therapy, *Front. Microbiol.* **5**, 1–13 (2014).
227. B. Kantor, T. J. McCown, P. Leone, S. J. Gray, *Clinical Applications Involving CNS Gene Transfer* (Elsevier, 2014; <http://linkinghub.elsevier.com/retrieve/pii/B9780128001493000020>).
228. J. M. Bergen, I. K. Park, P. J. Horner, S. H. Pun, Nonviral approaches for neuronal delivery of nucleic acids, *Pharm. Res.* **25**, 983–998 (2008).
229. R. A. Kroll, E. A. Neuwelt, Outwitting the blood-brain barrier for therapeutic purposes: Osmotic opening and other means *Neurosurgery* **42**, 1083–1100 (1998).
230. W. M. Pardridge, Blood-brain barrier delivery *Drug Discov. Today* **12**, 54–61 (2007).
231. N. Hosseinkhah, K. Hynynen, A three-dimensional model of an ultrasound contrast agent gas bubble and its mechanical effects on microvessels., *Phys. Med. Biol.* **57**, 785–808 (2012).
232. X. Shang, P. Wang, Y. Liu, Z. Zhang, Mechanism of Low-Frequency Ultrasound in Opening Blood – Tumor Barrier by Tight Junction, *J Mol Neurosci* **43**, 364–369 (2011).
233. F. Vlachos, Y.-S. Tung, E. E. Konofagou, Permeability assessment of the focused ultrasound-induced blood-brain barrier opening using dynamic contrast-enhanced MRI., *Phys. Med. Biol.* **55**, 5451–66 (2010).
234. A. B. Etame, R. J. Diaz, M. A. O. Reilly, C. A. Smith, T. G. Mainprize, K. Hynynen, J. T. Rutka, Enhanced delivery of gold nanoparticles with therapeutic potential into the brain using MRI-guided focused ultrasound, *Nanomedicine Nanotechnology, Biol. Med.* **8**, 1133–1142 (2012).
235. A. Burgess, C. a Ayala-Grosso, M. Ganguly, J. F. Jordão, I. Aubert, K. Hynynen, Targeted delivery of neural stem cells to the brain using MRI-guided focused ultrasound to disrupt the blood-brain barrier., *PLoS One* **6**, e27877 (2011).
236. O. M. Merkel, R. Urbanics, P. Bedocs, Z. Rozsnyay, L. Rosivall, M. Toth, T. Kissel, J. Szebeni, In vitro and in vivo complement activation and related anaphylactic effects associated

with polyethylenimine and polyethylenimine-graft-poly(ethylene glycol) block copolymers, *Biomaterials* **32**, 4936–4942 (2011).

237. A. Malek, F. Czubayko, A. Aigner, PEG grafting of polyethylenimine (PEI) exerts different effects on DNA transfection and siRNA-induced gene targeting efficacy., *J. Drug Target.* **16**, 124–139 (2008).

238. H. Petersen, P. M. Fechner, A. L. Martin, K. Kunath, S. Stolnik, C. J. Roberts, D. Fischer, M. C. Davies, T. Kissel, Polyethylenimine-graft-poly(ethylene glycol) copolymers: Influence of copolymer block structure on DNA complexation and biological activities as gene delivery system, *Bioconjug. Chem.* **13**, 845–854 (2002).

239. C. E. Thomas, T. a Storm, Z. Huang, M. a Kay, Rapid uncoating of vector genomes is the key to efficient liver transduction with pseudotyped adeno-associated virus vectors., *J. Virol.* **78**, 3110–3122 (2004).

240. C. H. Miao, R. O. Snyder, D. B. Schowalter, G. Patijn, B. Donahue, B. Winther, M. Kay, The Kinetics of rAAV Integration in the Liver, *Nat. Genet.* **18**, 231–236 (1998).

241. S. J. Gray, S. B. Foti, J. W. Schwartz, L. Bachaboina, B. Taylor-Blake, J. Coleman, M. D. Ehlers, M. J. Zylka, T. J. McCown, R. J. Samulski, Optimizing promoters for recombinant adeno-associated virus-mediated gene expression in the peripheral and central nervous system using self-complementary vectors., *Hum. Gene Ther.* **22**, 1143–53 (2011).

242. J. J. Rodríguez, A. Verkhratsky, Neuroglial roots of neurodegenerative diseases?, *Mol. Neurobiol.* **43**, 87–96 (2011).

243. D. Davila, K. Thibault, T. a Fiacco, C. Agulhon, Recent molecular approaches to understanding astrocyte function in vivo., *Front. Cell. Neurosci.* **7**, 272 (2013).

244. Y.-S. Tung, F. Vlachos, J. Feshitan, M. Borden, E. E. Konofagou, The mechanism of interaction between focused ultrasound and microbubbles in blood-brain barrier opening in mice, *J. Acoust. Soc. Am.* **130**, 3059 (2011).

245. W. T. Godbey, K. K. Wu, A. G. Mikos, Poly(ethylenimine) and its role in gene delivery, *J. Control. Release* **60**, 149–160 (1999).
246. T. Pringsheim, N. Jette, A. Frolikis, T. D. L. Steeves, The prevalence of Parkinson's disease: A systematic review and meta-analysis, *Mov. Disord.* **29**, 1583–1590 (2014).
247. S. Bhattacharjee, U. Sambamoorthi, Co-occurring chronic conditions and healthcare expenditures associated with Parkinson's disease : A propensity score matched analysis, *Park. Relat. Disord.* **19**, 746–750 (2013).
248. J. Jankovic, W. Poewe, Therapies in Parkinson's disease, *Curr. Opin. Neurol.* **25**, 433–447 (2012).
249. A. Toulouse, A. M. Sullivan, Progress in Parkinson's disease-Where do we stand?, *Prog. Neurobiol.* **85**, 376–392 (2008).
250. L. V Kalia, A. E. Lang, Parkinson's disease, *Lancet* **386**, 896–912 (2015).
251. E. Garbayo, E. Ansorena, M. J. Blanco-Prieto, Drug development in Parkinson's disease: From emerging molecules to innovative drug delivery systems, *Maturitas* **76**, 272–278 (2013).
252. L. F. Lin, D. H. Doherty, J. D. Lile, S. Bektesh, F. Collins, GDNF: a glial cell line-derived neurotrophic factor for midbrain dopaminergic neurons., *Science* **260**, 1130–1132 (1993).
253. P. T. Kotzbauer, P. Lampe, R. O. Heuckeroth, J. P. Golden, D. J. Creedon, E. M. Johnson, J. Milbrandt, Neurturin, a relative of glial-cell-line-derived neurotrophic factor. *Nature* **384**, 467–470 (1996).
254. R. T. Bartus, E. M. Johnson, Clinical tests of neurotrophic factors for human neurodegenerative diseases, part 1: Where do we stand and where must we go next?, *Neurobiol. Dis.* **97**, 156–168 (2016).
255. R. T. Bartus, E. M. Johnson, Clinical tests of neurotrophic factors for human neurodegenerative diseases, part 2: Where do we stand and where must we go next?, *Neurobiol. Dis.* **97**, 169–178 (2016).

256. J. H. Kordower, A. Bjorklund, Trophic factor gene therapy for Parkinson's disease., *Mov. Disord.* **28**, 96–109 (2013).
257. K. Hynynen, N. J. Mcdannold, N. Vykhodtseva, F. A. Jolesz, Noninvasive MR Imaging-guided Focal Opening of the Blood-Brain Barrier in Rabbits, *Radiology* **220**, 640–646 (2001).
258. P. Ghanouni, K. B. Pauly, W. J. Elias, J. Henderson, J. Sheehan, S. Monteith, M. Wintermark, Transcranial MRI-Guided Focused Ultrasound: A Review of the Technologic and Neurologic Applications, *Am. J. Roentgenol.* **205**, 150–159 (2015).
259. W. J. Elias, N. Lipsman, W. G. Ondo, P. Ghanouni, Y. G. Kim, W. Lee, M. Schwartz, K. Hynynen, A. M. Lozano, B. B. Shah, D. Huss, R. F. Dallapiazza, R. Gwinn, J. Witt, S. Ro, H. M. Eisenberg, P. S. Fishman, D. Gandhi, C. Helpert, R. Chuang, K. B. Pauly, T. S. Tierney, M. T. Hayes, G. R. Cosgrove, T. Yamaguchi, K. Abe, T. Taira, J. W. Chang, C. H. Halpern, R. Chuang, K. Butts Pauly, T. S. Tierney, M. T. Hayes, G. R. Cosgrove, T. Yamaguchi, K. Abe, T. Taira, J. W. Chang, A Randomized Trial of Focused Ultrasound Thalamotomy for Essential Tremor, *N. Engl. J. Med.* **375**, 730–739 (2016).
260. I. Schlesinger, a Eran, a Sinai, I. Erikh, M. Nassar, D. Goldsher, M. Zaaroor, MRI guided focused ultrasound thalamotomy for essential tremor, *Mov. Disord.* **29**, S423 (2014).
261. J. S. Suk, Q. Xu, N. Kim, J. Hanes, L. M. Ensign, PEGylation as a strategy for improving nanoparticle-based drug and gene delivery, *Adv. Drug Deliv. Rev.* **99**, 28–51 (2016).
262. J. Nance, Elizabeth; Zhang, C.; Shih, T.; Xu, Q.; Schuster, B.; Hanes, Brain-Penetrating Nanoparticles Improve Paclitaxel Efficacy in Malignant Glioma Following Local Administration, *ACS Nano* **8**, 10655–10664 (2014).
263. P. Mastorakos, A. L. da Silva, J. Chisholm, E. Song, W. K. Choi, M. P. Boyle, M. M. Morales, J. Hanes, J. S. Suk, Highly compacted biodegradable DNA nanoparticles capable of overcoming the mucus barrier for inhaled lung gene therapy, *Proc. Natl. Acad. Sci.* , 201502281 (2015).

264. J. S. Suk, A. J. Kim, K. Trehan, C. S. Schneider, L. Cebotaru, O. M. Woodward, N. J. Boylan, M. P. Boyle, S. K. Lai, W. B. Guggino, J. Hanes, Lung gene therapy with highly compacted DNA nanoparticles that overcome the mucus barrier, *J. Control. Release* **178**, 8–17 (2014).
265. B. P. Mead, P. Mastorakos, J. S. Suk, A. L. Klibanov, J. Hanes, R. J. Price, Targeted Gene Transfer to the Brain via the Delivery of Brain-Penetrating DNA Nanoparticles with Focused Ultrasound, *J. Control. Release* **223**, 109–117 (2016).
266. A. M. Fletcher, T. H. Kowalczyk, L. Padegimas, M. J. Cooper, D. M. Yurek, Transgene expression in the striatum following intracerebral injections of DNA nanoparticles encoding for human glial cell line-derived neurotrophic factor., *Neuroscience* **194**, 220–6 (2011).
267. D. M. Yurek, A. M. Fletcher, M. Mcshane, T. H. Kowalczyk, M. R. Weatherspoon, M. D. Kaytor, M. J. Cooper, G. Assem, DNA Nanoparticles: Detection of Long-Term Transgene Activity in Brain Using Bioluminescence Imaging, *Mol. Imaging* **10**, 327–339 (2011).
268. A. Björklund, D. Kirik, C. Rosenblad, B. Georgievska, C. Lundberg, R. J. Mandel, Towards a neuroprotective gene therapy for Parkinson's disease: use of adenovirus, AAV and lentivirus vectors for gene transfer of GDNF to the nigrostriatal system in the rat Parkinson model., *Brain Res.* **886**, 82–98 (2000).
269. C.-Y. Lin, H.-Y. Hsieh, C.-M. Chen, S.-R. Wu, C.-H. Tsai, C.-Y. Huang, M.-Y. Hua, K.-C. Wei, C.-K. Yeh, H.-L. Liu, Non-invasive, Neuron-Specific Gene Therapy by Focused Ultrasound-Induced Blood-Brain Barrier Opening in Parkinson's Disease Mouse Model, *J. Control. Release* **10**, 72–81 (2016).
270. D. M. Yurek, A. M. Fletcher, G. M. Smith, K. B. Seroogy, A. G. Ziady, J. Molter, T. H. Kowalczyk, L. Padegimas, M. J. Cooper, Long-term transgene expression in the central nervous system using DNA nanoparticles., *Mol. Ther.* **17**, 641–50 (2009).
271. A. Eslamboli, B. Georgievska, R. M. Ridley, H. F. Baker, N. Muzyczka, C. Burger, R. J.

- Mandel, L. Annett, D. Kirik, Continuous low-level glial cell line-derived neurotrophic factor delivery using recombinant adeno-associated viral vectors provides neuroprotection and induces behavioral recovery in a primate model of Parkinson's disease., *J. Neurosci.* **25**, 769–77 (2005).
272. B. Georgievska, D. Kirik, A. Bjo, Overexpression of Glial Cell Line-Derived Neurotrophic Factor Using a Lentiviral Vector Induces Time- and Dose- Dependent Downregulation of Tyrosine Hydroxylase in the Intact Nigrostriatal Dopamine System, *J. Neurosci.* **24**, 6437–6445 (2004).
273. N. Tumer, P. J. Scarpace, M. D. Dogan, C. S. Broxson, M. Matheny, D. M. Yurek, C. S. Peden, C. Burger, N. Muzyczka, R. J. Mandel, Hypothalamic rAAV-mediated GDNF gene delivery ameliorates age-related obesity, *Neurobiol. Aging* **27**, 459–470 (2006).
274. F. P. Manfredsson, N. Tumer, B. Erdos, T. Landa, C. S. Broxson, L. F. Sullivan, A. C. Rising, K. D. Foust, Y. Zhang, N. Muzyczka, O. S. Gorbatyuk, P. J. Scarpace, R. J. Mandel, Nigrostriatal rAAV-mediated GDNF overexpression induces robust weight loss in a rat model of age-related obesity., *Mol. Ther.* **17**, 980–91 (2009).
275. O. Isacson, J. H. Kordower, Future of cell and gene therapies for Parkinson's disease, *Ann. Neurol.* **64**, 122–138 (2008).
276. W. M. Pardridge, R. J. Boado, Pharmacokinetics and safety in rhesus monkeys of a monoclonal antibody-gdnf fusion protein for targeted blood-brain barrier delivery, *Pharm. Res.* **26**, 2227–2236 (2009).
277. E. Garbayo, C. N. Montero-Menei, E. Ansorena, J. L. Lanciego, M. S. Aymerich, M. J. Blanco-Prieto, Effective GDNF brain delivery using microspheres-A promising strategy for Parkinson's disease, *J. Control. Release* **135**, 119–126 (2009).
278. S. Sarkar, J. Raymick, S. Imam, Neuroprotective and Therapeutic Strategies against Parkinson's Disease: Recent Perspectives., *Int. J. Mol. Sci.* **17** (2016),

doi:10.3390/ijms17060904.

279. N. I. Bohnen, R. L. Albin, R. A. Koeppe, K. A. Wernette, M. R. Kilbourn, S. Minoshima, K. A. Frey, Positron emission tomography of monoaminergic vesicular binding in aging and Parkinson disease., *J. Cereb. Blood Flow Metab.* **26**, 1198–1212 (2006).
280. M. Decressac, A. Ulusoy, B. Mattsson, B. Georgievska, M. Romero-Ramos, D. Kirik, A. Björklund, GDNF fails to exert neuroprotection in a rat α -synuclein model of Parkinson's disease., *Brain* **134**, 2302–11 (2011).
281. M. Decressac, B. Kadkhodaei, B. Mattsson, A. Laguna, T. Perlmann, A. Björklund, A. Björklund, A-Synuclein-Induced Down-Regulation of Nurr1 Disrupts GDNF Signaling in Nigral Dopamine Neurons, *Sci. Transl. Med.* **4**, 1–15 (2012).
282. D. Kirik, C. Rosenblad, A. Bjo, R. J. Mandel, Long-Term rAAV-Mediated Gene Transfer of GDNF in the Rat Parkinson' s Model: Intrastratial But Not Intranigral Transduction Promotes Functional Regeneration in the Lesioned Nigrostriatal System, *J. Neurosci.* **20**, 4686–4700 (2000).
283. R. T. Bartus, J. H. Kordower, E. M. Johnson, L. Brown, B. R. Kruegel, Y. Chu, T. L. Baumann, a. E. Lang, C. W. Olanow, C. D. Herzog, Post-mortem assessment of the short and long-term effects of the trophic factor neurturin in patients with α -synucleinopathies, *Neurobiol. Dis.* **78**, 162–171 (2015).
284. W. C. Olanow, R. T. Bartus, T. L. Baumann, S. Factor, N. Boulis, M. Stacy, D. Turner, W. Marks, P. Larson, P. Starr, J. Jankovic, R. Simpson, R. Watts, B. Guthrie, K. Poston, J. M. Henderson, M. Stern, G. Baltuch, C. G. Goetz, C. Herzog, J. H. Kordower, R. Alterman, A. M. Lozano, A. E. Lang, Gene delivery of neurturin to putamen and substantia nigra in Parkinson disease: A double-blind, randomized, controlled trial, *Ann. Neurol.* **78**, 162–171 (2015).
285. J. H. Kordower, C. W. Olanow, H. B. Dodiya, Y. Chu, T. G. Beach, C. H. Adler, G. M. Halliday, R. T. Bartus, Disease duration and the integrity of the nigrostriatal system in

- Parkinson's disease, *Brain* **136**, 2419–2431 (2013).
286. A. Carpentier, M. Canney, A. Vignot, V. Reina, K. Beccaria, C. Horodyckid, C. Karachi, D. Leclercq, C. Lafon, J. Chapelon, L. Capelle, P. Cornu, M. Sanson, K. Hoang-xuan, Clinical trial of blood-brain barrier disruption by pulsed ultrasound, *Sci. Transl. Med.* **8**, 1–8 (2016).
287. S. L. Hardie, J. Hirsh, An improved method for the separation and detection of biogenic amines in adult *Drosophila* brain extracts by high performance liquid chromatography, *J. Neurosci. Methods* **153**, 243–249 (2006).
288. B. P. Mead, N. Kim, G. W. Miller, D. Hodges, P. Mastorakos, A. L. Klibanov, J. W. Mandell, J. Hirsh, J. S. Suk, J. Hanes, R. J. Price, ∇ Jung, S. Suk, J. Hanes, R. J. Price, Novel Focused Ultrasound Gene Therapy Approach Noninvasively Restores Dopaminergic Neuron Function in a Rat Parkinson's Disease Model, *Nano Lett.* (2017), doi:10.1021/acs.nanolett.7b00616.
289. T. Patel, J. Zhou, J. M. Piepmeier, W. M. Saltzman, Polymeric nanoparticles for drug delivery to the central nervous system., *Adv. Drug Deliv. Rev.* **64**, 701–5 (2012).
290. E. Shigetomi, X. Tong, K. Y. Kwan, D. P. Corey, B. S. Khakh, TRPA1 channels regulate astrocyte resting calcium and inhibitory synapse efficacy through GAT-3, *Nat. Neurosci.* **15**, 70–80 (2011).
291. Y. Kimura, Y. Mikami, K. Osumi, M. Tsugane, J. I. Oka, H. Kimura, Polysulfides are possible H₂S-derived signaling molecules in rat brain, *FASEB J.* **27**, 2451–2457 (2013).
292. Y. Chen, H. H. Willcockson, J. G. Valtchanoff, Influence of the vanilloid receptor TRPV1 on the activation of spinal cord glia in mouse models of pain, *Exp. Neurol.* **220**, 383–390 (2009).
293. T. Mannari, S. Morita, E. Furube, M. Tominaga, S. Miyata, Astrocytic TRPV1 ion channels detect blood-borne signals in the sensory circumventricular organs of adult mouse brains, *Glia* **61**, 957–971 (2013).
294. M. Mulier, J. Vriens, T. Voets, TRP channel pores and local calcium signals, *Cell Calcium* **66**, 19–24 (2017).

295. S. M. Brierley, P. A. Hughes, A. J. Page, K. Y. Kwan, C. M. Martin, T. A. O'Donnel, N. J. Cooper, A. M. Harrington, B. Adam, T. Liebrechts, G. Holtmann, D. P. Corey, Y. Rychkov, Grigory, A. Blackshaw, The Ion Channel TRPA1 is Required for Normal Mechanosensation and is Modulated by Algesic Stimuli., *Gastroenterology* **137**, 5124–5136 (2010).
296. M. J. Caterina, M. a Schumacher, M. Tominaga, T. a Rosen, J. D. Levine, D. Julius, The capsaicin receptor: a heat-activated ion channel in the pain pathway., *Nature* **389**, 816–824 (1997).
297. N. Bazargani, D. Attwell, Astrocyte calcium signaling: the third wave., *Nat. Neurosci.* **19**, 182–9 (2016).
298. P. Mastorakos, C. Zhang, S. Berry, Y. Oh, S. Lee, C. G. Eberhart, G. F. Woodworth, J. S. Suk, J. Hanes, P. Mastorakos, C. Zhang, S. Berry, Y. Oh, S. Lee, J. S. Suk, P. J. Hanes, S. Suk, J. Hanes, P. Mastorakos, C. Zhang, S. Berry, Y. Oh, S. Lee, C. G. Eberhart, P. E. G. Pei, J. S. Suk, J. Hanes, S. Suk, J. Hanes, P. Mastorakos, C. Zhang, S. Berry, Y. Oh, S. Lee, C. G. Eberhart, P. E. G. Pei, J. S. Suk, J. Hanes, P. Mastorakos, C. Zhang, S. Berry, Y. Oh, S. Lee, J. S. Suk, P. J. Hanes, Highly PEGylated DNA Nanoparticles Provide Uniform and Widespread Gene Transfer in the Brain, *Adv. Healthc. Mater.* **4**, 1–32 (2015).
299. S. Russell, J. Bennett, J. A. Wellman, D. C. Chung, Z. F. Yu, A. Tillman, J. Wittes, J. Pappas, O. Elci, S. McCague, D. Cross, K. A. Marshall, J. Walshire, T. L. Kehoe, H. Reichert, M. Davis, L. Raffini, L. A. George, F. P. Hudson, L. Dingfield, X. Zhu, J. A. Haller, E. H. Sohn, V. B. Mahajan, W. Pfeifer, M. Weckmann, C. Johnson, D. Gewaily, A. Drack, E. Stone, K. Wachtel, F. Simonelli, B. P. Leroy, J. F. Wright, K. A. High, A. M. Maguire, Efficacy and safety of voretigene neparvovec (AAV2-hRPE65v2) in patients with RPE65-mediated inherited retinal dystrophy: A randomised, controlled, open-label, phase 3 trial, *Lancet* **390**, 849–860 (2017).
300. T. Hirsch, T. Rothoeft, N. Teig, J. W. Bauer, G. Pellegrini, L. De Rosa, D. Scaglione, J. Reichelt, A. Klausegger, D. Kneisz, O. Romano, A. Secone Seconetti, R. Contin, E. Enzo, I.

- Jurman, S. Carulli, F. Jacobsen, T. Luecke, M. Lehnhardt, M. Fischer, M. Kueckelhaus, D. Quaglino, M. Morgante, S. Bicciato, S. Bondanza, M. De Luca, Regeneration of the entire human epidermis using transgenic stem cells, *Nature* **551**, 327–332 (2017).
301. J. R. Mendell, S. Al-Zaidy, R. Shell, W. D. Arnold, L. R. Rodino-Klapac, T. W. Prior, L. Lowes, L. Alfano, K. Berry, K. Church, J. T. Kissel, S. Nagendran, J. L'Italien, D. M. Sproule, C. Wells, J. A. Cardenas, M. D. Heitzer, A. Kaspar, S. Corcoran, L. Braun, S. Likhite, C. Miranda, K. Meyer, K. D. Foust, A. H. M. Burghes, B. K. Kaspar, Single-Dose Gene-Replacement Therapy for Spinal Muscular Atrophy, *N. Engl. J. Med.* **377**, 1713–1722 (2017).
302. J. H. Sampson, G. Archer, C. Pedain, E. Wembacher-Schröder, M. Westphal, S. Kunwar, M. a Vogelbaum, A. Coan, J. E. Herndon, R. Raghavan, M. L. Brady, D. a Reardon, A. H. Friedman, H. S. Friedman, M. I. Rodríguez-Ponce, S. M. Chang, S. Mittermeyer, D. Croteau, R. K. Puri, Poor drug distribution as a possible explanation for the results of the PRECISE trial., *J. Neurosurg.* **113**, 301–309 (2010).
303. A. M. Mehta, A. M. Sonabend, J. N. Bruce, Convection-Enhanced Delivery, *Neurotherapeutics* **14**, 358–371 (2017).
304. F. P. Manfredsson, A. C. Rising, R. J. Mandel, AAV9: a potential blood-brain barrier buster., *Mol. Ther.* **17**, 403–405 (2009).
305. G. M. Thomsen, M. Alkaslasi, J.-P. Vit, G. Lawless, M. Godoy, G. Gowing, O. Shelest, C. N. Svendsen, Systemic injection of AAV9-GDNF provides modest functional improvements in the SOD1G93A ALS rat but has adverse side effects, *Gene Ther.* **24**, 245–252 (2017).
306. H. Yin, R. L. Kanasty, A. A. Eltoukhy, A. J. Vegas, J. R. Dorkin, D. G. Anderson, Non-viral vectors for gene-based therapy, *Nat. Rev. Genet.* **15**, 541–555 (2014).
307. T. Zhang, W. Guo, C. Zhang, J. Yu, J. Zu, J. Xu, S. Li, J.-H. Tian, P. C. Wang, J.-F. Zing, X.-J. Liang, Transferrin-Dressed Virus-like Ternary Nanoparticles with Aggregation-Induced Emission for Targeted Delivery and Rapid Cytosolic Release of siRNA, *ACS Appl Mater*

Interfaces **46**, 417–428 (2017).

308. K. B. Johnsen, T. Moos, Revisiting nanoparticle technology for blood-brain barrier transport: Unfolding at the endothelial gate improves the fate of transferrin receptor-targeted liposomes, *J. Control. Release* **222**, 32–46 (2016).

309. W. Olbricht, M. Sistla, G. Ghandi, G. Lewis, A. Sarvazyan, Time-reversal acoustics and ultrasound-assisted convection-enhanced drug delivery to the brain, *J. Acoust. Soc. Am.* **134**, 1569–1575 (2013).

310. K. Nightingale, M. S. Soo, R. Nightingale, G. Trahey, Acoustic Radiation Force Impulse Imaging: in Vivo Demonstration of Clinical Feasibility, *Ultrasound Med. Biol.* **28**, 227–235 (2002).

311. H. a Hancock, L. H. Smith, J. Cuesta, A. K. Durrani, M. Angstadt, L. Φ. Palmeri, E. K. Ψ, V. Frenkel, Investigations into pulsed-high intensity focused ultrasound enhanced delivery : Preliminary evidence for a novel mechanism, *Ultrasound Med. Biol.* **35**, 1722–1736 (2010).

312. H. A. Hancock, L. H. Smith, J. Cuesta, A. K. Durrani, M. Angstadt, M. L. Palmeri, E. Kimmel, V. Frenkel, Investigations into Pulsed High-Intensity Focused Ultrasound-Enhanced Delivery: Preliminary Evidence for a Novel Mechanism, *Ultrasound Med. Biol.* **35**, 1722–1736 (2009).

313. E. Cao, J. F. . Cordero-Morales, B. Liu, F. Qin, D. Julius, TRPV1 channels are intrinsically heat sensitive and negatively regulated by phosphoinositide lipids, *Neuron* **77**, 1–23 (2013).

314. M. Simard, M. Nedergaard, The neurobiology of glia in the context of water and ion homeostasis, *Neuroscience* **129**, 877–896 (2004).

315. M. Zonta, M. C. Angulo, S. Gobbo, B. Rosengarten, K.-A. Hossmann, T. Pozzan, G. Carmignoto, Neuron-to-astrocyte signaling is central to the dynamic control of brain microcirculation, *Nat. Neurosci.* **6**, 43–50 (2002).

316. G. R. J. Gordon, H. B. Choi, R. L. Rungta, G. C. R. Ellis-Davies, B. A. MacVicar, Brain metabolism dictates the polarity of astrocyte control over arterioles, *Nature* **456**, 745–749

(2008).

317. T. Takano, G.-F. Tian, W. Peng, N. Lou, W. Libionka, X. Han, M. Nedergaard, Astrocyte-mediated control of cerebral blood flow, *Nat. Neurosci.* **9**, 260–267 (2006).

318. Y. Bernardinelli, J. Randall, E. Janett, I. Nikonenko, S. König, E. V. Jones, C. E. Flores, K. K. Murai, C. G. Bochet, A. Holtmaat, D. Muller, Activity-dependent structural plasticity of perisynaptic astrocytic domains promotes excitatory synapse stability, *Curr. Biol.* **24**, 1679–1688 (2014).

319. M. Iino, K. Goto, W. Kakegawa, H. Okado, M. Sudo, A. Miwa, Y. Takayasu, I. Saito, K. Tsuzuki, S. Ozawa, Glia-Synapse Interaction Through Ca²⁺-Permeable AMPA Receptors in Bergmann Glia, *Science* (80-.). **292**, 926–929 (2001).

320. S. Wiese, M. Karus, A. Faissner, Astrocytes as a source for extracellular matrix molecules and cytokines, *Front. Pharmacol.* **3 JUN**, 1–13 (2012).

321. H. R. Parri, T. M. Gould, V. Crunelli, Spontaneous astrocytic Ca²⁺ oscillations in situ drive NMDAR-mediated neuronal excitation, *Nat. Neurosci.* **4**, 803–812 (2001).

322. V. Parpura, T. A. Basarsky, F. Liu, K. Jeftinija, S. Jeftinija, P. G. Haydon, Glutamate-mediated astrocyte–neuron signalling, *Nature* **369**, 744–747 (1994).

323. E. a Newman, Glial cell inhibition of neurons by release of ATP., *J. Neurosci.* **23**, 1659–1666 (2003).

324. J.-P. Mothet, L. Pollegioni, G. Ouanounou, M. Martineau, P. Fossier, G. Baux, Glutamate receptor activation triggers a calcium-dependent and SNARE protein-dependent release of the gliotransmitter D-serine, *Proc. Natl. Acad. Sci.* **102**, 5606–5611 (2005).

325. Q. Y. Liu, A. E. Schaffner, Y. H. Chang, D. Maric, J. L. Barker, Persistent activation of GABA(A) receptor/Cl(-) channels by astrocyte-derived GABA in cultured embryonic rat hippocampal neurons, *J. Neurophysiol.* **84**, 1392–1403 (2000).

326. J. Zhou, T. R. Patel, R. W. Sirianni, G. Strohbehn, M.-Q. Zheng, N. Duong, T. Schafbauer,

- A. J. Huttner, Y. Huang, R. E. Carson, Y. Zhang, D. J. Sullivan, J. M. Piepmeier, W. M. Saltzman, Highly penetrative, drug-loaded nanocarriers improve treatment of glioblastoma, *Proc. Natl. Acad. Sci.* **110**, 11751–11756 (2013).
327. Y. Wang, F. YUAN, Delivery of Viral Vectors to Tumor Cells : Extracellular Transport , Systemic Distribution , and Strategies for Improvement, *Ann. Biomed* **34**, 114–127 (2006).
328. V. Frenkel, Ultrasound mediated delivery of drugs and genes to solid tumors, *Adv. Drug Deliv. Rev.* **60**, 1193–1208 (2008).
329. S. McGuire, D. Zaharoff, F. Yuan, Nonlinear dependence of hydraulic conductivity on tissue deformation during intratumoral infusion, *Ann. Biomed. Eng.* **34**, 1173–1181 (2006).
330. Y. H. Bae, K. Park, Targeted drug delivery to tumors: Myths, reality and possibility, *J. Control. Release* **153**, 198–205 (2011).
331. M. Milosevic, A. Fyles, D. Hedley, R. Hill, The Human Tumor Microenvironment : Invasive (Needle) Measurement of Oxygen and Interstitial Fluid Pressure, *Semin. Radiat. Oncol.* **14**, 249–258 (2004).
332. K. F. Timbie, U. Afzal, A. Date, C. Zhang, J. Song, G. Wilson Miller, J. S. Suk, J. Hanes, R. J. Price, MR image-guided delivery of cisplatin-loaded brain-penetrating nanoparticles to invasive glioma with focused ultrasound, *J. Control. Release* , 1–12 (2017).
333. S. Lee, H. Han, H. Koo, J. H. Na, H. Y. Yoon, K. E. Lee, H. Lee, H. Kim, I. C. Kwon, K. Kim, Extracellular matrix remodeling in vivo for enhancing tumor-targeting efficiency of nanoparticle drug carriers using the pulsed high intensity focused ultrasound, *J. Control. Release* **263**, 68–78 (2017).
334. H. Han, H. Lee, K. Kim, H. Kim, Effect of high intensity focused ultrasound (HIFU) in conjunction with a nanomedicines-microbubble complex for enhanced drug delivery, *J. Control. Release* **266**, 75–86 (2017).
335. G. Samiotaki, M. E. Karakatsani, A. Buch, S. Papadopoulos, S. Y. Wu, S. Jambawalikar, E.

- E. Konofagou, Pharmacokinetic analysis and drug delivery efficiency of the focused ultrasound-induced blood-brain barrier opening in non-human primates, *Magn. Reson. Imaging* **37**, 273–281 (2017).
336. A. Maruo, C. E. Hamner, A. J. Rodrigues, T. Higami, J. F. Greenleaf, H. V. Schaff, Nitric oxide and prostacyclin in ultrasonic vasodilatation of the canine internal mammary artery, *Ann. Thorac. Surg.* **77**, 126–132 (2004).
337. S.-M. Zou, P. Erbacher, J.-S. Remy, J.-P. Behr, Systemic linear polyethylenimine (L-PEI)-mediated gene delivery in the mouse, *J. Gene Med.* **2**, 128–134 (2000).
338. T. Vasculature, G. Kong, R. D. Braun, M. W. Dewhirst, Characterization of the Effect of Hyperthermia on Nanoparticle Extravasation from, , 3027–3032 (2001).
339. K. Y. Kwan, A. J. Allchorne, M. A. Vollrath, A. P. Christensen, D. S. Zhang, C. J. Woolf, D. P. Corey, TRPA1 Contributes to Cold, Mechanical, and Chemical Nociception but Is Not Essential for Hair-Cell Transduction, *Neuron* **50**, 277–289 (2006).
340. M. J. Caterina, A. Leffler, Malmberg A.B., W. J. Martin, J. Trafton, P.-Z. K.R., M. Koltzenburg, A. I. Basbaum, D. Julius, Impaired Nociception and Pain Sensation in Mice Lacking the Capsaicin Receptor, *Science* (80-.). **288**, 306–313 (2000).
341. P. Mastorakos, C. Zhang, S. Berry, Y. Oh, S. Lee, C. G. Eberhart, G. F. Woodworth, S. Suk, J. Hanes, P. Mastorakos, C. Zhang, S. Berry, Y. Oh, S. Lee, C. G. Eberhart, P. E. G. Pei, Highly PEGylated DNA Nanoparticles Provide Uniform and Widespread Gene Transfer in the Brain, (2015), doi:10.1002/adhm.201400800.
342. G. P. Tang, J. M. Zeng, S. J. Gao, Y. X. Ma, L. Shi, Y. Li, H. P. Too, S. Wang, Polyethylene glycol modified polyethylenimine for improved CNS gene transfer: Effects of PEGylation extent, *Biomaterials* **24**, 2351–2362 (2003).
343. S. Yamano, J. Dai, S. Hanatani, K. Haku, T. Yamanaka, M. Ishioka, T. Takayama, C. Yuvienco, S. Khapli, A. M. Moursi, J. K. Montclare, Long-term efficient gene delivery using

- polyethylenimine with modified Tat peptide., *Biomaterials* **35**, 1705–15 (2014).
344. J. J. . Green, R. Langer, D. G. Anderson, A Combinatorial Polymer Library Approach Yields Insight into Nonviral Gene Delivery, *Acc Chem Res.* **15**, 1203–1214 (2008).
345. P. Mastorakos, L. Adriana, J. . Chisholm, E. Song, W. K. Choi, M. M. Morales, M. P. Boyle, J. Hanes, J. S. Suk, Highly compacted biodegradable DNA nanoparticles capable of overcoming the mucus barrier for inhaled lung gene therapy Highly compacted biodegradable DNA nanoparticles capable of overcoming the mucus barrier for inhaled lung gene therapy, *PNAS* **112**, 8720–8725 (2015).
346. S. T. . Tzeng, H. Guerrero-Cazares, E. E. . Martinez, J. C. . Sunshine, A. Quinones-Hinojosa, J. J. . Green, Non-Viral Gene Delivery Nanoparticles Based on Poly(Beta-amino esters) for Treatment of Glioblastoma, *Biomaterials* **32**, 5402–5410 (2012).
347. B. A. Piras, Y. Tian, Y. Xu, N. A. Thomas, D. M. O'Connor, B. A. French, Systemic injection of AAV9 carrying a periostin promoter targets gene expression to a myofibroblast-like lineage in mouse hearts after reperfused myocardial infarction, *Gene Ther.* **23**, 469–478 (2016).
348. V. Brochard, B. Combadière, A. Prigent, Y. Laouar, A. Perrin, V. Beray-berthat, O. Bonduelle, D. Alvarez-fischer, J. Callebert, J. Launay, C. Duyckaerts, R. A. Flavell, E. C. Hirsch, S. Hunot, Infiltration of CD4+ Lymphocytes into the Brain Contributes to Neurodegeneration in a Mouse Model of Parkinson Disease, *J. Clinical Investig.* **119**, 182–192 (2009).
349. B. D. Bradaric, A. Patel, J. A. Schneider, P. M. Carvey, B. Hendey, Evidence for angiogenesis in Parkinson's disease, incidental Lewy body disease, and progressive supranuclear palsy, *J. Neural Transm.* **119**, 59–71 (2012).
350. N. Dudvarski Stankovic, M. Teodorczyk, R. Ploen, F. Zipp, M. H. H. Schmidt, Microglia–blood vessel interactions: a double-edged sword in brain pathologies, *Acta Neuropathol.* **131**, 347–363 (2016).
351. P. S. Whitton, Inflammation as a causative factor in the aetiology of Parkinson's disease,

Br. J. Pharmacol. **150**, 963–976 (2009).

352. C. Jiang, M. Mei, B. Li, X. Zhu, W. Zu, Y. Tian, Q. Wang, Y. Guo, Y. Dong, X. Tan, A non-viral CRISPR/Cas9 delivery system for therapeutically targeting HBV DNA and pcsk9 in vivo, *Cell Res.* **27**, 440–443 (2017).

353. R. Batra, D. A. Nelles, E. Pirie, S. M. Blue, R. J. Marina, H. Wang, I. A. Chaim, J. D. Thomas, N. Zhang, V. Nguyen, S. Aigner, S. Markmiller, G. Xia, K. D. Corbett, M. S. Swanson, G. W. Yeo, Elimination of Toxic Microsatellite Repeat Expansion RNA by RNA-Targeting Cas9, *Cell* **170**, 899–912.e10 (2017).

354. Y. Boucher, L. T. Baxter, R. K. Jain, Interstitial pressure gradients in tissue- isolated and subcutaneous tumours: implications for therapy., *Cancer Res.* **50**, 4478–4484 (1990).

355. Z. I. Kovacs, S. Kim, N. Jikaria, F. Qureshi, B. Milo, B. K. Lewis, M. Bresler, S. R. Burks, J. A. Frank, Disrupting the blood–brain barrier by focused ultrasound induces sterile inflammation, *Proc. Natl. Acad. Sci.* , 201614777 (2016).

356. H.-L. Liu, Y.-Y. Wai, P.-H. Hsu, L.-A. Lyu, J.-S. Wu, C.-R. Shen, J.-C. Chen, T.-C. Yen, J.-J. Wang, In vivo assessment of macrophage CNS infiltration during disruption of the blood-brain barrier with focused ultrasound: a magnetic resonance imaging study., *J. Cereb. Blood Flow Metab.* **30**, 177–86 (2010).

357. A. Louveau, I. Smirnov, T. J. Keyes, J. D. Eccles, S. J. Rouhani, J. D. Peske, N. C. Derecki, D. Castle, J. W. Mandell, K. S. Lee, T. H. Harris, J. Kipnis, Structural and functional features of central nervous system lymphatic vessels, *Nature* **523**, 337–341 (2015).

358. H. Salmon, K. Franciszkievicx, D. Damotte, M.-C. Dieu-Nosjean, P. Validire, A. Trautmann, F. Mami-Chouaib, E. Donnadieu, Matrix architecture defines the preferential localization and migration of T cells into the stroma of human lung tumors, *J. Clin. Invest.* **122**, 899–910 (2012).

359. A. C. Naj, G. Jun, G. W. Beecham, L. S. Wang, B. N. Vardarajan, J. Buros, P. J. Gallins, J.

D. Buxbaum, G. P. Jarvik, P. K. Crane, E. B. Larson, T. D. Bird, B. F. Boeve, N. R. Graff-Radford, P. L. De Jager, D. Evans, J. A. Schneider, M. M. Carrasquillo, N. Ertekin-Taner, S. G. Younkin, C. Cruchaga, J. S. K. Kauwe, P. Nowotny, P. Kramer, J. Hardy, M. J. Huentelman, A. J. Myers, M. M. Barmada, F. Y. Demirci, C. T. Baldwin, R. C. Green, E. Rogaevea, P. S. George-Hyslop, S. E. Arnold, R. Barber, T. Beach, E. H. Bigio, J. D. Bowen, A. Boxer, J. R. Burke, N. J. Cairns, C. S. Carlson, R. M. Carney, S. L. Carroll, H. C. Chui, D. G. Clark, J. Corneveaux, C. W. Cotman, J. L. Cummings, C. Decarli, S. T. Dekosky, R. Diaz-Arrastia, M. Dick, D. W. Dickson, W. G. Ellis, K. M. Faber, K. B. Fallon, M. R. Farlow, S. Ferris, M. P. Frosch, D. R. Galasko, M. Ganguli, M. Gearing, D. H. Geschwind, B. Ghetti, J. R. Gilbert, S. Gilman, B. Giordani, J. D. Glass, J. H. Growdon, R. L. Hamilton, L. E. Harrell, E. Head, L. S. Honig, C. M. Hulette, B. T. Hyman, G. A. Jicha, L. W. Jin, N. Johnson, J. Karlawish, A. Karydas, J. A. Kaye, R. Kim, E. H. Koo, N. W. Kowall, J. J. Lah, A. I. Levey, A. P. Lieberman, O. L. Lopez, W. J. MacK, D. C. Marson, F. Martiniuk, D. C. Mash, E. Masliah, W. C. McCormick, S. M. McCurry, A. N. McDavid, A. C. McKee, M. Mesulam, B. L. Miller, C. A. Miller, J. W. Miller, J. E. Parisi, D. P. Perl, E. Peskind, R. C. Petersen, W. W. Poon, J. F. Quinn, R. A. Rajbhandary, M. Raskind, B. Reisberg, J. M. Ringman, E. D. Roberson, R. N. Rosenberg, M. Sano, L. S. Schneider, W. Seeley, M. L. Shelanski, M. A. Slifer, C. D. Smith, J. A. Sonnen, S. Spina, R. A. Stern, R. E. Tanzi, J. Q. Trojanowski, J. C. Troncoso, V. M. Van Deerlin, H. V. Vinters, J. P. Vonsattel, S. Weintraub, K. A. Welsh-Bohmer, J. Williamson, R. L. Woltjer, L. B. Cantwell, B. A. Dombroski, D. Beekly, K. L. Lunetta, E. R. Martin, M. I. Kamboh, A. J. Saykin, E. M. Reiman, D. A. Bennett, J. C. Morris, T. J. Montine, A. M. Goate, D. Blacker, D. W. Tsuang, H. Hakonarson, W. A. Kukull, T. M. Foroud, J. L. Haines, R. Mayeux, M. A. Pericak-Vance, L. A. Farrer, G. D. Schellenberg, Common variants at MS4A4/MS4A6E, CD2AP, CD33 and EPHA1 are associated with late-onset Alzheimer's disease, *Nat. Genet.* **43**, 436–443 (2011).

360. J. Herz, A. J. Filiano, A. Smith, N. Yogev, J. Kipnis, Myeloid Cells in the Central Nervous

System, *Immunity* **46**, 943–956 (2017).

361. M. T. Heneka, M. J. Carson, J. El Khoury, G. E. Landreth, F. Brosseron, D. L. Feinstein, A. H. Jacobs, T. Wyss-Coray, J. Vitorica, R. M. Ransohoff, K. Herrup, S. a Frautschy, B. Finsen, G. C. Brown, A. Verkhratsky, K. Yamanaka, J. Koistinaho, E. Latz, A. Halle, G. C. Petzold, T. Town, D. Morgan, M. L. Shinohara, V. H. Perry, C. Holmes, N. G. Bazan, D. J. Brooks, S. Hunot, B. Joseph, N. Deigendesch, O. Garaschuk, E. Boddeke, C. a Dinarello, J. C. Breitner, G. M. Cole, D. T. Golenbock, M. P. Kummer, Neuroinflammation in Alzheimer's disease, *Lancet Neurol.* **14**, 388–405 (2015).

362. M. T. Heneka, M. P. Kummer, E. Latz, Innate immune activation in neurodegenerative disease, *Nat. Rev. Immunol.* **14**, 463–477 (2014).

363. W. Peng, T. M. Achariyar, B. Li, Y. Liao, H. Mestre, E. Hitomi, S. Regan, T. Kasper, S. Peng, F. Ding, H. Benveniste, M. Nedergaard, R. Deane, Suppression of glymphatic fluid transport in a mouse model of Alzheimer's disease, *Neurobiol. Dis.* **93**, 215–225 (2016).

364. B. T. Kress, J. J. Iliff, M. Xia, M. Wang, H. S. Wei Bs, D. Zeppenfeld, L. Xie, B. S. Hongyi Kang, Q. Xu, J. A. Liew, B. A. Plog, F. Ding, R. D. PhD, M. Nedergaard, Impairment of paravascular clearance pathways in the aging brain, *Ann. Neurol.* **76**, 845–861 (2014).